NUMERICAL STUDY OF THE NONLINEAR ROSSBY WAVE CRITICAL LEVEL

NUMERICAL STUDY OF THE NONLINEAR ROSSBY WAVE CRITICAL LEVEL DEVELOPMENT IN A BAROTROPIC ZONAL FLOW.

by

MICHEL BÉLAND

A thesis submitted to the Faculty of Graduate Studies and Research in partial fulfilment of the requirements for a degree of Doctor of Philosophy.

Department of Meteorology
McGill University
Montréal

March, 1977

RÉSUMÉ

Afin d'étudier l'évolution dans le temps et dans l'espace du niveau critique de l'onde de Rossby, l'équation du tourbillon barotrope non-linéaire est solutionnée à l'aide d'un modèle numérique. Le profil de vent initial a la forme d'une tangente hyperbolique, et une onde est entretenue à la frontière nord du courant; une condition de rayonnement de Sommerfeld est utilisée à la frontière sud. Des intégrations linéaires, quasi-linéaires et non-linéaires sont effectuées, et les résultats sont comparés à ceux d'études antérieures.

On démontre entre autres choses que pour de faibles amplitudes de l'onde incidente (de sorte que les intéractions non-linéaires ne demeurent importantes que dans la couche critique) un état stationnaire est atteint, à l'extérieur de la couche critique. Cet état est caractérisé par un flux de momentum nul au sud et au nord de la couche critique, de sorte que l'onde incidente est totalement réfléchie au niveau critique, en accord avec une théorie antérieure. L'évolution vers cet état stationnaire, ainsi que la structure de la couche critique sont cependant très différentes de celles obtenues lors d'intégrations précédentes par d'autres auteurs. A partir de ces résultats, on discute brièvement de la propagation méridionale des ondes de Rossby vers l'équateur, et de leur influence sur la circulation tropicale.

ABSTRACT

The fully nonlinear barotropic vorticity equation is integrated in time to study the development of a Rossby wave critical level. The initial conditions consist of a hyperbolic tangent shear flow, and a steady forced wave at the northern boundary; a radiation condition is used at the southern boundary. Linear, quasilinear and nonlinear integrations are made, and the results are compared with previous studies.

For small values of the perturbation amplitude, such that nonlinear interactions are important only in the critical layer, a steady-state is obtained in the outer domain, in which the Reynolds stress vanishes both above and below the critical level, and the forced wave is totally reflected as suggested by previous analytical nonlinear steady-state solutions; the approach to that steady-state, and the structure of the critical layer are however quite different from the quasilinear integrations performed by other authors. Some conclusions are drawn with respect to the forcing of the equatorial regions by meridionally propagating mid-latitude Rossby waves.

ACKNOWLEDGEMENTS

The author would like to thank Professor J. Derome, who acted as thesis supervisor, for originally bringing up this problem to his attention, and for his continued guidance, criticisms and suggestions. I wish also to thank Dr. T. Warn, whose work on the theoretical aspects of this problem has led to many fruitful discussions and suggestions; his guidance and his help in learning and understanding nonlinear critical layer theory was invaluable.

I would also like to acknowledge the cooperation of the programmers of the Division de Recherche en Prévision Numérique, and of the Atmospheric Environment Service of Canada for extended use of their CDC 7600 computer, and also for financial support through a grant during the earlier part of this work. Finally, I wish to thank Ms. Sandra Yip for her drafting of the figures, and Ms. Marcia Doleyres who typed the manuscript.

TABLE OF CONTENTS

LIST OF FIGURES

LIST OF SYMBOLS

a	earth's radius (6371 km)
A_n, B_n	sine and cosine Fourier coefficient of n^{th} harmonic.
c	phase speed of a wave (usually in the east-west direction)
f	Coriolis parameter ($f=2\omega\sin\phi$)
$\vec{g}$	gravitational acceleration
H	atmospheric scale height
$\vec{i}$, $\vec{j}$	Cartesian unit vectors; $\vec{i}$ points to the east, $\vec{j}$ to the north
k, l	x and y wavenumbers
L	shear scale length
N	Brunt Vaisala frequency, or number of harmonics
p	pressure
t	time
u, v	x and y components of velocity vector
x, y	cartesian coordinates; x increases to the east, y to the north
α	x wavenumber
β	planetary vorticity gradient
δ	aspect ratio (K^2L^2)
ε	non dimensional perturbation amplitude
ζ	vorticity
ϕ	latitude
$\phi(y,t)$	complex wave function
λ	x wavelength
$\Psi(x,y,t)$	total stream function (zonal and perturbation)
$\Psi'(x,y,t)$	perturbation stream function
ρ	density

ω earth's angular velocity

$\overline{(\ )}$ indicates a zonal average $\left(\frac{1}{2\pi}\int_0^{2\pi}(\ )\,d\lambda\right)$

" ' " indicates a deviation from a zonal average

CHAPTER 1. INTRODUCTION

In order to avoid any ambiguity in the discussion to follow, we shall first define the terms "critical level", hereafter abbreviated C.L., and "critical layer". By critical level we want to refer to the singular point occurring in linearized hydrodynamic shear flow equations, when the phase speed of a disturbance in the direction of flow matches the speed of the basic flow. By critical layer we want to refer to a region situated around the critical level, having a width which is a function of certain non-dimensional parameters of the problem at hand , usually time, viscosity or a wave amplitude, and where nonlinear and/or viscous terms are important.

Critical levels are by no means restricted to atmospheric shear flow equations. They appear in almost every type of shear flow equations, be it that of a plasma flowing in a magnetic bottle, or that of an ocean current in which waves are imbedded. In this particular study, we shall restrict ourselves to the atmosphere, and even then, to a particular type of atmospheric wave motion. We already know that several types of wave motions are possible in the atmosphere. To each type is associated a wave propagation equation, and these equations, upon linearization, and after the assumption of inviscidness has been made, usually possess a critical level singularity. We list below, for the most well-known of these waves, mainly gravity and Rossby waves, the governing equations that result:

(1) Vertical propagation of gravity waves.

$$\Psi_{zz} + \left\{ \frac{N^2}{(\bar{u}-c)^2} - \frac{\bar{u}_{zz}}{(\bar{u}-c)} - k^2 \right\} \Psi = 0$$

(2) Vertical propagation of Rossby waves.

$$\Psi_{zz} + \left\{ \frac{N^2}{f_0^2} \left(\frac{\beta}{\bar{u}-c} - k^2 + l^2 \right) - \frac{1}{4H^2} \right\} \Psi = 0$$

(3) Lateral propagation of Rossby waves.

$$\Psi_{yy} + \left\{ \frac{\beta - \bar{u}_{yy}}{\bar{u}-c} - k^2 \right\} \Psi = 0$$

In these equations, ψ stands for the perturbation stream function, N is the Brunt-Vaisala frequency, H is the scale height, and the other parameters have the usual meaning. To obtain these three equations, a solution of the form $e^{ik(x-ct)}$ was assumed. The critical level is thus situated at the point where $\bar{u} = c$. This, however, does not render the equations necessarily singular. We must also make sure that at this same point the numerator of the terms containing $(\bar{u}-c)$ or $(\bar{u}-c)^2$ in the denominator are not equal to 0. In the third equation for example, if $\beta - \bar{u}_{yy} = 0$ and $\frac{d\bar{u}}{dy} \neq 0$ at the C.L. there is no critical level singularity, and the solutions (and their derivatives) are regular. In other words, even though there might be a point where $\bar{u} = c$, there might not be a critical level singularity. Equations 1, 2, and 3 are so-called steady-state equations. That is, if we define a new x-coordinate $\xi = k(x-ct)$, the flow will appear steady since we are now moving with the wave. However, critical levels also exist for the time-dependent versions of

1-3, in the sense that as $t \to \infty$, and the solutions become steady, the singularity will appear in the equations.

The question we might now ask ourselves is the following: how does one go about solving the singular propagation equations?

We can separate the scientists who treated the problem in two large groups, mainly those who were interested in the critical level problem as a mathematical curiosity worth solving for its own sake, and those who dealt with it as a "nuisance" preventing them from tackling a more general or interesting problem. Chapter 3 looks in detail at the work of the scientists of the first group. Let us mention here that in the last 25 years or so, a tremendous amount of work has been done on the steady-state problems, starting with a very good review of the linear problem by C.C. Lin (1955), and continuing further as more sophisticated mathematical techniques were used, such as matched asymptotic expansions techniques and multiple scaling techniques, until the nonlinear problems were solved by Benney and Bergeron (1969), Davis (1969), Kelly and Maslowe (1970), Maslowe (1972, 1973) and a few others. The linear time-dependent problems were also tackled, by use of the Laplace transform method by Booker and Bretherton (1966) and Dickinson (1970) to name a few. Right now, active research is going on in order to solve the nonlinear time-dependent problem, as indicated for example in Warn and Warn (1976). The reader might now well ask himself what is meant by the "nonlinear" problem, since the critical level was defined for the linearized equations (that is, equations where the nonlinear terms were dropped). This will be

answered by looking at the work of the scientists of the second group.

To exemplify this type of approach, let us look for example at the problem of the vertical propagation of Rossby waves. It is well known that while the flow is generally westerly in the temperate latitudes, it is easterly near the equator so that if a Rossby wave of zero phase speed crosses from the westerly regime to the easterly regime, it will encounter a critical level, and the equation describing its propagation becomes singular at that point. For someone interested in the vertical propagation problem, this singularity is sometimes viewed as a nuisance, and must be removed. There are 2 ways to remove it. We recall that a number of assumptions were made in deriving the propagation equations, in particular that of linearity, and that of inviscidness. Now the nonlinear term, generally in the form of the Jacobian $J(\psi, \nabla^2\psi)$ contains a third order derivative in y, while the viscous term, generally of the form $\nu\nabla^4\psi$ contains a fourth order derivative in y. The linear inviscid equation, however, contains only a second order derivative in y, and it is the coefficient multiplying this term which disappears as $\bar{u}$-c goes to 0. So retaining either the nonlinear term or the viscous term, or both, removes the singularity. Therefore a choice has to be made: so far, the viscous term, in most studies, has been chosen; there are many reasons for this, the most obvious being that it is the simplest choice to make. This however contradicts the inviscidness assumption; now we know that on the scales of motion usually considered in meteorology, the

atmosphere can be considered for all purposes to be approximately inviscid, although it is conceivable that due to the large shears developing near the C.L., the viscous terms will eventually become important. What about the nonlinear terms? It has been demonstrated by Lin (1957) and more specifically for our problem by Warn and Warn (1976), that indeed in the critical layer, the nonlinear terms become as important as the linear advection terms in a finite time. Moreover, steady-state analytical results indicate that completely different results are obtained when nonlinear terms are retained in the critical layer, instead of the viscous terms. Unfortunately, so far, the nonlinear time-dependent problem has not yet been solved, either by analytical means or numerical means.

This work is therefore dedicated to solving the nonlinear time-dependent problem for the lateral propagation of Rossby waves, by means of a numerical model. By nonlinear, we mean specifically that the amplitude of the nonlinear terms will be small enough that their effect will be felt mainly in this critical layer region; therefore we still have a "critical level" problem. In doing so, we will seek answers to the following questions: (1) is it possible to reach some steady-state similar to those predicted by analytical studies; (2) if so, are the time scales and amplitudes involved realistic enough that the results should be used in steady-state models of wave propagation, particularly concerning the lateral and vertical propagation of Rossby waves; (3) what are the effects of adding viscosity, or modifying the mean flow

initially, or using different types of forcing?; (4) in light of the answers, is the Rossby wave critical level an important physical mechanism significantly modifying the propagation characteristics of the medium, or is it more or less a mathematical curiosity? The answers to these questions will be found in the following chapters. Chapter 2 gives a derivation of the model equations. Chapter 3 contains a survey of the available analytical and numerical results pertinent to our problem. Chapter 4 is devoted to the numerical model itself; we have tried to be explicit enough so that the experiments can be repeated by any independent investigator. In Chapter 5, we discuss the results of a set of linear integrations, which are compared to the analytical results of Dickinson (1970). Finally, the results of the nonlinear integrations, and of various experiments are presented in Chapter 6.

CHAPTER 2. THE MODEL EQUATIONS

2.1 DERIVATION

We shall be using the approximate meteorological equations for large scale flows (large-scale flows meaning flows with a scale of O (1000 km) at least). These are:

$$\frac{du}{dt} = -\frac{1}{\rho}\frac{\partial p}{\partial x} + fv \tag{2.1}$$

$$\frac{dv}{dt} = -\frac{1}{\rho}\frac{\partial p}{\partial y} - fu \tag{2.2}$$

$$\frac{\partial p}{\partial z} = -\rho g$$

where $f = 2\omega\sin\phi$. The effect of the earth's rotation appears as the linear term in u and v, and thus, these equations are not mathematically very different from the Euler equation. Here, x and y represent the two cartesian coordinates, x pointing eastward, and y pointing northward. The sphericity of the earth is accounted for by two assumptions: (1) we will require cyclic periodicity in x, thus modeling the closed nature of atmospheric flow along a latitude circle; (2) we will replace the variable Coriolis force with a linear approximation. That is, we choose a central latitude ϕ_0, (at which y now vanishes) and use Taylor's theorem to write

$$f = f_0 + \frac{\partial f}{\partial y}\Big|_{y=0} y + O(y^2)$$

But

$$\frac{\partial f}{\partial y}\Big|_{y=0} = \frac{\partial}{a\partial\phi}(2\omega\sin\phi)\Big|_{y=0} = \frac{2\omega}{a}\cos\phi_0 = \beta$$

where the constant β gives the rate of change of f with latitude, so that in equation (2.1) and (2.2),

$$f = f_0 + \beta y$$

This is the so-called β-plane approximation. The equations thus formally describe motion on a plane, with the addition of the β term. Defining the vertical component of the vorticity to be given by

$$\zeta = \frac{\partial v}{\partial x} - \frac{\partial u}{\partial y} + f$$

it is possible to form the so-called barotropic vorticity equation, using (2.1) and (2.2). We shall further assume the fluid to be incompressible ($\nabla \cdot \vec{v} = 0$), and two dimensional ($w = 0$, $\frac{\partial}{\partial z}( ) = 0$), so that

$$\nabla_H \cdot \vec{v} = \frac{\partial u}{\partial x} + \frac{\partial v}{\partial y} = 0$$

and the only component of vorticity present is ζ. We end up with

$$\frac{\partial \zeta}{\partial t} + \vec{v}_H \cdot \nabla \zeta = 0 \qquad (2.3)$$

Because $\nabla_H \cdot \vec{v} = 0$, we may define a streamfunction Ψ (x, y, t) such that

$$\vec{v} = \vec{k} \times \nabla_H \Psi$$

where $\vec{k}$ is a unit vector pointing in the positive z direction, and

$$\zeta = \nabla_H^2 \Psi + f$$

Hence, equation (2.3) becomes, with $\nabla_H^2 = \nabla^2$ from now on,

$$\frac{\partial}{\partial t}\nabla^2\Psi + J(\Psi, \nabla^2\Psi) + \beta\Psi_x = 0 \qquad (2.4)$$

Equation (2.4) is the non-divergent barotropic vorticity equation. It approximates the planetary wave motions in the temperate latitudes (Burger (1958), Pedlosky (1964)), and was shown by Charney (1963) to be a valid approximation in the tropics under certain restrictions. We will thus use it to model (in a crude way) the meridional propagation of Rossby waves towards the equator, and study their behaviour as they encounter a critical level.

The condition of cyclic periodicity in the x direction is accounted for by defining a length λ such that a displacement of all the variables in the x direction by λ leaves them unchanged. A natural choice for this length is the earth's circumference at some latitude ϕ_0; thus,

$$\lambda = 2\pi a \cos\phi_0$$

where a denotes the earth's radius. With this boundary condition, the streamfunction is first partitioned into a mean part and a perturbation part

$$\Psi = \bar{\Psi}(y,t) + \Psi'(x,y,t) \qquad (2.5)$$

where

$$\Psi'(x,y,t) = \sum_{m=1}^{M} \left\{ A^m(y,t)\sin k_m x + B^m(y,t)\cos k_m x \right\} \qquad (2.6)$$

and k_m is the wavenumber, defined as

$$k_m = \frac{2\pi m}{\lambda} = \frac{m}{a\cos\phi_0}$$

When (2.5) is substituted into (2.4), and the $\overline{(\ )}$ operator, defined as

$$\overline{(\ )} = \frac{1}{\lambda}\int_0^{\lambda} (\ )\, d\pi$$

is applied to the resulting equation, there results the following equation:

$$\frac{\partial \bar{\zeta}}{\partial t} + \overline{J(\psi', \nabla^2\psi')} = 0 \qquad (2.7)$$

Using the fact that the perturbation wind is non-divergent, $\overline{J(\psi', \nabla^2\psi')}$ is easily shown to be equal to $-\frac{\partial^2 \overline{u'v'}}{\partial y^2}$; since $\bar{\zeta} = -\frac{\partial \bar{u}}{\partial y}$, one can integrate (2.7) once with respect to y, to obtain an equation governing the mean flow. (the constant of integration has been set equal to zero, since (2.8.a) is really just the zonal average of the u momentum equation):

$$\frac{\partial \bar{u}}{\partial t} = -\frac{\partial}{\partial y}\overline{(uv)} \qquad (2.8.a)$$

where

$$\bar{u} = -\frac{\partial \bar{\psi}}{\partial y} \; ; \quad u' = -\frac{\partial \psi'}{\partial y} \; ; \quad v' = \frac{\partial \psi'}{\partial x}$$

That is, the forcing of the mean flow is done by the action of the wave momentum flux convergence. The second equation is obtained by subtracting (2.7) from (2.4); this yields:

$$\frac{\partial}{\partial t}\nabla^2\psi' + \bar{u}\frac{\partial}{\partial x}\nabla^2\psi' + J(\psi',\nabla^2\psi') - \overline{J(\psi',\nabla^2\psi')} + (\beta - \bar{u}_{yy})\frac{\partial\psi'}{\partial x} = 0 \qquad (2.8.b)$$

It is the perturbation vorticity equation, and it is nonlinear because of the Jacobian term.

2.2 NON DIMENSIONALIZATION

In order to explore more easily the range of parameters of interest, and facilitate the analysis of the results, equation (2.8.b) was non-dimensionalized in the following fashion. Let L be a typical shear scale length, u_m the maximum initial zonal wind speed, and ϕ_s the amplitude of the forced wave at the northern boundary. We also define

$$y = Ly^* \; ; \; \bar{u} = u_m u^* \; ; \; \psi = \phi_s \psi^* ; \; x = x^*/k$$

where a "*" denotes a non-dimensional quantity. The Laplacian operator now becomes

$$\nabla^2 = \frac{1}{L^2}\nabla^{2*}$$

where

$$\nabla^{2*} = \frac{\partial^2}{\partial y^{2*}} + \delta\frac{\partial^2}{\partial x^{2*}}$$

and

$$\delta = k^2L^2$$

is the aspect ratio. The longer the zonal wavelength, the smaller it is. This is why for long waves one is sometimes justified in dropping the x-derivative of the Laplacian (see for example Dickinson (1970)). Substituting the above definitions into (2.8.b) and balancing each term, we obtain the following after dividing through by ϕ_s:

$$\frac{1}{TL^2} \sim \frac{U_m k}{L^2} \sim k\left(\beta - \frac{U_m}{L^2}\right) \sim \frac{\phi_s k}{L^3}$$

Multiplying the above by L^2/ku_m leads to

$$\frac{1}{TkU_m} \sim 1 \sim \left(\frac{\beta L^2}{U_m} - 1\right) \sim \frac{\phi_s}{LU_m}$$

A balance between the first two terms, that is the advection term and the vorticity tendency term gives the non-dimensional time scale

$$t = t^*/ku_m$$

We shall define also

$$\beta = \left(\frac{U_m}{L^2}\right)\beta^* \; ; \quad \varepsilon = \frac{\phi_s}{LU_m}$$

so that equation (2.8.b) can now be written in non-dimensional quantities as

$$\frac{\partial}{\partial t}\nabla^2\psi' + \bar{U}\frac{\partial}{\partial x}\nabla^2\psi' + (\beta - \bar{U}_{yy})\frac{\partial \psi'}{\partial x} + \varepsilon J(\psi', \nabla^2\psi') - \varepsilon \overline{J(\bar{\psi}, \nabla^2\psi')} = 0 \qquad (2.9)$$

where stars have been dropped. We see that it is almost identical in form to (2.8.b) apart from the nonlinear parameter ε which now multiplies the Jacobian, and is a measure of the nonlinearity, or, more specifically, of the amplitude of the forced wave. Equation (2.8.a) also becomes

$$\frac{\partial \bar{U}}{\partial t} = -\varepsilon^2 \frac{\partial}{\partial y}\overline{(v\psi)} \qquad (2.10)$$

We now see that there are three parameters of interest: δ, ε and β (when diffusion is present, ν is to be considered). We already know that ε determines the importance of the nonlinear term. We shall look at the meaning of δ and β in the following section. Since $\sin(k_n x)$ and $\cos(k_n x)$ now become $\sin(nx)$ and $\cos(nx)$, k_n should be replaced by n in equation (2.6), and k_n^2 by $n^2\delta$.

Equation (2.9) will be further decomposed into two other equations, one for $A^n(y,t)$ and one for $B^n(y,t)$, using the Fourier series for ψ'. Before doing so, however, we have to choose a correct form for the Jacobian. It is well-known that the analytic Jacobian preserves certain integral constraints, some of which are mean square vorticity (also called enstrophy), mean kinetic energy and mean vorticity, in a closed domain, across the boundaries of which there is no inflow of outflow. In particular, Arakawa (1966) showed that when expressed over a grid with second order finite differences,

1) $J^{++}(\zeta,\psi) = \frac{\partial \zeta}{\partial x}\frac{\partial \psi}{\partial y} - \frac{\partial \zeta}{\partial y}\frac{\partial \psi}{\partial x}$ — conserves neither enstrophy nor vorticity.

2) $J^{+\times}(\zeta,\psi) = \frac{\partial}{\partial x}\left(\zeta\frac{\partial \psi}{\partial y}\right) - \frac{\partial}{\partial y}\left(\zeta\frac{\partial \psi}{\partial x}\right)$ — conserves only kinetic energy

3) $J^{\times+}(\zeta,\psi) = \frac{\partial}{\partial y}\left(\psi\frac{\partial \zeta}{\partial x}\right) - \frac{\partial}{\partial x}\left(\psi\frac{\partial \zeta}{\partial y}\right)$ — conserves only enstrophy.

whereas the sum of 1), 2), and 3) divided by 3 conserves all three integral constraints. Since in our model $\overline{\psi}$ is not carried explicitly, we cannot use $J^{\times+}$; we therefore chose to use $J^{+\times}$, which conserves kinetic energy. The derivation of the final three predictive equations is given in Appendix A. They are written as follows:

$$\frac{\partial}{\partial t} S^{A^p} = p\left[\bar{u} S^{B^p} + B^p(\beta - \bar{u}_{yy})\right] - \frac{\epsilon}{2} \sum_{\ell=1}^{N} \left\{ \ell \left[C_1^{p+\ell,\ell} + C_1^{p-\ell,\ell} - C_1^{\ell-p,\ell} + C_4^{p+\ell,\ell} - C_4^{|\ell-p|,\ell} \right] + p\left[D_1^{p+\ell,\ell} + D_1^{\ell-p,\ell} - D_1^{p-\ell,\ell} + D_4^{p+\ell,\ell} + D_4^{|\ell-p|,\ell} \right] \right\} \quad (2.11)$$

$$\frac{\partial}{\partial t} S^{B^p} = p\left[-\bar{u} S^{A^p} - A^p(\beta - \bar{u}_{yy})\right] - \frac{\epsilon}{2} \sum_{\ell=1}^{N} \left\{ \ell \left[C_2^{p-\ell,\ell} - C_2^{\ell-p,\ell} - C_2^{p+\ell,\ell} + C_3^{p+\ell,\ell} + C_3^{|p-\ell|,\ell} \right] - p\left[D_2^{p+\ell,\ell} - D_2^{\ell-p,\ell} + D_2^{p-\ell,\ell} + D_3^{|\ell-p|,\ell} - D_3^{p+\ell,\ell} \right] \right\} \quad (2.12)$$

$$\frac{\partial \bar{u}}{\partial t} = \epsilon^2 \sum_{\ell=1}^{N} \frac{\ell}{2} \left(A^\ell S^{B^\ell} - B^\ell S^{A^\ell} \right) \quad (2.13)$$

where the following definitions have been used:

$$S^{B^m} = B^m_{yy} - m^2\delta B^m \quad ; \quad S^{A^m} = A^m_{yy} - m^2\delta A^m$$

$$C_1^{m,m} = \frac{\partial}{\partial y}\left(S^{A^m} A^m\right) \quad ; \quad C_2^{m,m} = \frac{\partial}{\partial y}\left(S^{A^m} B^m\right) \quad ; \quad C_3^{m,m} = \frac{\partial}{\partial y}\left(S^{B^m} A^m\right) \quad ; \quad C_4^{m,m} = \frac{\partial}{\partial y}\left(S^{B^m} B^m\right)$$

$$D_1^{m,m} = S^{A^m} A^m_y \quad ; \quad D_2^{m,m} = S^{A^m} B^m_y \quad ; \quad D_3^{m,m} = S^{B^m} A^m_y \quad ; \quad D_4^{m,m} = S^{B^m} B^m_y$$

and it is required that $|p-\ell|>0$, $p+\ell \in N$, N represents the number of Fourier components allowed by the model, and only interaction terms with positive indices are retained. These three equations form the basic set which was integrated in time. In some of the experiments, a diffusion term was added to the perturbation equations. The form of the diffusion term was linear, and written as $\nu\nabla^4\psi'$; in terms of A^n and B^n, it is easily shown to be equal to $\nu\nabla^2 S^{A^m}$ and $\nu\nabla^2 S^{B^m}$, respectively added to the right hand side of equations (2.11) and (2.12).

2.3 RANGES OF INTEREST FOR δ AND β

Since our study is aimed at the critical level development, we must be careful in the choice of the parameters so as to stay away from instability (numerical or dynamical), and make sure that the waves will indeed propagate towards the C.L., and in a time short enough for the model to be integrable on a computer.

2.3.1 BAROTROPIC INSTABILITY

The first criterion we should satisfy is the Rayleigh-Kuo criterion for stability (even though it is defined for a linear equation). It says that

$$\beta - \bar{u}_{yy} > 0 \quad \text{or} \quad \beta - \bar{u}_{yy} < 0$$

everywhere in the domain of interest to avoid barotropic instability. We will choose the following initial profile for the mean zonal wind:

$$\bar{u} = \tanh y$$

To find the maximum of $\bar{u}_{yy}$, we set $\bar{u}_{yyy} = 0$; this gives

$$\operatorname{sech}^2 y(2\tanh^2 y - \operatorname{sech}^2 y) = 0$$

It is easy to see that the solution corresponding to the maximum value of $\bar{u}_{yy}$ is given by

$$\tanh y = (\operatorname{sech} y)/1.414$$

from which we get that

$$(\bar{u}_{yy})\text{max.} = 0.78 \text{ at } y = -0.66$$

So we must set $\beta > 0.78$ at initial time, if we want to avoid the possibility of barotropic instability.

2.3.2 PROPAGATION

Upon substituting a solution of the form $\Psi = \phi(y) e^{im\alpha}$ in the linear steady-state barotropic vorticity equation for constant zonal wind $\bar{u}$, there results

$$\phi_{yy} + \left(\frac{\beta}{\bar{U}} - m^2\delta\right)\phi = 0$$

Defining the parameter $\ell^2 = \left(\frac{\beta}{\bar{U}} - m^2\delta\right)$, solutions are easily seen to be of the form $e^{\pm i\ell y}$; if ℓ is imaginary, we have both amplifying and decaying solutions; use of given boundary conditions usually results in rejection of the amplifying solution. In the problem we are dealing with, we want the forced wave to be able to propagate towards the C.L., without any amplification or attenuation, at least for that part of the wind profile where $\bar{U}$ = constant.

Thus, for the waves to propagate without attenuation or amplification, we require

$$\frac{\beta}{\bar{U}} - m^2\delta \geq 0 \quad , \quad 0 < \bar{U} < \beta/m^2\delta$$

We have $\bar{u} = \tanh y \leq 1$, initially, and we already require $\beta > 0.78$; so this leads to

$$m^2\delta < 0.78$$

Since for the forced wave, n = 1, we finally get

$$\delta < 0.78$$

which sets an upper bound on the value of δ if we want the forced wave to propagate southward without attenuation towards the C.L.

2.3.3 TIME REQUIRED TO SET UP THE CRITICAL LAYER

Geisler and Dickinson (1974) defined a parameter, called t_c in their paper which is a measure of the flux divergence across the C.L.; it is indicative of the time required for a linear steady solution to be set up in the critical layer. In terms of dimensional quantities, it is given by

$$t_c = \frac{(\beta - \bar{U}_{yy})}{k \bar{U}_y^2}$$

Substituting non-dimensional variables, and using the fact that $\bar{U}_{yy}=0$, $\bar{U}_y=1$ near the critical level, we get that

$$t_c = \beta$$

So we must choose a sufficiently low value of β if we want the linear steady solution to be set up in a reasonably short time (roughly $\lesssim 10 t_c$.).

2.3.4 COMPUTATIONAL INSTABILITY

It is hard to obtain a precise stability criterion for the time scheme we used, which, as will be seen in Chapter 4 is an Adams- Moulton method, using an Adams-Bashforth scheme as a predictor. However, following Henrici (1964), we feel it is quite safe to require

$$\omega \Delta t < 1$$

which is the equivalent criterion for a leapfrog scheme. We know that for Rossby waves,

$$\omega = k\left(\bar{U} - \frac{\beta}{k^2+\ell^2}\right)$$

where ℓ denotes now the y-wavenumber. There are two cases:

1) Short waves.

Then, we can approximate $\omega \simeq \bar{u}k$, and we want to satisfy $\bar{u}k\Delta t < 1$; in non-dimensional units, this becomes

$$\bar{U}\Delta t < 1$$

and since $\bar{u} \leqslant 1$, we finally get $\Delta t < 1$.

2) Long waves.

The highest frequencies will be given by $\bar{u} < 0$, so that we can write

$$|\omega|_{max} = k\left(|\bar{U}| + \frac{\beta}{k^2+\ell^2} \right)$$

The smallest "ℓ" wavenumber is π/D, where $D \to \infty$, since we will be considering a semi-infinite domain, whereas the smallest "k" wavenumber is wavenumber 1, where $k \sim 1/a$, a being the earth's radius. In terms of non-dimensional quantities, we get, since $K > \ell_{min}$, that

$$\left[|\bar{U}| + \frac{\beta}{\delta} \right] \Delta t < 1$$

2.3.5 EXAMPLE

Many of the integrations to be described hereafter were done with the following values of the non-dimensional parameters: $\varepsilon = 0.018$, $\delta = 0.16$, $\beta = 1.6$, $\Delta t = 0.036$, $\Delta y = 0.00625$; this choice corresponds to the following values of the dimensional parameters: L = 1000 km, $k = 4\times10^{-7}\ m^{-1}$ (roughly equal to wavenumber 2 at 40 degrees latitude), $u_m = 10 m\text{-}s^{-1}$, $\beta = 1.6\times10^{-11} m^{-1}\text{-}s^{-1}$, $\Delta y = 6.25$ km, $\Delta t = 2.5$hrs, $\Phi_s = 1.8\times10^{5}\ m^2\text{-}s^{-1}$. It can be observed that all the criteria are

satisfied by this choice, so that stability of the model could be expected, at least in the linear stage of the integrations. The computational stability criterion for long waves gave $\omega\Delta t = 0.396$, which, as required, is smaller than 1. Values of ε, δ, β and Δt as a function of the dimensional parameters k, u_m, L, and ϕ_s, β can be obtained using the definitions of section 2.2.

2.4 BOUNDARY CONDITIONS

We have already mentioned the cyclic boundary condition in the x-direction. There are also two boundary conditions to be specified in the y-direction. The domain we shall be considering for this model extends from $y = -\infty$ to $y = y_0 > 0$. $y = y_0$ corresponds to the northern boundary. At this point, a wave will be switched-on, as a function of time, of which both the amplitude and phase will be known; the amplitudes of the remaining harmonics, for the nonlinear integrations, will be set to zero at that point; i.e.,

$$\psi'(x, y_0, t) = A(t)\sin x + B(t)\cos x \qquad (2.14)$$

The reason behind this choice is that we wish to consider a problem where nonlinear interactions are important only in the critical layer. This is one way of satisfying that condition. The southern boundary condition is a little more problematic to define. So far three different methods have been used. The first is to assume there is a wall and set the amplitudes of the waves to zero at y = 0, say. The second also assumes there is a wall, but sets up a sponge layer (a region where some viscosity is introduced) in front of it, in order to

absorb the waves. The third method, used by Geisler and Dickinson (1974) is to extend the wind profile with a linear wing of negative winds far away from the region of interest, up to a wall, in order that the transients and the propagating or decaying waves are eventually absorbed as they encounter a linear critical level. The first method produces ringing in the channel, as the waves initiated at switch-on time bounce back and forth between the two walls, unless one switches on the wave very slowly. The reason for this is that the frequencies of these transients are too large for them to see a C.L. in the channel, and eventually get absorbed. The second method is better, although sponge layers have unpredictable behaviour as linear or nonlinear waves cross them; part of the wave can be reflected as happens with any change in the index of refraction of a medium, and it is never known exactly how this affects the solution. This approach was tried by Ward (1975), and found to give incorrect results. Method 3 is better still, although the highest frequency modes excited by the switch-on never see a critical level; moreover, this method has the cumbersome effect of extending the domain of integration enormously, just to get rid of transients. This leads to a very large number of gridpoints, only a small fraction of which are actually needed to solve the problem at hand. It prevents the use of a fine resolution, unless one has a mammoth computer, capable of digesting all the arrays needed. For these reasons, we decided to try a fourth method, that is to implement a time-dependent radiation condition at $y = 0$, in order to allow the transients, and the waves to

propagate freely to $-\infty$ outside the domain of integration, without any reflection. This is a better approximation also to what we think happens in the real atmosphere, as there are no walls present at the equator, nor sponge layers, nor 200 ms^{-1} easterly winds. A full description of the radiation condition we shall use is given in Béland and Warn (1975). However, we will rederive it here, for the sake of completeness. Let us consider the problem of a Rossby wave, switched on at the northern boundary, at $y=y_0>0$. The linear governing equation, for a constant zonal wind $\bar{u}$, is

$$\frac{\partial}{\partial t}\nabla^2\psi + \bar{u}\frac{\partial}{\partial x}\nabla^2\psi + \beta\psi_x = 0 \qquad (2.15)$$

Let us first look at the plane wave solution $e^{i(kx + \ell y - \omega t)}$. After substitution of this solution in (2.15), we obtain the well-known dispersion formula

$$\omega = k\bar{u} - \frac{k\beta}{k^2+\ell^2}$$

The phase speed of the Rossby wave is defined as

$$\vec{c}_p = \frac{\omega}{k^2+\ell^2}\left(k\vec{i} + \ell\vec{j}\right)$$

while the group velocity is given by

$$\vec{c}_g = \left[\bar{u} + \frac{\beta(k^2-\ell^2)}{(k^2+\ell^2)^2}\right]\vec{i} + \frac{2\beta k\ell}{(k^2+\ell^2)^2}\vec{j}$$

with the convention that $k>0$. Waves propagating energy towards $y<0$ must have $(c_g)_y<0$; so for these waves, $k\ell<0$, or because of our convention, $\ell<0$. This means that the lines $(kx + \ell y)$ = constant, slope from the north-east to the south-west (we adopt the usual convention that x points to the east, and y to the north). For the

steady problem ($\frac{\partial(\,)}{\partial t} = 0$), let $\Psi = Ae^{ikx}$ at $y = y_0$, and let $\Psi = \phi(y)e^{ikx}$ be a solution; after substituting into (2.15), there comes

$$\phi_{yy} + \left(\frac{\beta}{\bar{U}} - k^2\right)\phi = 0$$

Two cases arise:

(a) $\frac{\beta}{\bar{U}} - k^2 < 0$; $\bar{U} > \frac{\beta}{k^2}$: Non-propagating waves. This leads to an evanescent wave, and there is no problem in choosing the correct solution, which is the decaying one.

(b) $\frac{\beta}{\bar{U}} - k^2 > 0$; $0 < \bar{U} < \frac{\beta}{k^2}$: Propagating waves.

The solution is now

$$\Psi = A_1 e^{i(\ell y + kx)} + B_1 e^{-i(\ell y - kx)}$$

where $\ell = (\beta/\bar{u} - k^2)^{\frac{1}{2}}$

Using the boundary condition at $y = y_0$ gets rid of one arbitrary constant. However, how does one determine the other? This is where the radiation condition comes into play: simply stated, it tells us to choose the solution which gives a southward propagation of energy, the only energy source being at $y = y_0$. This in turn implies that $(c_g)_y < 0$, or $k\ell < 0$, or $\ell < 0$; thus, $A_1 = 0$, and we have a fully determined solution. It is possible to prove formally, by looking at the initial value problem that this is indeed the correct solution. We shall be using the following initial and boundary conditions:

$$\Psi(x,0,t) = \phi(0,t)e^{ikx} = F(t)e^{ikx}$$

$$\nabla^2\Psi(x,y,0) = 0$$

In the model, y = 0 corresponds to the southern boundary, where the radiation condition will be applied. We will further assume that from $y = 0$ to $y = -\infty$, $\bar{u}$ is a constant negative wind, and the amplitude of the waves at $y = 0$ is small enough that the linearized barotropic vorticity equation offers a valid approximation. Let $\Psi(x,y,t) = \phi(y,t)e^{inx}$ be a solution of (2.15) (all quantities are now non-dimensional). We get, after substituting in (2.15)

$$\phi_{yyt} - n^2\delta\phi_t + in\bar{u}(\phi_{yy} - n^2\delta\phi) + in\beta\phi = 0 \quad ; \quad n = 1, 2, 3\ldots\ldots, N$$

We solve this equation by using a Laplace transform method; let

$$\tilde{\phi} = \mathcal{L}(\phi)$$

$$\mathcal{L}(\phi) = \int_0^\infty e^{-\Lambda t}\phi(t)\,dt$$

The Laplace transformed equation and B.C's become

$$\tilde{\phi}_{yy}(\Lambda + in\bar{u}) + \tilde{\phi}(in\beta - in^3\delta\bar{u} - \Lambda\delta n^2) = 0$$

$$\tilde{\phi}(0,\Lambda) = \tilde{F}(\Lambda)$$

Defining $c_r = \bar{u} - \beta/n^2\delta$, we get, rearranging terms,

$$\tilde{\phi}_{yy} - n^2\delta\tilde{\phi}\left\{\frac{\Lambda + inc_n}{\Lambda + in\bar{u}}\right\} = 0$$

Let

$$\ell = n\delta^{1/2}\left\{\frac{\Lambda + inc_n}{\Lambda + in\bar{u}}\right\}^{1/2}$$

and choose $\mathrm{Re}(\ell) > 0$; then, requiring the solution to be bounded at $y = -\infty$, we get

$$\tilde{\phi}(y,\Lambda) = F(\Lambda)e^{\ell y}$$

Thus we see that in the initial value problem, there is no arbitrariness

in choosing the correct solution. Using the inverse Laplace transform,

$$\phi(y,t) = \frac{1}{2\pi i}\int_{c-i\infty}^{c+i\infty} F(\Delta)\, e^{\ell y} e^{\Delta t}\, d\Delta$$

where as usual, c must be chosen such that all the singularities of $F(s)e^{\ell y}$ lie to the left of the line Re(s) = c in the complex s plane. Making use of the convolution theorem, we can rewrite the above as

$$\phi(y,t) = \int_0^t F(t-\tau)\, w(\tau)\, d\tau$$

where

$$w(\tau) = \frac{1}{2\pi i}\int_{c-i\infty}^{c+i\infty} e^{\ell y}\, e^{\Delta\tau}\, d\Delta$$

Differentiating with respect to y, and setting y = 0, we get

$$\phi_y(0,t) = \int_0^t \phi(0,t-\tau)\, \mu w(\tau)\, d\tau$$

with

$$\mu w(\tau) = \frac{1}{2\pi i}\int_{c-i\infty}^{c+i\infty} \ell\, e^{\Delta\tau}\, d\Delta$$

Noting that as $s\to\infty$, $\ell \to m\delta^{\frac{1}{2}}$, we get

$$\mu w(\tau) = \left\{ \frac{1}{2\pi i}\int_c (\ell - m\delta^{1/2}) e^{\Delta\tau}\, d\Delta + \frac{1}{2\pi i}\int m\delta^{1/2} e^{\Delta\tau}\, d\Delta \right\}$$

Substituting the definition of ℓ in the first integral, and using the fact that

$$\frac{1}{2\pi i}\int e^{\Delta\tau}\, d\Delta = \Delta(\tau)$$

where $\Delta(\tau)$ is the so-called delta function, we obtain

$$\mu w(\tau) = m\delta^{1/2}\Delta(\tau) + \frac{m\delta^{1/2}}{2\pi i}\int_c \left\{ \left(\frac{\Delta + im\zeta_n}{\Delta + im\bar{v}} \right) - 1 \right\} e^{\Delta\tau}\, d\Delta$$

After substituting the above expression for $\mu w(\tau)$ in the left-hand side of the equation for $\phi_y(0,t)$, we finally get:

$$\phi_y(0,t) - m\delta^{1/2}\phi(0,t) = \int_0^t \phi(0,t-\tau)\, h(\tau)\, d\tau \qquad (2.16)$$

where

$$h(\tau) = \frac{m\delta^{1/2}}{2\pi i}\int_c \left[\left(\frac{\Delta + im\zeta_n}{\Delta + im\bar{v}} \right)^{1/2} - 1 \right] e^{\Delta\tau}\, d\Delta$$

Using Abramowitz and Stegun, p. 1024, formula 29.3.48, the above can be evaluated, and after a simple manipulation, the result comes out to be

$$h(\tau) = \frac{-\beta}{2\delta^{1/2}} e^{-i\tau\left(m\bar{v} - \frac{\beta}{2m\delta}\right)} \left\{ J_1\left(\frac{\beta\tau}{2m\delta}\right) + i J_0\left(\frac{\beta\tau}{2m\delta}\right) \right\} \qquad (2.17)$$

However, in the model, the unknown variable is not ϕ, but rather $\frac{\partial\phi}{\partial t}$; so the boundary condition (2.16) has to be written for $\frac{\partial\phi}{\partial t}$; to achieve this, take $\frac{\partial}{\partial t}$ of (2.16):

$$\frac{\partial}{\partial y}\phi_t - m\delta^{1/2}\phi_t = \frac{d}{dt}\left\{ \int_0^t \phi(0,t-\tau)\, h(\tau)\, d\tau \right\} \Big|_{y=0}$$

Using Leibnitz' rule to evaluate the right-hand side, we get

$$\text{R.H.S.} = \phi(0,0^+)\, h(t) + \int_0^t \frac{\partial}{\partial t}\phi(0,t-\tau)\, h(\tau)\, d\tau$$

We now have to evaluate $\phi(0,0^+)$ from the boundary condition $\nabla^2\psi = 0$ at $t = 0^+$; we get, using the definition of $\nabla^2\psi$,

$$\phi_{yy} - m^2\delta\phi = 0 \Big|_{t = 0^+}$$

the solution of which is

$$\phi = A e^{m\delta^{1/2} y} + B e^{-m\delta^{1/2} y} \Big|_{t = 0^+}$$

The two constants A and B can be easily evaluated, using the boundary conditions at $y = y_0$ and at $y \to -\infty$.

Since we require $\phi(y,t)$ to remain bounded as $y \to -\infty$, we set B = 0; we have also

$$\Phi(y_0,0^+) = G(0^+) = A e^{m\delta^{1/2} y_0}$$

where G(t) is the forcing. So $A = G(0^+)/e^{m\delta^{1/2} y_0}$, and we get

$$\phi(0,0^+) = G(0^+) e^{-m\delta^{1/2} y_0}$$

The correct radiation condition for $\frac{\partial \phi}{\partial t}$ can now be written

$$\frac{\partial}{\partial y}\left[\frac{\partial \phi}{\partial t}\right]_{y=0} - m\delta^{1/2}\left[\frac{\partial \phi}{\partial t}\right]_{y=0} = G(0^+) e^{-m\delta^{1/2} y_0} h(t) + \int_0^t \frac{\partial}{\partial t}\phi(0,t-\tau)\, h(\tau)\, d\tau$$

We have seen earlier that in our model, $\Psi_n(x,y,t) = A_n \sin nx + B_n \cos nx$ while for the derivation, we have used the form $\Psi_m(x,y,t) = \mathrm{Re}\{\phi_m(y,t) e^{inx}\}$, or, equivalently, $\Psi_n = \mathrm{Re}\{\Phi_m\} \cos nx - \mathrm{Im}\{\phi_m\} \sin nx$. We thus have the correspondence $\mathrm{Re}\{\phi_m\} = B^n$, and $\mathrm{Im}\{\phi_m\} = -A^n$. Similarly, $h(\tau)$ can be written as $\mathrm{Re}\{h(\tau)\} + i\,\mathrm{Im}\{h(\tau)\}$. Using these definitions, the above radiation condition can then be written as a set of two coupled equations for $\frac{\partial A^n}{\partial t}$ and $\frac{\partial B^n}{\partial t}$.

$$\left[\frac{\partial}{\partial y}\left(\frac{\partial B}{\partial t}\right) - m\delta^{1/2}\frac{\partial B}{\partial t}\right]_{y=0} = \left[B(0^+)\,\mathrm{Re}\{h(t)\} + A(0^+)\,\mathrm{Im}\{h(t)\}\right]_{y=0} \tag{2.18.a}$$
$$+ \left[\int_0^t \left\{\frac{\partial}{\partial t} B(t-\tau)\,\mathrm{Re}\{h(\tau)\} + \frac{\partial A}{\partial t}(t-\tau)\,\mathrm{Im}\{h(\tau)\}\right\} d\tau\right]_{y=0}$$

$$\left[\frac{\partial}{\partial y}\left(\frac{\partial A}{\partial t}\right) - m\delta^{1/2}\frac{\partial A}{\partial t}\right]_{y=0} = \left[B(0^+)\,\mathrm{Im}\{h(t)\} - A(0^+)\,\mathrm{Re}\{h(t)\}\right]_{y=0} \tag{2.18.b}$$
$$- \left[\int_0^t \left\{\frac{\partial}{\partial t} B(t-\tau)\,\mathrm{Im}\{h(\tau)\} - \frac{\partial A}{\partial t}(t-\tau)\,\mathrm{Re}\{h(\tau)\}\right\} d\tau\right]_{y=0}$$

This concludes the derivation of the model equations. Equations (2.11), (2.12) and (2.13) will be used to study the evolution in time of the Rossby wave C.L.; these equations will be solved subject to the boundary conditions (2.14) and (2.18), while the profile $\bar{u} = \tanh y$ will be specified initially. As yet, there exist no analytical solutions to the nonlinear time-dependent problem for Rossby waves (or any other waves, as a matter of fact, with a varying (in y) wind profile). However, some interesting conclusions have been reached using simpler equations. They will be reviewed in the following chapter, together with the available numerical results obtained by solving the linear and quasilinear (and even nonlinear, although in a very unsatisfactory way) problems.

CHAPTER 3. PREVIOUS RESULTS

3.1 STEADY-STATE LINEAR PROBLEM

If we neglect the nonlinear terms in (2.8a) and (2.8b) the system reduces to the following:

$$\left(\frac{\partial}{\partial t} + \bar{u}\frac{\partial}{\partial x}\right)\nabla^2\psi' + \left(\beta - \bar{u}_{yy}\right)\frac{\partial \psi'}{\partial x} = 0$$

where ψ' is the perturbation stream function and $\bar{u} = \bar{u}(y)$ is the mean zonal wind speed. If we assume a solution of the form

$$\psi'(x,y,t) = \phi(y)\, e^{i\alpha(x-ct)}$$

then, we get

$$(\bar{u}-c)(\phi_{yy} - \alpha^2\phi) + (\beta - \bar{u}_{yy})\phi = 0$$

where α is the (real) wavenumber, and c the real phase velocity. (we assume here that $\beta - \bar{u}_{yy} > 0$ everywhere in the domain). This equation is similar in type to the Rayleigh equation, except for the beta term, and it was solved by Kuo (1949). The two basic solutions, obtained by using the method of Frobenius (see appendix B) are written as:

$$\phi_a = b_1 y + b_2 y^2 + b_3 y^3 + \ldots$$

$$\phi_b = c_{-1} + c_0\phi_a \ln y + c_1 y + c_2 y^2 + c_3 y^3 + \ldots$$

where the values of the coefficients c_n and b_n are given in appendix B. Two problems show up: first, it is apparent that the perturbation zonal wind has a logarithmic singularity at y = 0 (we again assume the domain of interest extends from $y = y_0$ to $y = -\infty$). This comes from the ϕ_b solution, which upon differentiation with respect to y yields a $\ln y$ term.

This is obviously physically incorrect. The second problem appears when one wants to go from $y>0$ to $y<0$. How do we write ln y for $y<0$? It can be shown (Lin (1944, 1945) and Kuo (1949) that the inclusion of viscosity in the critical layer region yields new solutions in which u' is not singular anymore. These solutions also show that in order to match the inviscid solution for $y > 0$, above the C.L., with the solution for $y < 0$, under the C.L., the lny term, for $y < 0$, should be written as $\ln|y| - i\pi$. This is the so-called $-\pi$ phase shift, a result of retaining the viscous terms in the critical layer region. Using this information, the inviscid solutions can now be written as follows:

for $y > 0$: $$\phi^+ = A^+\phi_a + B^+\phi_b$$

for $y < 0$: $$\phi^- = A^-\phi_a + B^-\phi_b$$

where for $y<0$, $\ln y = \ln|y|$. The viscous matching then requires $B^+ = B^- = B$. and $A^+ = A^- - Bc_i i\pi$. Thus, there is a jump in the constant A as one crosses the C.L., here located at $y = 0$. It is an easy matter to show that this jump is related to the jump in the wave momentum flux across the C.L., averaged over one wavelength (this quantity is equivalent to the Reynolds stress). Let $\alpha = 1$, and $c = 0$ for simplicity. Then we can write

$$\psi' = \frac{1}{2}\left\{(A\phi_a + B\phi_b)e^{ix} + c.c.\right\}$$

where c.c. denotes the complex conjugate. With $u' = -\frac{\partial\psi'}{\partial y}$, and $v' = \frac{\partial\psi'}{\partial x}$,

one gets

$$\overline{u'v'} = (i/4)(A^*B - AB^*)\,(\phi_{ay}\phi_b - \phi_{by}\phi_a).$$

Noting that the Wronskian of the two solutions ϕ_a and ϕ_b is defined as

$$W = \begin{vmatrix} \phi_a & \phi_b \\ \phi_{ay} & \phi_{by} \end{vmatrix} = \phi_a\phi_{by} - \phi_b\phi_{ay} = \text{constant}$$

the above expression for $\overline{u'v'}$ can be further simplified. The constant can be shown to equal -1, by evaluating W at y=0, and using the fact that $\lim_{y\to 0} \phi_a\phi_{by} = 0$.

Thus we get that

$$\overline{u'v'} = -(i/4)(A^*B - AB^*).$$

Since $A^+ \neq A^-$, $B^+ = B^-$, one concludes that: (1) The Reynolds' stress is constant above and below the C.L., and (2) it has a different value above and below, or, in other words, there is a jump. In the special case where the wave momentum flux is to vanish at $y \to -\infty$, the jump can be shown (see Lin (1967)) to be

$$[\overline{u'v'}] = \frac{-\pi|B|^2(\bar{U}_{yy_c} - \beta)}{2\bar{U}_{y_c}}$$

(a subscript "c" indicates that the derivative is to be evaluated at the C.L.)

Summarizing the results of the steady-state linear problem, we can say the following:

1) u' has a logarithmic singularity at the C.L.

2) there is a $-\pi$ phase shift in the ln y term of the ϕ_b solution.

3) the wave momentum flux $\overline{u'v'}$ has a jump across the C.L.

Let us note that in the critical layer, the viscous terms were used to permit a matching of the inviscid solutions, so that properly speaking, we should be speaking of the linear "viscous" steady problem.

3.2 TIME-DEPENDENT LINEAR PROBLEM

This problem (for Rossby waves) was first solved by Dickinson (1970), using an equation similar to that used by Kuo. It is a simplified version of the linearized barotropic vorticity equation: he assumes the y (north-south) scale to be much smaller than the x-scale, so that the x-derivative can be dropped in the Laplacian (this is the long wave approximation), and also that the mean zonal wind $\bar{u}$ has a constant shear, so that one can write $\bar{u}(y) = \bar{u}'y$, where the prime denotes a y derivative. After substituting a solution of the form

$$\Psi(x,y,t) = \phi(y,t)\, e^{ikx}$$

he obtains the following equation:

$$\left(\frac{\partial}{\partial t} + \bar{u}'y \frac{\partial}{\partial x}\right)\Psi_{yy} + \beta\Psi_x = 0$$

He solves it as an initial value problem, in which a wave is switched on at $t = 0$, along some boundary $y=y_0 \gg 1$, using a Laplace transform method. He obtains a solution consisting of a transient oscillating in y and t, and a large time quasi-steady part very similar to the Tollmien-Kuo solutions discussed previously in 3.1. Warn and Warn (1976), in a review of Dickinson's paper, found a number of errors, so that the solution we give here is taken from their note: for $|yt| \gg 1$, and $t \gg 1$, that is for a region lying outside the critical layer:

$$\phi(y,t) = \phi(y,\infty) - \frac{a e^{-iyt}}{2yt^2} + o(t^{-3}) + o(y^{-2}t^{-1}) + o(y^{-1}t^{-2})$$

where $\phi(y,\infty)$ is the solution as $t\to\infty$, valid inside or outside the critical layer:

$$\phi(y,\infty) = -(\pi/2)\,y^{1/2}\,Y_1(2y^{1/2}) - i(\pi/2)\,y^{1/2}\,J_1(2y^{1/2}) \qquad y>0$$

$$\phi(y,\infty) = |y|^{1/2}\,K_1(2|y|^{1/2}) \qquad y<0$$

It can be shown by expanding the above expressions in powers of y that they can be rearranged in a form very similar to the Tollmien-Kuo solutions, and that the $-i\pi$ in the $y>0$ solution corresponds exactly to the $-i\pi$ phase shift of the ln y term. In other words, as $t\to\infty$, the large time behaviour develops an identical phase shift, even though no viscosity is present. This is due to the fact that now the problem is an initial value problem, and that the solution is completely determined by the initial conditions.

One should also notice the transient part originating from the switch-on: at a fixed point in y, the solution will oscillate in time with period $1/y$ and decay as $1/t^2$; at a fixed time t, it will show oscillations in y with wavelength $1/t$ and decaying as $1/y$. Dickinson goes on to show that the critical layer decreases in width as t^{-1}. The perturbation zonal velocity was also shown by Warn and Warn (1976) to grow indefinitely like ln t. ; thus the singularity is never realized in a finite time. The wave momentum flux eventually reaches a constant value for $y > 0$ and thereafter exhibits small decaying oscillations about its value at infinite time. Since $\overline{u'v'} = 0$ for $y<0$, a jump is thus realized.

Summarizing the above results, we can say that the large time behaviour of the forced linear time-dependent problem is very similar to that of the steady-state linear problem. In particular, one should expect:

1) a $-\pi$ phase shift in the ln y term.
2) a jump in the Reynolds stress $-\overline{u'v'}$.
3) a ln t growth of u'.
4) a decrease in width of the critical layer like t^{-1}.
5) a transient oscillation in time and in space superimposed on the large - time solution.

3.3 STEADY-STATE NONLINEAR PROBLEM

This problem was first solved by Benney and Bergeron (1969) and independently by Davis (1969), and later generalized by Haberman (1972). They solved the following equation:

$$(\bar{u}-c)\nabla^2\psi_x - \bar{u}_{yy}\psi_x + \varepsilon J(\psi,\nabla^2\psi) = \nu\nabla^4\psi$$

where

$$\psi(x,y) = \int^{y}(\bar{u}(y)-c)\,dy + \varepsilon\,\psi(x,y)$$

ε being the nonlinear parameter (a measure of the amplitude of the perturbation, ν an inverse Reynolds number, and $\bar{u}(y)$ a mean zonal flow. The C.L. is defined at $y = 0$, where $\bar{u}(0) = c$. These equations are similar to (2.4) and (2.5), except for the beta term which is absent here, and the viscous term. The addition of the beta term does not

change qualitatively the results, as long as $\beta - (u_{yy})_c \neq 0$, which is the case here, at the C.L. Benney and Bergeron defined the parameter

$$\lambda = \frac{\nu}{\varepsilon^{3/2}}$$

which is a measure of the effect of the viscosity versus that of the nonlinearities. For $\lambda \gg 1$, one recovers the results of the linear "viscous" problem, as the viscous terms are used in the critical layer to resolve the critical level singularity. For $\lambda \ll 1$, one uses the nonlinear Jacobian to resolve the singularity. This is the case treated by Benney and Bergeron, and Davis. The viscous terms will still be used however, but not in the primary balance. This is what is meant by "nonlinear" critical layer.

Using the method of matched asymptotic expansions, they obtained the following interesting results. There is no phase shift in the ln y term of the Tollmien solutions. That is, for $y<0$, $\ln y = \ln |y|$ and $A^+ = A^-$, $B^+ = B^-$. This leads in turn to the absence of any jump in $\overline{u'v'}$ across the C.L. In particular, if it is 0 for $y<0$, then it is also 0 for $y>0$; in the case where one is forcing a wave at $y = y_0 \gg 0$, this implies a total reflection at the C.L. (versus the absorption that resulted in the previous analysis). They also found that the mean flow had an $0(\varepsilon)$ distortion, or, equivalently, that the zero of the mean flow is moved at most by a distance of $0(\varepsilon)$. In the critical layer itself, the harmonics are $0(\varepsilon^{1/2})$ smaller than the fundamental, while they are $0(\varepsilon)$ smaller outside.

Haberman solved a very similar type of problem, allowing the parameter λ to cover a wider range of values. He retrieved most of Benney and Bergeron's results for the case $\lambda \ll 1$, and found that as λ is increased to values $\gg 1$, the linear viscous results are recovered. That is the ln y phase shift goes from 0 to $-i\pi$ as λ goes from values $\ll 1$ to values $\gg 1$. The Reynolds stress behaves accordingly.

Summarizing the above results, the nonlinear steady problem is characterized by the following conclusions:

1) there is no phase shift in the ln y term.
2) there is no jump in the Reynolds stress.
3) the mean flow distortion is $O(\varepsilon)$, the width of the critical layer is $O(\varepsilon^{1/2})$, and the amplitude of the harmonics in the critical layer is $O(\varepsilon^{1/2})$ smaller than that of the fundamental.

3.4 PREVIOUS NUMERICAL STUDIES

A number of numerical experiments were undertaken in order to study the time-dependent Rossby wave critical level problem. Some of the most important results will now be discussed.

3.4.1 LINEAR PROBLEM

Bennett and Young (1971) did a numerical integration of the linearized barotropic vorticity equation in time, using a linear wind profile and a forced wave at a northern boundary. Their intention was to study the propagation of planetary waves in the presence of a critical level. This situation is usually encountered in the tropics, where planetary

waves propagating southward from the temperate latitudes usually meet easterlies; if their phase speed is such that it matches the speed of the mean wind, they encounter a C.L. Their results agree with those of Dickinson (1970). They reach a quasi-steady-state, in which the wave transports zonal momentum northward, which, according to Eliassen and Palm (1961) is indicative of a southward energy transport. South of the C.L., the wave momentum flux is very small, and they conclude that "the wave-mean flow interaction represents an absorption of wave energy".

3.4.2 QUASILINEAR PROBLEM

Geisler and Dickinson (1974) took a further step ahead and considered the following "quasilinear" model:

$$\left(\frac{\partial}{\partial t}+\bar{u}\frac{\partial}{\partial x}\right)\left(\Psi_{xx}+\Psi_{yy}\right)+\left(\beta-\bar{u}_{yy}\right)\Psi_{x}=S(y,t)$$

$$\frac{\partial \bar{u}}{\partial t}=-\frac{\partial}{\partial y}\left(\overline{u'v'}\right)$$

where S is a vorticity source north of the C.L., and $\bar{u} = u_m \tanh(y/L)$ at $t = 0$, and $\Psi(x,y,t) = \mathrm{Re}\{\phi(y,t)e^{ikx}\}$. In other words, they allow the resulting forced wave to interact with itself to modify $\bar{u}$, while neglecting any self-interaction which would lead to the excitation of harmonics. They found that after the switch-on of the vorticity source far north of the C.L., a ledge develops in the mean flow profile, and the C.L. moves northward until $\beta - \bar{u}_{yy}$ (>0 at initial time) becomes negative; at that point, the C.L. stops its northward migration, and starts moving southward until $\beta - \bar{u}_{yy}$ changes sign again, and the process is repeated again, until eventually a steady-state is reached,

in which $\beta - \bar{u}_{yy} = 0$ at the C.L., the profile having a well defined ledge, and the C.L. being situated somewhat north of its initial position. This oscillation of $\beta - \bar{u}_{yy}$ is well correlated with an oscillation in the wave momentum flux $\overline{u'v'}$, which is positive when $\beta - \bar{u}_{yy}$ is positive, and negative in the other case. $\overline{u'v'}$ eventually decays to zero north of the C.L. (it is always zero south of the C.L.), indicating the presence of a reflected wave at the C.L. which transports as much energy northward as the forced wave does southward. The whole process is found to depend on a few critical parameters. The time required to set up the critical layer is controlled by the parameter

$$t_c = \frac{\beta - \bar{u}_{yy}}{k \bar{u}_y^2}$$

The longer the wavelength, and the smaller the shear, at initial time, the longer it takes to initiate the process. They also found that the steady-state deformation of the mean flow was proportional to the strength of the source, and to t_c.

We shall now discuss in more detail these results. One of the steady-state features is that $\beta - \bar{u}_{yy} = 0$ at the C.L. What does this imply? Since we are in the steady-state, we can use the results of 3.1, and set $\beta - \bar{u}_{yy}$ to 0 in the Tollmien-Kuo solutions. It is easy to check that apart from changing the values of the coefficients a_n, b_n, and c_n, this has the important result of eliminating the "ln y" term from the ϕ_b solution. Therefore there is no phase shift problem, and since the Reynolds stress, as before, remains constant above and below the C.L., with $A^+ = A^-$ and $B^+ = B^-$, the jump disappears. Since

$\overline{u'v'}$ is 0 under the C.L., at the steady-state, it is also 0 everywhere. Thus Geisler and Dickinson's result is not surprising: the singularity has been removed by the fact that $\beta - \bar{u}_{yy} = 0$ where $\bar{u} = 0$. In a way, there is no longer a "critical level problem". We recall that Benney and Bergeron also had $\overline{u'v'} = 0$ everywhere; however, and this is the interesting part, their profile had $(\bar{u}_{yy})_c \neq 0$ (in their problem, it is equivalent to $(\beta - \bar{u}_{yy})_c \neq 0$). So even though an identical result is obtained (at least for $\overline{u'v'}$), the mean flow configuration seems to be different . We have to point out here that Benney and Bergeron get a mean flow distortion term, which must be added to the original profile. It is possible that when it is taken into account to evaluate $\bar{u}_{yy}$, the result is also zero like in Geisler and Dickinson's analysis. Yet, even then, one would have to account for the presence in the critical layer of all the harmonics, which, as mentioned before, are an essential result of Benney and Bergeron's analysis, while they are altogether absent in Geisler and Dickinson's model. According to Warn and Warn (1976), this seems to be hard to justify. In fact, they have shown that for $t = O(\varepsilon^{-1/2})$, the nonlinear Jacobian becomes of O(1) (in the critical layer), and therefore it is not permitted to neglect it as Geisler and Dickinson did, if one wants to make consistent approximations.

All these considerations very naturally lead us to the next step, which is to perform a fully nonlinear integration, and hopefully resolve this dilemma. In other words, is $\beta - \bar{u}_{yy}$ effectively reduced to 0 in

the steady-state, even in the fully nonlinear problem? And then, is it possible to reach a steady-state similar to the one obtained by Benney and Bergeron? Or is the steady-state similar to Geisler and Dickinson's? Answers to these questions will be found in the following pages. Before discussing our model results, we shall however review an attempt that was made to solve the nonlinear problem numerically.

3.4.3 NONLINEAR PROBLEM

Ward (1974) attempted to solve numerically the nonlinear time-dependent problem. His model equations are similar to ours. He adopted a linear wind profile. In his thesis, he describes, among other results, two types of nonlinear integrations. In the first one, one wave is forced, and the other higher harmonics are allowed to develop through nonlinear interactions with the forced wave. In the other, two waves are forced, and again higher harmonics are allowed to develop. In both types, $\frac{\partial \bar{u}}{\partial t}$ is either set to zero or allowed to change.

Before we go on discussing his results, a few remarks should be made. The nonlinear amplitude parameter he uses has a value of 0.32, so that $\varepsilon^{1/2} = 0.56$. Now recall that the width of the critical layer is of $O(\varepsilon^{1/2})$. The implications are that: (1) the model is presumably nonlinear everywhere, because of such a big value of ε, and thus the problem is altogether different from that treated by Benney and Bergeron, where nonlinearities are important only in the critical layer, and (2), since his domain extends from $y = 1.6$ to $y = -1.6$, we conclude that

the critical layer boundary is dangerously close to the walls, so that the possibility of contamination from the southern computational boundary is very real. The numerical model itself, in our opinion, is not well suited for such a study: the resolution (Δy = 250 km) is much too coarse to resolve the fine details of the nonlinear interactions in the critical layer, the Jacobian is neither energy-preserving or enstrophy-preserving, and finally, the southern boundary is a solid wall. It is thus not surprising that his integrations never exceed 6 or 8 days, and even at that time, the results should be treated with caution.

For the first type of integrations, he observes the following: in the case where $\frac{\partial \bar{u}}{\partial t} = 0$, $\overline{u'v'}$ drops to zero after 6 days; the nonlinear amplitudes exceed the linear amplitudes by a factor of 2 or 3 in the evanescent region (south of the C.L.). As we shall see later, we got an altogether different result. For the case where $\frac{\partial \bar{u}}{\partial t} \neq 0$, up to 6 days, the integration proceeds as in the quasilinear case. This is not surprising, as it takes some time for the nonlinear terms to start modifying the results. In the second type of integrations, the model is obviously nonlinear everywhere. The case $\frac{\partial \bar{u}}{\partial t} \neq 0$ yields the following results: there is a northward migration of the C.L., but without any ledge formation in the mean wind profile; in other words, there is no tendency for the mean flow to develop a curvature such as to drive $\beta - \bar{u}_{yy}$ to zero at the C.L. He also observes a greater penetration of wave energy south of the C.L. After 6 days, however, the integration starts diverging, and again, no steady-state is reached. We shall see later that our results disagree with his.

Summing up the preceding considerations, we see that the nonlinear time-dependent problem is still unsolved analytically, and that the only numerical approach to it does not give satisfactory answers, due in part to the crudeness of the model, and also to the fact that only the very early transient development was studied, and for a very limited choice of parameters (in fact, only one set). In the text to follow, we intend to do a thorough examination of the problem, exploring the full range of parameters involved, and integrating until some steady-state is reached (at least in the outer solution, i.e., away from the C.L.). To achieve this goal, great care was given to the finite difference version of the governing equations; this we will now describe, before going on to discuss the results themselves.

CHAPTER 4. THE NUMERICAL MODEL

In order to be able to integrate the model equations on a computer, they have to be approximated by a corresponding set of finite difference equations. It is well-known that finite difference equations have solutions of their own, which may (or may not) bear any resemblance with the analytical solutions they are supposed to approximate. And if, as in our case, the analytical equations possess regions of rapid variation, one has to be extremely careful in the choice of a numerical scheme. We will now describe the choices we made, and reasons supporting these choices.

4.1 SPATIAL DIFFERENCING

The domain of integration can be thought of as a channel encircling the earth; the northern boundary, situated at $y = y_0 > 0$, consists of a wavy wall, along which flows a westerly current. This current has a north-south shear (of hyperbolic tangent type), and somewhere between the southern boundary and the northern boundary, the speed goes to zero: this will be referred to as the C.L. Further south, the flow is easterly, until the "radiation" boundary is reached. Waves impingent on this boundary are allowed to pass through, without any reflections, as long as the flow remains essentially linear. What happens during the integration is as follows: as the flow goes along the northern boundary, steady waves ($c = 0$) are generated; these waves propagate

southward until they reach the zero wind line, that is, their C.L. There an interaction takes place, which we want to study. What goes through the C.L. eventually reaches the radiation boundary and simply escapes outside. Since the waves are in an evanescent regime south of the C.L., their amplitudes are very small when they reach this point, and the assumption that they can be treated linearly was always well verified.

Free modes can also be generated at switch-on time. However, it can be shown (Warn, private communication) that for the particular configuration chosen, the only allowed modes are a set for which $c < -1 - \beta/\delta$, with $\delta < 0.5$. Thus, these modes are regular (they do not have a C.L.), and neutral. Since many of the experiments were done with $\delta = 0.16$, they were not excluded by this criterion. However, inspection of the results seems to indicate that no such free modes were present, or, if they were, that their amplitude was small enough to be unnoticeable.

As mentioned before, the x-derivatives are evaluated exactly (apart from the fact that only a limited number of waves can be carried). Grid points are used to evaluate the y-derivatives. The choice of a grid length was done in the following way: a set of nonlinear integrations were done, until eventually halfing the gridlength did not produce any important change in the results up to a given integration time. This yielded the following choice:

$$\Delta y = 0.00625 \qquad (6.25 \text{ km})$$

As we shall see later, such a fine grid length is needed if one wants to integrate long enough to reach a nonlinear steady-state. The width of the channel was chosen to represent roughly the propagation of a wave from the temperate latitudes to the equator; this in turn yielded a choice of 601 grid points. The C.L. was positioned at n = 201, that is, 401 grid points south of the forcing. Again, it was checked that the distance between the forcing boundary and the C.L. did not affect significantly the critical level development. We doubled the distance from the C.L. to the forcing boundary: the wave structure (amplitude and phase) remained almost unchanged in the corresponding or overlapping parts of the domain. A small delay was introduced because it took longer for the wave to reach the C.L. Otherwise, everything else proceeded in a similar fashion. Fig.4.1 shows the mean wind profile, and the domain configuration.

Most of the y-derivatives were of $O(\Delta y^2)$ accuracy. That is :

$$f_y = \frac{\partial f}{\partial y} = \frac{f(y+\Delta y) - f(y-\Delta y)}{2\Delta y} + O(\Delta y^2)$$

$$f_{yy} = \frac{\partial^2 f}{\partial y^2} = \frac{f(y+\Delta y) + f(y-\Delta y) - 2f(y)}{\Delta y^2} + O(\Delta y^2)$$

The $\bar{u}_{yy}$ term was evaluated with a fourth-order scheme, and so were the perturbation vorticities in some cases.

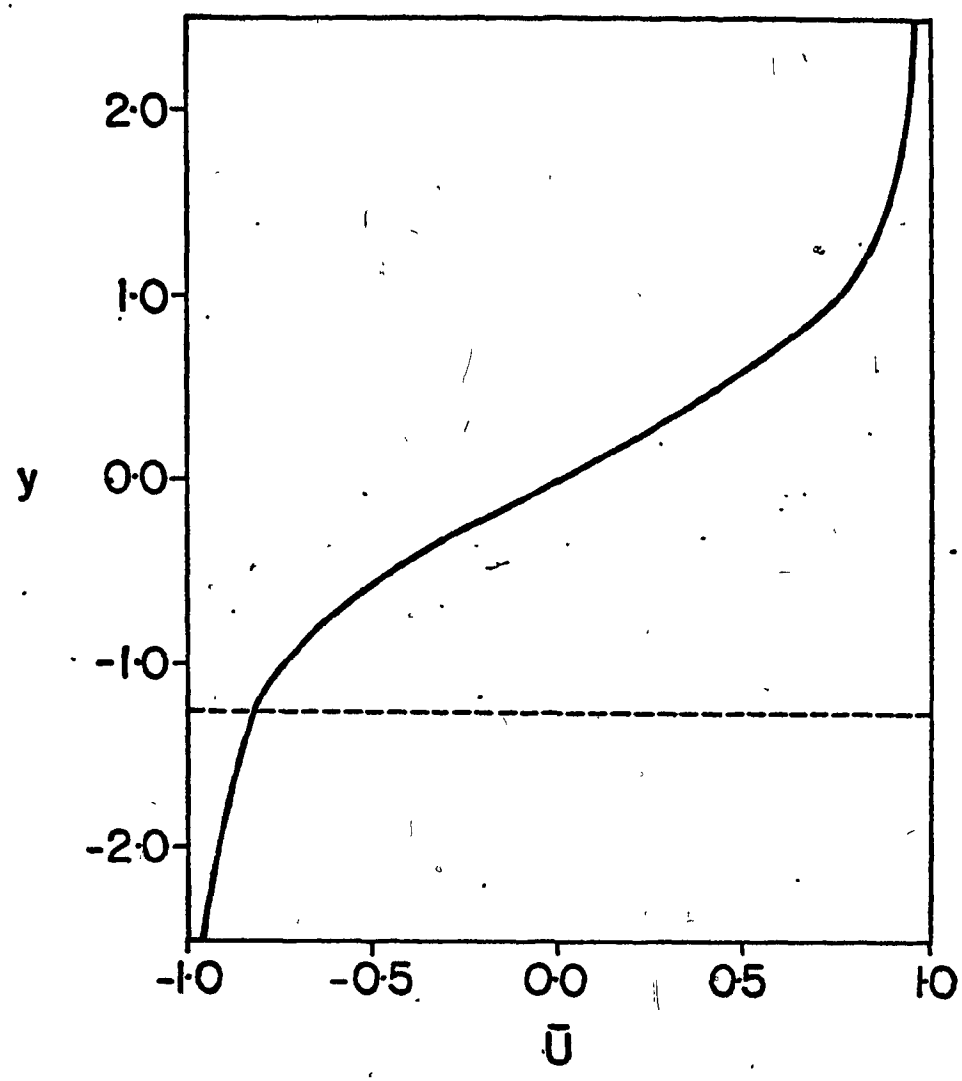

Fig. 4.1 - Hyperbolic tangent shear flow profile in dimensionless units. Wave source is at y=2.5. Dashed line represents southern boundary of fine mesh ($\Delta y=0.00625$) integration.

$$(f_{yy})_{final} = f_{yy} - \frac{\Delta y^2}{12}(f_{yy})_{yy} + O(\Delta y^4)$$

However, we found that with such a small Δy, the improvement in accuracy was not worth the extra amount of computing time required for a fourth-order scheme. A fourth-order scheme would in fact probably be more useful for the nonlinear Jacobian.

At the two boundaries, i.e. n = 1 and n = 601, these formulas cannot be used. This is one of the problems created by the use of finite difference equations: how does one evaluate $\frac{\partial f}{\partial y}$ or $\frac{\partial^2 f}{\partial y^2}$ at the boundaries? There is, as yet, no exact way to solve the problem. Several approximations exist, either in the form of an off-centered scheme, or in the form of an extrapolation formula. The off-centered schemes considered were the following :

$$f_y = \pm \frac{[f(y \pm \Delta y) - f(y)]}{\Delta y} + O(\Delta y)$$

$$f_y = \mp \frac{[3f(y) - 4f(y \pm \Delta y) + f(y \pm 2\Delta y)]}{2\Delta y} + O(\Delta y^2)$$

$$f_{yy} = \frac{[f(y) + f(y \pm 2\Delta y) - 2f(y \pm \Delta y)]}{\Delta y^2} + O(\Delta y)$$

$$f_{yy} = \frac{[2f(y) - 5f(y \pm \Delta y) + 4f(y \pm 2\Delta y) - f(y \pm 3\Delta y)]}{\Delta y^2} + O(\Delta y^2)$$

The extrapolation formulas considered were the following:

$$F_1 = F_2$$

$$F_1 = 2F_2 - F_3 \qquad \text{(linear)}$$

$$F_1 = F_4 - 3F_3 + 3F_2 \qquad \text{(quadratic)}$$

The following quantities have to be evaluated at either one or the two boundaries: $(A_n)_y$, $(B_n)_y$, $(A_n)_{yy}$, $(B_n)_{yy}$ and $\bar{u}$. In order to choose the best possible scheme at the southern boundary, the following experiment was performed: a nonlinear integration was done with the southern boundary 200 grid points from the C.L., and another with the same boundary displaced 400 grid points from the C.L. Since a radiation condition is used in both, we assumed that the results obtained from the second integration, at a point situated 200 grid points from the C.L. were true, and we adjusted the B.C.'s of the first integration so as to yield a similar result. This showed that the best choice was:

$$\bar{v}_1 = \bar{v}_2$$

$$[(A_m)_{yy}]_1 = [(A_m)_{yy}]_2$$

$$[(B_m)_{yy}]_1 = [(B_m)_{yy}]_2$$

That is we assumed the values of $\bar{u}$ and the values of the perturbation vorticity at the boundary to equal their respective values at the first interior point. $(A_n)_y$ and $(B_n)_y$ were given by the off-centered second order scheme (this derivative has to be evaluated in the

radiation condition). At the northern boundary the choice is more arbitrary; since we are forcing a wave at this boundary however, the consequences are in a way less important. In any case, we chose a second-order off-centered scheme for $(A_n)_{yy}$ and $(B_n)_{yy}$.

4.2 TIME DIFFERENCING

Five different schemes were tested with the model. They are the following:

1) Matsuno's simulated backward difference method.

$$f_*(t+\Delta t) - f(t) = \frac{\partial f}{\partial t}\Big|_t \Delta t$$

$$f(t+\Delta t) - f(t) = \frac{\partial f}{\partial t}\Big|_{t+\Delta t} \Delta t$$

where a "*" denotes a tentative (first guess) value.

2) Leapfrog method

$$f(t+\Delta t) = f(t-\Delta t) + 2\Delta t \frac{\partial f}{\partial t}$$

3) Adams-Bashforth method

$$f(t+\Delta t) = f(t) + \left(\frac{3}{2}\frac{\partial f}{\partial t}\Big|_t - \frac{1}{2}\frac{\partial f}{\partial t}\Big|_{t-\Delta t}\right)\Delta t \qquad (4.1)$$

4) Adams-Moulton method.

$$f(t+\Delta t) = f(t) + \frac{1}{2}\left(\frac{\partial f}{\partial t}\Big|_t + \frac{\partial f}{\partial t}\Big|_{t+\Delta t}\right)\Delta t \qquad (4.2)$$

where $\frac{\partial f}{\partial t}\Big|_{t+\Delta t}$ is obtained by using scheme (3), for example.

(5) Lorenz' scheme

$$f_*(t+\Delta t) = f(t) + \frac{\partial f}{\partial t}\Big|_t \Delta t$$

$$f(t+\Delta t) = f(t) + \frac{1}{2}\left(\frac{\partial f}{\partial t}\Big|_t + \frac{\partial f}{\partial t}\Big|_{t+\Delta t}\right)\Delta t$$

For linear and quasilinear integrations, all these schemes worked well, except possibly for scheme 1, which required the use of a much smaller time step (by a factor of 3 or 4); even then some damping is present. This was recognized by Matsuno (1966), who in fact does not recommend use of his scheme for long term integrations, which is our case. For nonlinear integrations, scheme 1 fails completely, as the model becomes unstable, even with a very small time step. Scheme 2 has the advantage, with scheme 3, of being a one step method. It has, however, the undesirable effect of time-splitting (one of the two numerical solutions changes sign every time step). This can be corrected by the use of time filter, first designed by Robert (1966) and later analysed by Asselin (1972). With a value for the filter parameter of 0.002, the integration behaved quite well, and the results were quite similar to those of the other 3 schemes, even after 2400 time steps, which was the usual length of the integration period (with $\Delta t = 0.036$). Scheme 3 was highly recommended by Lilly (1965), as he found it was the best overall scheme he tested: it allows a time step comparable to that of the leapfrog scheme, has no time-splitting, and a very small amplification term. As shown by Henrici (1962, 1964), it can be

used in conjunction with scheme 4, as in the case of a multi-step method: scheme 3 is then used as a predictor, and scheme 4 as a corrector. One can then iterate, and reduce the numerical error to a pre-specified value. This was the scheme adopted by Dietrich (1973); he found it to give very precise results. This is the scheme we finally chose to adopt. It was found that one iteration only was necessary for convergence. The time step, as mentioned before was $\Delta t = 0.036$. Let us note finally that scheme 5 is really a slightly modified version of scheme 4, since it differs only in the predictor. When tested, it yielded results which were similar(to 1%) to scheme 4.

4.3 THE POISSON EQUATION

The two predictive equations for A_n and B_n are of the non-homogenous Poisson type. Defining $\phi(y,t) = \frac{\partial A_n}{\partial t}$ or $\frac{\partial B_n}{\partial t}$, and letting the right hand side of equations (2.11) and (2.12) equal some function F(y,t), we can rewrite (2.11) and (2.12) in the form:

$$\phi_{yy} - n^2\phi = F(y,t) \qquad (4.3)$$

F(y,t) is a known function of y and t; the problem is then to solve for the perturbation stream function tendency. Once $\phi(y,t)$ is known, (4.1) and (4.2) are used to advance one step in time, and the whole process is repeated again. There are many schemes available to solve such an equation. We chose the so-called "direct" method, because of

its simplicity and speed. First, a particular solution is sought for the finite difference version of (4.3); the grid points are numbered from m = 1 to m = M, and (4.3) is written as

$$\phi^p_{m+1} + \phi^p_{m-1} - (2+m^2\delta\Delta y^2)\phi^p_m = F_m\Delta y^2 = c_m \qquad (4.4)$$

where superscript "p" denotes the particular solution. Using arbitrary "guess" values for ϕ^p_{m-1} and ϕ^p_m, ϕ^p_{m+1} is calculated, and the process is repeated until ϕ^p_M is obtained. A few things should be said about this particular solution: first, it can be shown that it grows roughly like m^2; to see this, let $n^2\delta\Delta y^2 \ll 2$ (in our model, for n=6, and the values quoted before, $n^2\delta\Delta y^2 \sim O(10^{-4})$); then, by an iteration procedure, it can be shown that

$$\phi^p_m \simeq \sum_{\ell=2}^{\ell=m-1} (m-\ell)c_\ell + (m-1)\phi_2 - (m-2)\phi_1$$

In particular, if we let $c_\ell = c$, a constant, and $\phi_2 = \phi_1 = \phi$, then, for $m \gg 1$,

$$\phi^p_m \simeq \frac{m^2}{2}\, c + \phi$$

In second place, associated with the finite-differencing, there is a round-off error; this round-off error, because of the marching process eventually grows sufficiently to contaminate the result (it grows also like m^2). So some care must be taken to eliminate this source of error. We will come back to this later. Finally, we should mention that the guess values used during the integration were the values of the streamfunction tendency at the previous time step, thus forcing the particular solution to be quite near the true solution. The

homogeneous solution to (4.4) is obtained by substituting $\phi_m^h = e^{rm}$ (where the superscript "h" now stands for homogeneous). We obtain the basic solution:

$$\phi_m^h = D_1 e^{\alpha m} + D_2 e^{\beta m} \qquad (4.5)$$

where:

$$\alpha = \ln \frac{(2 + m^2\delta\Delta y^2) + \sqrt{(2+m^2\delta\Delta y^2)^2 - 4}}{2}$$

$$\beta = \ln \frac{(2 + m^2\delta\Delta y^2) - \sqrt{(2+m^2\delta\Delta y^2)^2 - 4}}{2}$$

It is easily shown that in the limit as $\Delta y \to 0$, and $n^2\delta \ll 1$, $\alpha \cong m\delta^{\frac{1}{2}}\Delta y$, $\beta \cong -n\delta^{\frac{1}{2}}\Delta y$, that is, we recover the analytic homogeneous solution (since $(m-1)\Delta y = y$). The solution is redefined in terms of the following parameters: let $\lambda = \frac{\alpha+\beta}{2}$, $r = \frac{\alpha-\beta}{2}$, and make the substitution m = m-M; then, (4.5) becomes

$$\phi_m^h = D_1(e^{(\lambda + r)(m-M)}) + D_2 (\sinh r(m-M)\, e^{\lambda(m-M)}) \qquad (4.6)$$

The constant D_1 is easily evaluated in the following manner: at the northern boundary, the stream function tendency is specified and

equal to, say, F; we then get

$$\phi_M = \phi_M^p + \phi_M^h = D_1 + \phi_M^p = F$$

$$D_1 = F - \phi_M^p$$

The constant D_2 is obtained by using the radiation condition (2.18). However, since $\frac{\partial A_n}{\partial t}$ and $\frac{\partial B_n}{\partial t}$ are coupled in (2.18.a) and (2.18.b), a little algebra is necessary in order to get D_2. This is done in Appendix C. Once D_1 and D_2 are known, the total solution is simply written

$$\phi_m = \phi_m^p + \phi_m^h$$

This solution now has to be corrected for round-off error, which, however small, might eventually contaminate the integration after a few thousand time steps. We shall use a method developed by Dietrich (private communication) : we back-substitute ϕ_m into (4.4), and evaluate the corresponding c_m, which can now be written as $c_m + \varepsilon_m$, where c_m is the exact original right hand side, and ε_m corresponds to the error introduced in the forcing field evaluated using our solution ϕ_m. Once ε_m is known, a new particular solution χ_m^p is calculated for the forcing field "$-\varepsilon_m$". Since the solution ϕ_M is exact, we use a guess value of 0 for χ_M^p and χ_{M-1}^p, and we repeat the marching procedure described before to get χ_1^p. The homogeneous "error" solution χ_m^h is of the same type as (4.6):

$$\chi_m^h = D_3 \left[e^{(\lambda + r)(m-M)} \right] + D_4 \left[\sinh r(m-M) e^{\lambda(m-M)} \right] \qquad (4.7)$$

Again, D_3 is easily evaluated, using the fact that Φ_M is exact, so that we get $\mathcal{I}_M^h = 0$; this gives $D_3 = 0$; D_4 is evaluated using the radiation condition (see Appendix C). The complete solution is then given by

$$\Phi_m = \phi_m + \mathcal{I}_m$$

The procedure can be repeated any number of times, until a prescribed error limit is reached. In our integrations, one error scan was found to be sufficient for convergence. Let us mention finally that the scheme was tested up to wave number 24 ($\delta = 23.04$), with 601 grid points, for a 2400 time step integration. The solution was well-behaved, and when compared with the results of the linear theory, was found to be very precise.

4.4 THE FORCING

Unless otherwise specified, the following procedure was adopted for the switch-on: at m=M, or $y=(M-1)\Delta y=y_0$, the streamfunction tendency was specified. We rewrite (2.6) in the following way:

$$\Psi_0'(x,y,t,) = \alpha_n(y,t) \cos (nx - \beta_n(y,t)) \qquad (4.8)$$

where:

$$\alpha_n(y,t) = \sqrt{A_n^2(y,t) + B_n^2(y,t)}$$

$$\beta_n(y,t) = \tan^{-1}(A_n(y,t)/B_n(y,t)).$$

We choose $\alpha_1(y_0,t) = 1, \alpha_n(y_0,t) = 0$ for $n > 1$, and $\beta_1(y_0,t) = \pi/4$.

The unit amplitude for $\alpha_1(y_0,t)$ was achieved in a certain lapse of time, usually 96 Δt. The above two considerations completely determine $\frac{\partial A_n}{\partial t}$ and $\frac{\partial B_n}{\partial t}$ at $y = (M-1)\Delta y$.

More formally, we have :

$$N \geq n > 1; \quad t > 0; \quad \frac{\partial A_n}{\partial t} = 0 \quad ; \quad \frac{\partial B_n}{\partial t} = 0$$

$$n=1 \; ; \quad 0 < t \leq 96\,\Delta t; \quad \frac{\partial A_n}{\partial t} = 1/(96\,\Delta t\,\sqrt{2}) \; ; \quad \frac{\partial B_n}{\partial t} = 1/(96\Delta t\,\sqrt{2})$$

$$n > 0; \quad t > 96\,\Delta t; \quad \frac{\partial A_n}{\partial t} = 0 \; ; \quad \frac{\partial B_n}{\partial t} = 0$$

The reason behind the slow switch-on is to prevent the buildup of a large gradient in the wave momentum flux near the forcing boundary. This gradient, if allowed to become important, deforms the mean flow considerably, and the characteristics of the initial wind profile are changed significantly. In fact, after a certain number of experiments, we found out that the best procedure was to let the integration be linear during the switch-on, allowing the fundamental harmonic to build up slowly throughout the channel without affecting the mean flow, and only then allowing the integration to be quasilinear or nonlinear. It was verified that the results did not depend on the switch-on procedure as such. As long as the switch-on time is large enough to prevent the wave momentum flux from affecting the mean flow next to the forcing boundary, the results are quite insensitive to the following manipulations: doubling or quadrupling the switch-on time only delays the linear stage of the critical layer build-up, without affecting the nonlinear stage very much; letting $\bar{u}$ be constant (in time) in the upper

200 grid points leaves the results essentially unchanged, as the mean flow deformation there is always $O(10^{-4})$ or less; letting the integration be nonlinear during switch-on time did produce a slight deformation of the mean flow near the forcing boundary; however, for values of $\varepsilon<0.1$, this deformation was eventually smoothed out, and the results were not affected significantly.

This therefore completes the description of the numerical model. Before going on to describe the results of nonlinear integrations, we will briefly comment on a set of linear integrations, designed to test the coding, and compare them with the analytical results available, in order to check the accuracy of the finite difference equations (at least, the linear part of it).

CHAPTER 5. LINEAR INTEGRATIONS

5.1 STANDARD INTEGRATION

In order to check the coding, a standard integration was performed, the results of which were compared with Dickinson's (1970) analysis. The wind profile is somewhat different, since he used a linear wind profile, versus our hyperbolic tangent profile. However, in the critical layer region, both profiles have a more or less linear shear, and as will be seen, the results, at least qualitatively, do not seem to be affected at all by this fact. He also made a long wave approximation (that is, he neglected the x-part of the Laplacian), while we kept this term. Since $\delta = 0.16$, this term is small, and again, its presence does not lead to different results.

One result predicted by Dickinson is that the width of the critical layer should decrease as t^{-1}. Fig. 5.1 gives a plot of the width as a function of time. It can be seen to effectively decrease as t^{-1}. The width of the critical layer was estimated from the momentum flux divergence at the C.L. We measured the distance required for $\overline{u'v'}$ to decrease by 2 orders of magnitude across the C.L., from the linear steady-state value north of the C.L., to its value south of the C.L. ($\overline{u'v'} = 0$ for $y < 0$).

Another result is that the perturbation zonal wind u' should increase as ln t at the C.L. (Warn and Warn (1976). Fig. 5.2 gives a plot of u' at three points : $y = \pm 0.025$, and $y = 0$. At the C.L., it effectively increases like ln t (notice the logarithmic scale); away from the C.L., it starts increasing until eventually the critical

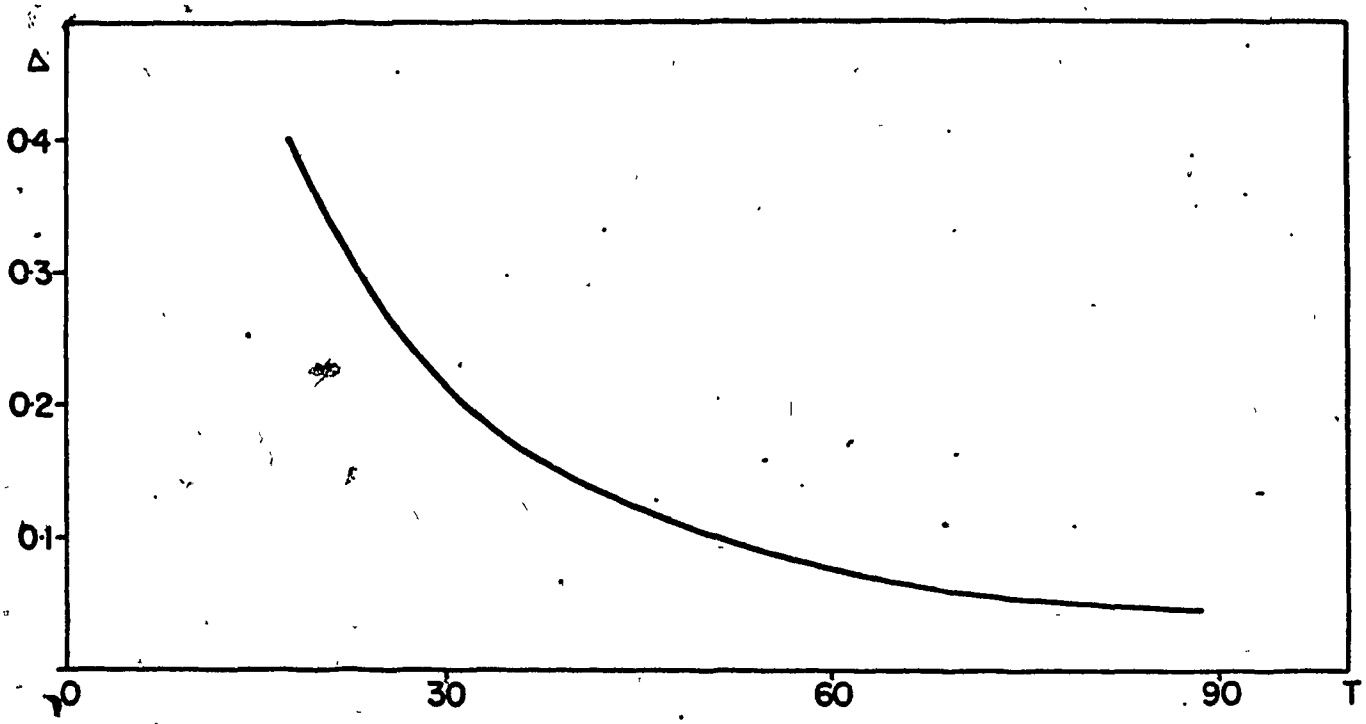

Fig. 5.1 - Width of critical layer as a function of time, as measured from Reynolds stress jump in linear integration; $\beta = 1.6$, $\delta = 0.16$.

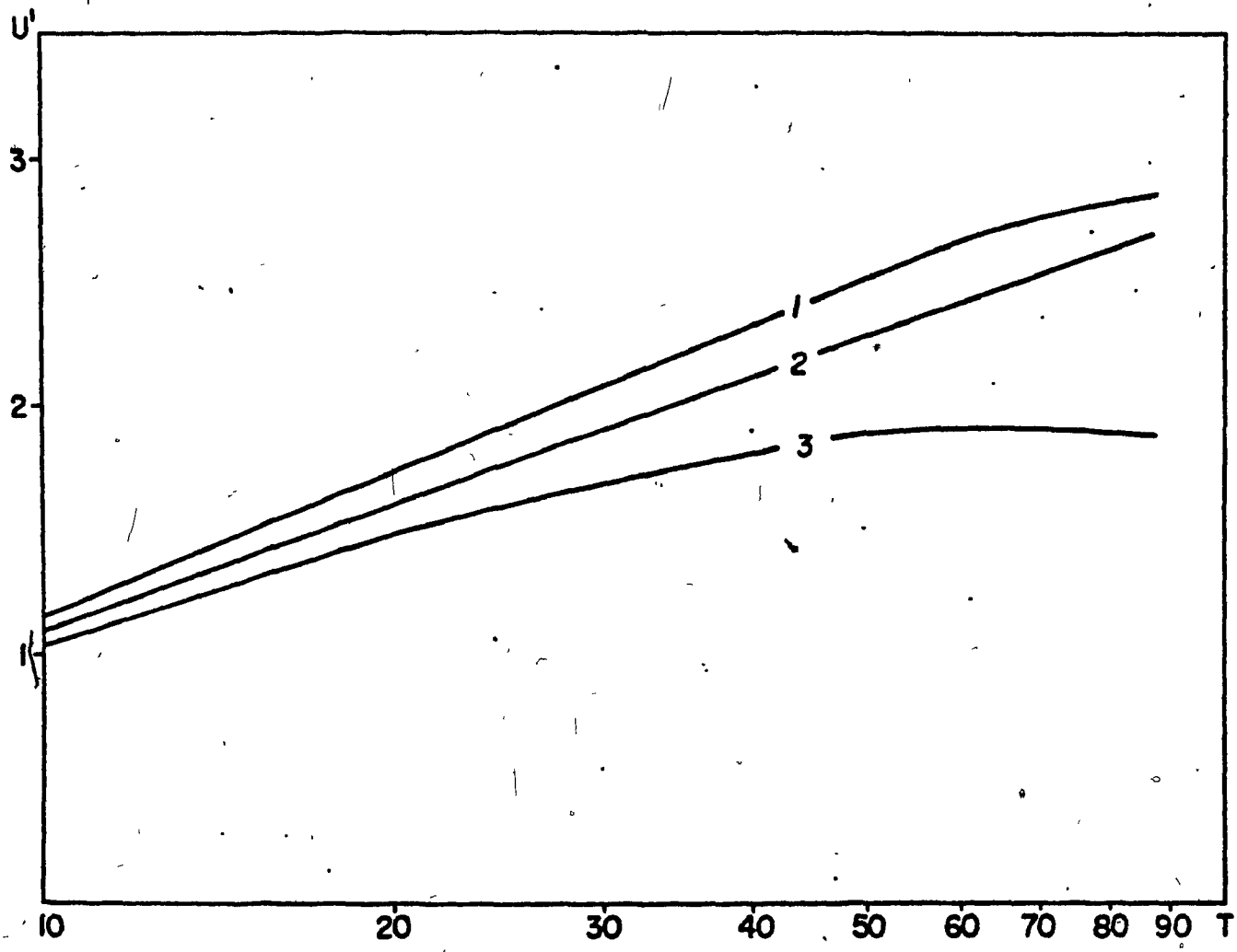

Fig. 5.2 - Perturbation zonal wind as a function of time in linear integration; 1. y=0.025, 2. y=0.0, 3. y=-0.025.

layer thickness is such that the 2 points $y = \pm 0.025$ are outside of the critical layer: the growth then stops, and u' thereafter oscillates in time around some constant value (this is not shown on the graph).

According to Dickinson's results, a jump should develop in time for $\overline{u'v'}$. Since there are no energy sources south of the C.L., it vanishes for $y < 0$; north of the C.L., it should reach a steady-state value, depending only on the wave amplitude and phase at the forcing level (all other parameters being held constant). Fig. 6.1 gives a plot of $\overline{u'v'}$ at a point situated just below the forcing, while Fig. 6.2 gives a similar plot for a point situated below the C.L. It is seen that the numerical result reproduces almost exactly the analytical result. In particular, one should note the presence of small decaying oscillations around the steady-state values; they are due to the presence of transients generated by the switch-on. As we have seen earlier, they also appear in Dickinson's solution as terms of the form e^{iyt}/yt^2. That is, at a fixed y, there is a decaying oscillation in time of frequency y. This is the reason why the oscillations have a higher frequency in Fig. 6.1 than in Fig. 6.2; the point above the C.L. is situated at a value of $y = 2.4$, while the point below is at $y = -0.625$ (the forcing is at $y = 2.5$). If one looks at $\overline{u'v'}$ at a given time, as a function of y instead (see Fig. 6.3.a for example) one sees the jump across the C.L., and also small oscillations in y, superimposed on a constant value. The oscillations have a wavenumber t, and their amplitude also decays as y^{-1}. (This is not apparent in

fig. 6.3.a , since the profile shown is for a nonlinear integration, and at that time, the configuration has already started to depart from that of the linear stage. The preceding remarks were however verified for linear integrations). That is, as one moves away from the C.L., the profile becomes less wavy, and as time increases, the oscillations develop shorter and shorter wavelengths.

So far, however, these are only qualitative comparisons. It is possible to get a measure of the accuracy of the model by evaluating the logarithmic phase shift (we recall that one of the features of Dickinson's solution as $t \to \infty$ is to exhibit a $-\pi$ phase shift in the ln y term). Writing

$$\ln y = \ln|y| - i\theta, \quad y < 0$$

where now $\theta = \theta(t)$ since we have a time-dependent problem, it is possible to evaluate, with a certain precision, this phase shift from the numerical results. This is done in the following way. Using Warn and Warn's results, we write

$$\phi(y,t) = \phi(y,\infty) + O(1/yt^2) \tag{5.1}$$

where $\phi(y,\infty)$ are essentially the Tollmien-Kuo solutions, corresponding to the steady-state inviscid problem, that is:

$$\phi(y,\infty) = A\phi_a + B\phi_b \tag{5.2}$$

From the numerical model, we also have that (see (4.8))

$$\phi(y,t) = \alpha(y,t,)e^{-i\beta(y,t)} \tag{5.3}$$

where $\alpha(y,t)$ and $\beta(y,t)$ respectively refer to the amplitude and phase of the wave as given by the numerical integration. Equating (5.1) and (5.3), and neglecting the $O(1/yt^2)$ term, we then obtain a relationship between A, B and the numerical solution. Letting the symbols "+" and "-" denote as usual the upper (above the C.L.) and lower (below the C.L.) solutions, we can write:

$$\begin{aligned} \phi^+ &= A^+\phi_a^+ + B^+\phi_b^+ \\ \phi^- &= A^-\phi_a^- + B^-\phi_b^- \end{aligned} \qquad (5.4.a)$$

So far, we have four unknowns (A^+, B^+, A^- and B^-) and only two equations. The other two equations are obtained by differentiating ϕ^+ and ϕ^- with respect to y; this gives:

$$\begin{aligned} \phi_y^+ &= A^+\phi_{ay}^+ + B^+\phi_{by}^+ \\ \phi_y^- &= A^-\phi_{ay}^- + B^-\phi_{by}^- \end{aligned} \qquad (5.4.b)$$

It is then a simple matter to obtain the values of the constants A and B from (5.4.a) and (5.4.b); using the fact that the Wronskian of the two solutions is simply -1, we get:

$$\begin{aligned} A^+ &= \phi_y^+\phi_b^+ - \phi^+\phi_{by}^+ \\ B^+ &= \phi^+\phi_{ay}^+ - \phi_y^+\phi_a^+ \\ A^- &= \phi_y^-\phi_b^- - \phi^-\phi_{by}^- \\ B^- &= \phi^-\phi_{ay}^- - \phi_y^-\phi_a^- \end{aligned} \qquad (5.5)$$

Once ϕ_a and ϕ_b are evaluated using the results of Appendix B, and since Φ and ϕ_y are known from the numerical integration, the constants A and B are easily evaluated; it was also verified that to O(1/yt), A and B are insensitive to the choice of a given y to evaluate (5.5)(i.e. they are indeed constants).

We recall from the results discussed in chapter 3 that matching between ϕ^+ and ϕ^- can be effected by writing $\ln y = \ln|y| - i\pi$ for $y<0$, or equivalently, letting the two constants A and B above and below the C.L. be related as follows with now $\ln y = \ln|y|$ for $y<0$:

$$B^+ = B^- = B$$

$$A^+ = A^- + i\pi B \frac{(\beta - \bar{u}_c'')}{\bar{u}_c'}$$

And effectively, as time increases, the numerical model yields exactly these results. Fig. 5.3, for example, is a plot of the real part of the logarithmic phase shift as a function of time; it is seen to converge to π quite nicely. Notice again the presence of a decaying oscillation in time. This is due to the presence of the e^{iyt}/yt^2 term in (5.4.a) and the e^{iyt}/yt term in (5.4.b). In other words, the result is accurate to O(1/yt) or $O(y^6)$ whichever is greater (the $O(y^6)$ error comes from the use of a finite number of terms in the Frobenius method). For example, in Fig. 5.3, at $t=86.4$, and for $y=0.5$, this gives absolute errors of O(0.02) and O(0.004) respectively for the O(1/yt) and $O(y^6)$ neglected terms. When an average in time is taken to eliminate the effect of the e^{iyt} term, we get a value for the phase shift of 3.15, a value quite close to π. The following values are

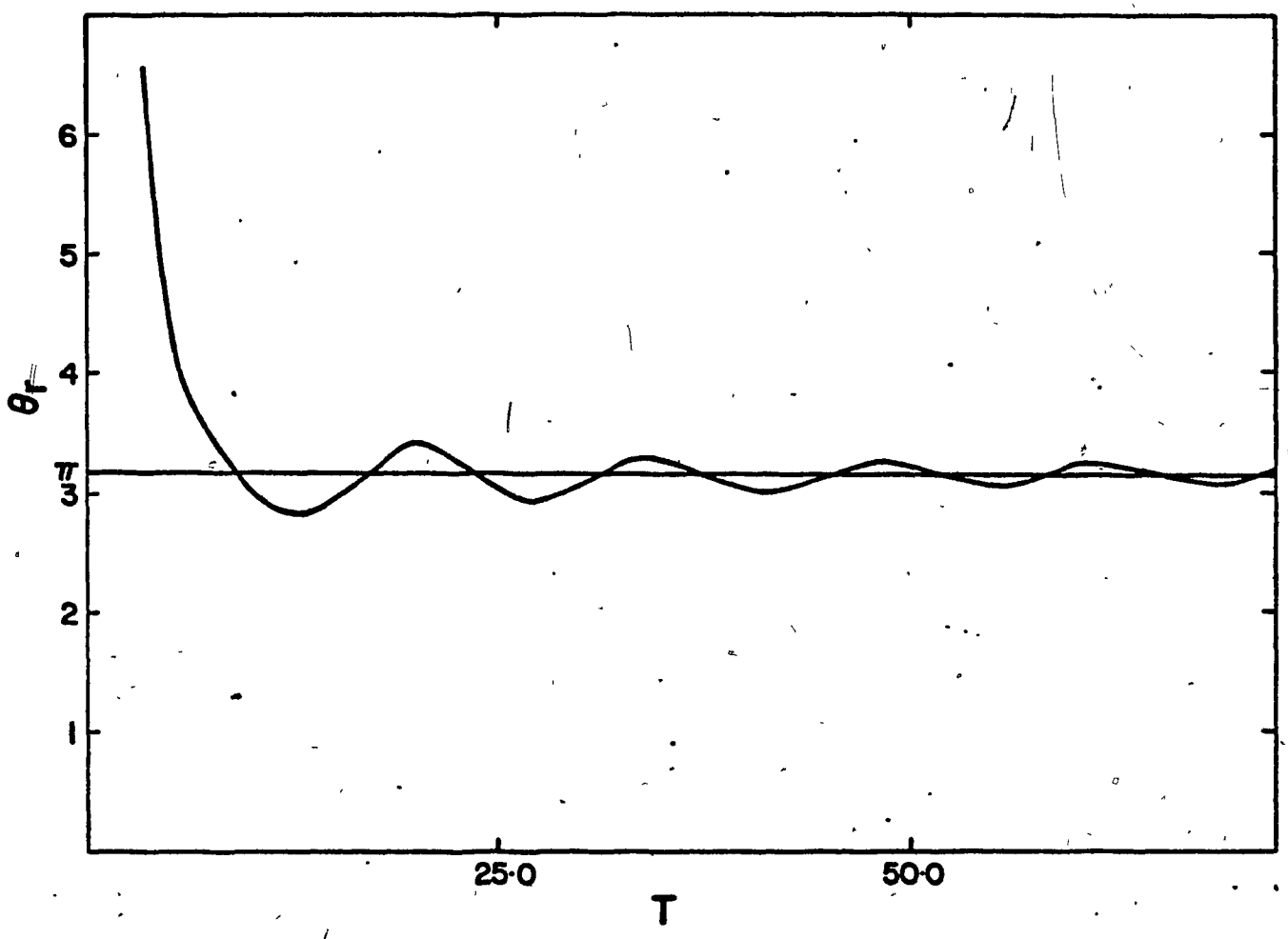

Fig. 5.3 - Real part of the logarithmic phase shift θ_r, as a function of time, in linear integration; $\beta = 1.6$, $\delta = 0.16$.

also obtained for the imaginary part of the phase shift, and B^+ and B^-. At this point, we should clarify the following: the so-called logarithmic phase shift is in general a complex number. At first sight it is hard to see how θ could have an imaginary part when we write for $y < 0$, $\ln y = \ln|y| - i\theta$. One should remember that this is really only a convenient way of writing the jump in the constant A across the C.L. This jump is determined by including neglected terms in the equation. It so happens that in the linear-viscous problem it can be interpreted as a $-i\pi$ phase shift in the ln y term of the Frobenius solution (and thus as an acceptable definition of the logarithm of a negative number). However, this is not generally the case: in Haberman's analysis, the phase shift can be seen to vary continuously from $-\pi$ to 0. Although it is still called a "logarithmic phase shift", it is hard to interpret it as the logarithm of a negative number. Moreover, it has so far been impossible to prove that the "phase shift" is always a real number, even though it has always turned out to be so for the problems already solved. Thus, for the nonlinear time-dependent problem, it is theoretically possible to have a complex phase shift.

$$\mathrm{Im}(\theta) = 0.05$$

$$B^+ = 0.44 + i\ 0.14$$

$$B^- = 0.45 + i\ 0.15$$

As can be seen, B^+ and B^- match almost exactly, and the phase shift is seen to be a real number to 3 significant figures.

Let us note finally that there is also another way of getting the real part of the phase shift, using (3.1); $\overline{u'v'}$ is obtained from the model, and it is easy to show that B is equal to $\phi(y,t)$ at the C.L. (y=0), again to $O(1/yt^2)$ (recall that $\phi_a(y=0) = 0$, and $\phi_b(y=0) = 1$). A π phase shift is again obtained; however, this method does not prove that the phase shift is real, contrary to the previous one, as only the real part of θ enters in the evaluation of $\overline{u'v'}$.

We should stress here the importance of this quantity. We have already shown that the real part is related to the jump in $\overline{u'v'}$, and thus to the energy flux: a zero part would thus imply total reflection of the wave at the C.L.. The complete phase shift (real and imaginary part, if it is non-zero) is also related to the amplitude and phase of the forced wave. In fact, knowledge of the Frobenius solution, and of A^+ and B^+ at all times at a forcing boundary is sufficient to determine the solution completely in the whole domain (above and under the C.L.) once this phase shift is known. This remains true for the non-linear problem, in the outer domain (i.e. away from the C.L.), up to a certain accuracy. The change in time of the logarithmic phase shift is directly related to the change in time of the slope of the phase of the forced wave, and thus to the change in time of $\overline{u'v'}$ and of the energy flux.

In summary, the results of the linear numerical integration show a high degree of accuracy, even for a long integration period (2400 time steps, or 250 days). The fact that the mean flow is of hyperbolic

tangent type, and that the x-part of the derivative is kept, contrary to Dickinson's analysis, does not seem to affect at all the critical layer development. All the fine scales generated by the transients in the linear theory are well represented, and their frequencies and amplitudes seem to correspond to the theory. The $-\pi$ logarithmic phase shift of the large time solution is recovered, indicating the adequacy of the grid length and the time step chosen, as well as the finite difference schemes. Of course, this experiment says nothing about the accuracy of the nonlinear finite difference Jacobian, there being no analytical solutions of the nonlinear problem we could use as a means of comparison.

5.2 FORCING EXPERIMENTS

Two types of forcing were tested; the first one was designed to study the effect of a finite time forcing : that is, the streamfunction amplitude at $y=y_0$ is brought back to zero after a given time. (See Fig. 5.4). Nothing particularly interesting happens in this case. The wave momentum fluxes north and south of the C.L. more or less follow the behaviour of the forced wave. Around the C.L. the momentum flux reaches a maximum some time after the forcing has been brought back to zero, and thereafter decays itself to zero. The effect can be thought of as that of a wave packet propagating towards the C.L.; when it reaches the C.L., it is "absorbed", and the amplitude eventually decays back to zero.

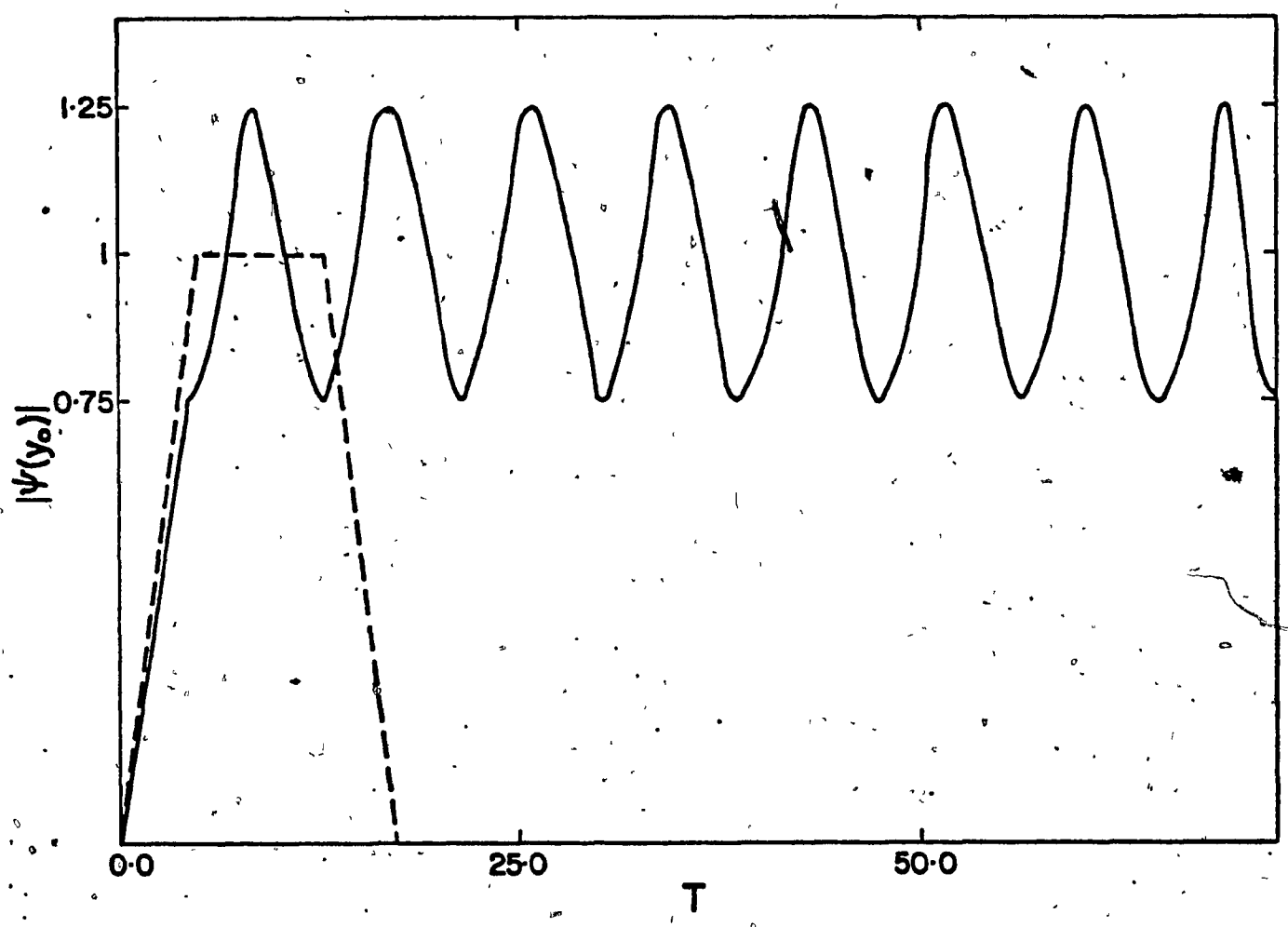

Fig. 5.4 - Amplitude of the forced wave at $y=y_0$ in forcing experiments, as a function of time; ——— second experiment, ------- first experiment.

The other type of forcing is a combination standing wave forcing, and stationary wave forcing (see Fig. 5.4). The amplitude of the standing wave was chosen to be 0.25, with a period of 120 time steps, or 4.32 time units. Now a standing wave is really the sum of two waves, each propagating in an opposite direction, with the same frequency, and half the amplitude. Since frequency is related to phase speed by $c = \omega/k$, and $\omega = 2\pi/T$, where T is the period, we have, with k = 1 for the forcing wave (in non-dimensional units) that $c = \pm 1.45$. Now we recall that $\bar{u} = \tanh y$, and is thus always smaller than c. This has the following implications: the wave propagating to the east, with c = 1.45, will be in an evanescent regime; the other wave, propagating to the west, with c = -1.45, will see no critical level, and will thus be able to propagate freely across the shear flow. This further implies that a non-zero positive $\overline{u'v'}$ should be observed south of the stationary wave's C.L. This is in fact what we get: in Fig. 5.5, we have a plot of $\overline{u'v'}$ as a function of time, south of the C.L. Clearly, the average of $\overline{u'v'}$ in time yields a positive value ($\sim 6 \times 10^{-3}$) which is not the case when forcing only with a stationary wave (see fig. 6.2 for example). This is interesting, for it offers a means by which energy can propagate southward to large distances without encountering critical levels. In the atmosphere, stationary waves are usually forced by orographic or land-sea temperature contrasts. If this stationary wave, for some reason, starts pulsating, it behaves exactly like a standing wave, and energy might be able to propagate towards the subtropical latitudes.

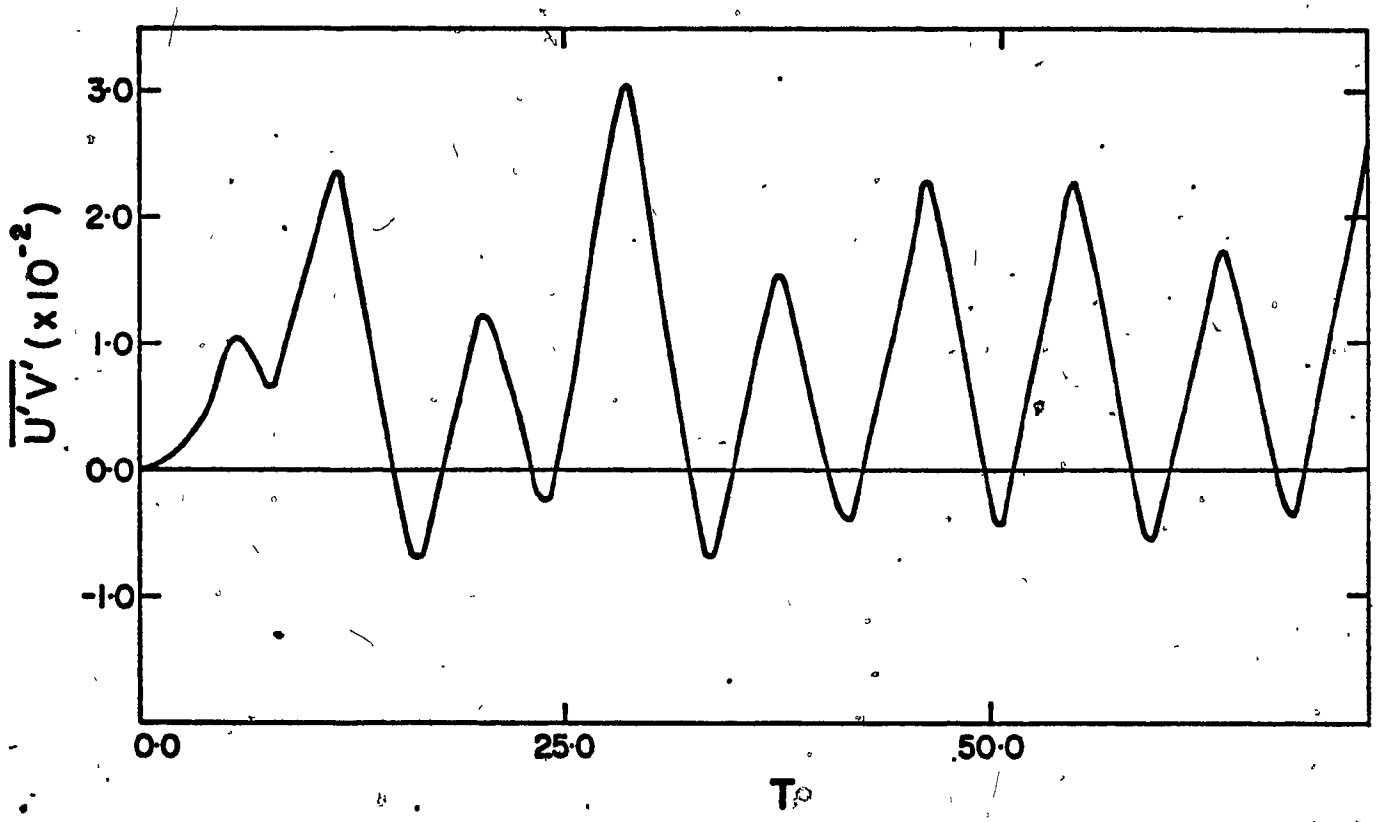

Fig. 5.5 - $\overline{u'v'}$ at y=-0.625 for coupled stationary and standing wave forcing, as a function of time; β=1.6, δ=0.16.

5.3 VARIATION OF THE δ PARAMETER

A series of runs where made with different δ values, namely δ = 0.04, 0.16, 0.36 and 0.64. For a shear scale length of 1000 km, these values correspond roughly to wave numbers 1, 2, 3 and 4, at $\varphi = 38^{0}$N. All other parameters were kept unchanged from their "standard" values. Using arguments similar to those invoked by Bennett and Young (1972), one can conclude that an increase in δ results in a decrease of the WKB-defined y-wave number: i.e.

$$\ell^2(y) = \left[\frac{\beta - \bar{v}_{yy}}{\bar{v}} - \delta \right]$$

decreases as δ increases, all other parameters being held constant. This in turn means that the wave momentum flux north of the C.L. should also decrease as δ increases, since if we assume a solution of the form $\psi = Ae^{i(kx+ly)}$, where ℓ is given by the above expression, it is easy to show that

$$-\overline{\frac{\partial \psi'}{\partial x}\frac{\partial \psi'}{\partial y}} = \overline{u'v'} \propto K\ell |A|^2$$

where we have assumed $\ell(y) \simeq \ell$, a constant. Thus an increase in δ produces a decrease in ℓ, and hence, a decrease in $\overline{u'v'}$. We list below the different steady-state values of a number of parameters of interest, as a function of δ :

δ	$\lvert B\rvert$	$\overline{u'v'}$	θ_-(deg.)
.04	.492	.60	-24
.16	.476	.56	-19
.36	.449	.51	-9.9
.64	.411	.42	2.5

$|B|$ is the modulus of the constant multiplying the φ_b solution. We have already noted that the jump across the C.L. in $\overline{u'v'}$ is proportional to $|B|^2$ (see (3.1)). It can be checked that this is true for the above values. θ_- is the phase of the forced wave south of the C.L. Since $\overline{u'v'}$ is constant and equal to zero in this region, θ_- is constant for $y < 0$. Fig. 5.6 gives a plot of θ_- as a function of δ. It is interesting to note that the relationship is linear; we see that since the phase of the forced wave is fixed to $\pi/4$ at $y=y_0$, the value of the phase south of the C.L. has to increase with δ in order for $\overline{u'v'}$ to decrease north of the C.L.

Apart from the above considerations, no significant differences whatsoever were observed in the critical layer development between our results and Dickinson's, obtained using the long wave approximation (i.e. $\delta = 0$). It seems that the only effect of δ is to change the phase and the amplitude of the wave slightly, leaving the mechanism of the critical layer formation and development unchanged.

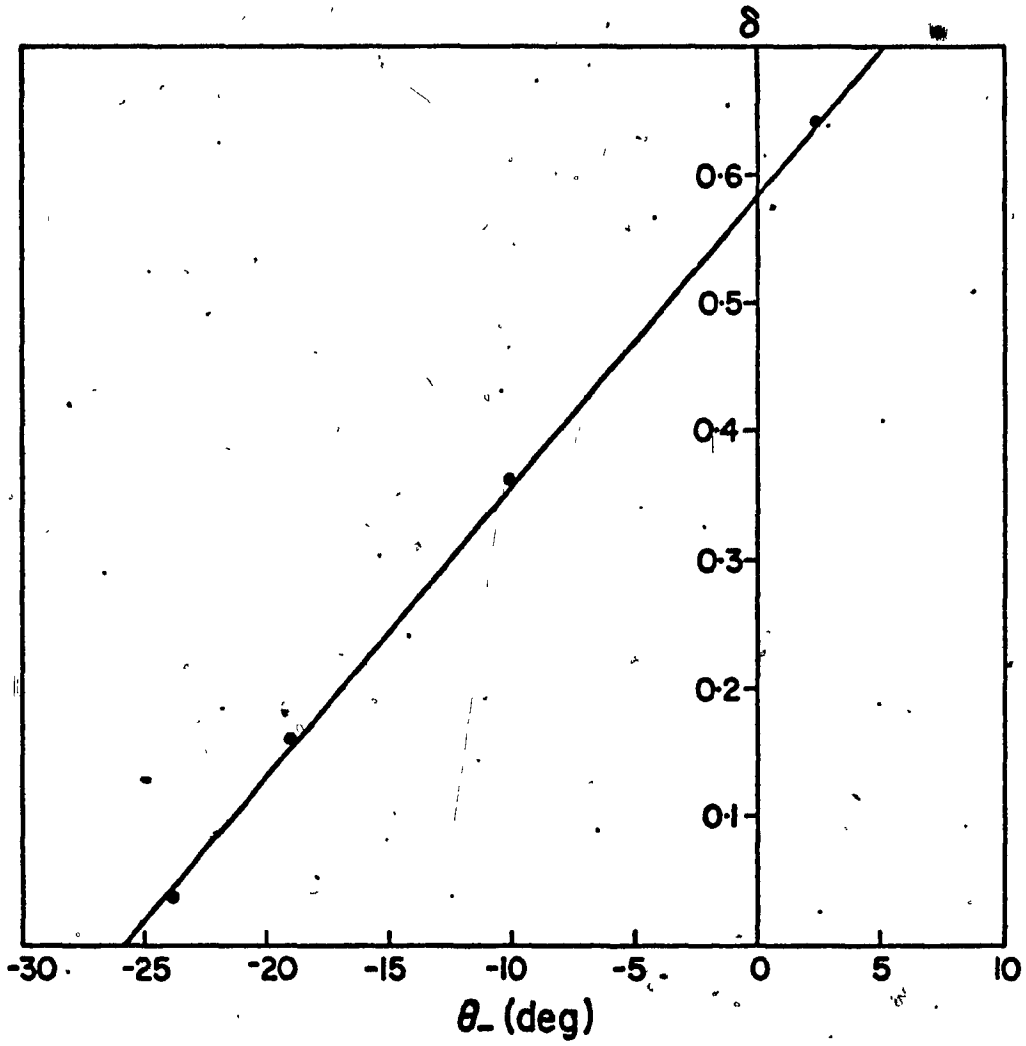

Fig. 5.6 - Phase of the forced wave as a function of δ for $y < 0$; $\beta = 1.6$.

5.4 VARIATION OF THE BETA PARAMETER

A series of runs were made with the following values of β: 1.0, 1.6 and 2.0, the other parameters having their standard value. Again, we should expect $\overline{u'v'}$ to change with β; that is, it should increase as β increases, since now $\ell(y)$ increases with β. We list below the values of parameters of interest as a function of β:

β	$\lvert B \rvert$	$\overline{u'v'}$	θ (deg.)
1.0	.477	.36	25
1.6	.476	.56	-19
2.0	.467	.69	-47

As expected, $\overline{u'v'}$ increases with β. Again the jump relationship is almost exactly verified for the above given values of $|B|$ and β. We had mentioned before that the parameter $t_c = \beta$ in non-dimensional units. And effectively, as β was increased, the development was found to be delayed accordingly. We have also plotted in Fig. 5.7 θ as a function of β. Again, it is interesting to note that the relationship seems to be linear. Also, for $\beta = 0.78$, that is at the lower limit for stability, we see that $\theta = 45$ deg., which is the phase of the forced wave at $y = y_0$.

Apart from these observations, the critical layer development proceeded as it did in the standard integration.

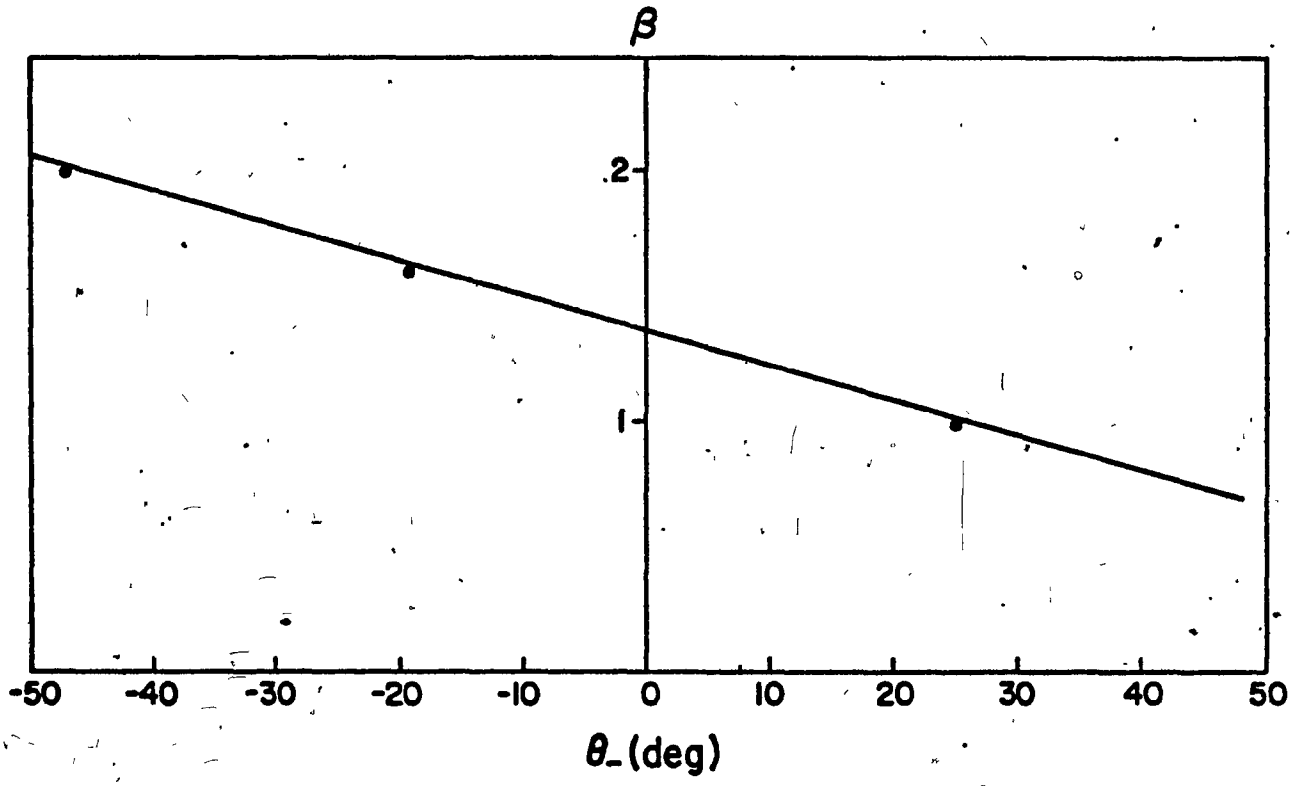

Fig. 5.7 - Phase of the forced wave as a function of β for $y < 0$; $\delta = 0.16$.

CHAPTER 6. NONLINEAR INTEGRATIONS

6.1 STANDARD INTEGRATION

The integration to be described will be referred to as the "standard" integration, for it will be used as a basis of comparison with other runs where the parameters will be allowed to vary, the forcing modified or diffusion terms will be added. The parameters used in the standard run are $\delta = 0.16$, $\varepsilon = 0.018$, $\beta = 1.6$, $N = 6$ (N designates the number of harmonics), and $\Delta t = 0.036$, $\Delta Y = .00625$. $\varepsilon = 0.018$ corresponds to $\phi_s = 1.8 \times 10^5 m^2 s^{-1}$ with $u_m = 10\ ms^{-1}$ and $L = 10^3 km$. All other details are the same as for the linear integrations. In describing the results, we will be looking at a number of different quantities, such as the wave momentum flux $\overline{u'v'}$, β_{eff} (i.e. $\beta + \sigma_{yy}$), etc.

In order to compare the evaluation of some of these quantities with the results obtained by Geisler and Dickinson (1974), we have done a quasi-linear integration, using the same set of parameters except that $N = 1$.

6.1.1 WAVE MOMENTUM FLUX

By wave momentum flux (denoted $\overline{u'v'}$), we mean the total wave momentum flux, that is the sum for the six harmonics. We shall first look at this quantity at two fixed points in y, as a function of time. The first point is located just south of the forcing level (more precisely at $y = 2.4$, the forcing being at $y = y_0 = 2.5$). Fig. 6.1 gives a plot of $\overline{u'v'}$ as a function of time at $y = 2.4$. One can observe three different regimes . The first one, (we call it the linear regime), is for all

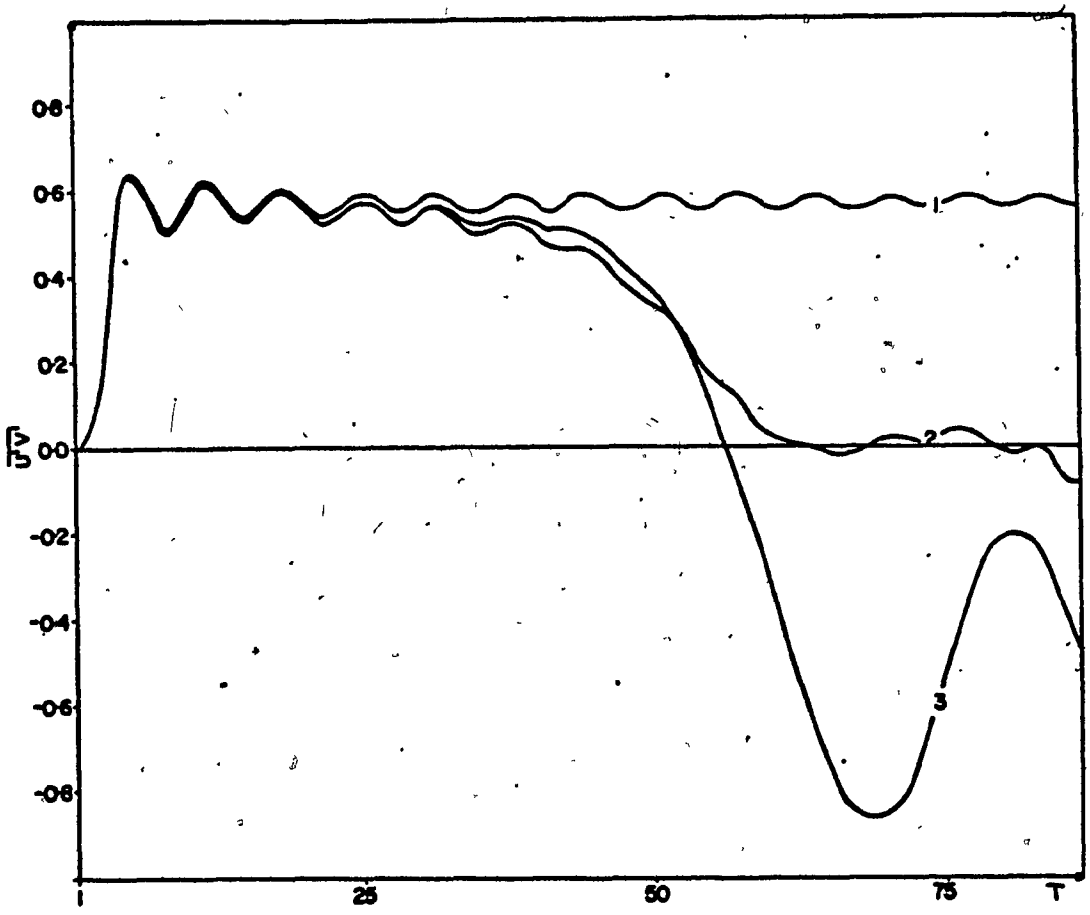

Fig. 6.1 - $\overline{u'v'}$ as a function of time at y=2.4; 1. linear integration, 2. nonlinear integration, 3. quasilinear integration; β=1.6, δ=0.16, ε=0.018, N=6.

purposes identical to what was observed in a linear integration. It corresponds to the stage where there is a slow build-up of the harmonics through nonlinear interactions. Regime 2 is characterized by a decrease in $\overline{u'v'}$ from the linear steady-state value to a value near 0. Notice that the small "e^{iyt}" oscillations superimposed on the mean linear value of $\overline{u'v'}$ still persist during this decay. Regime 3 is characterized by a slowly oscillating $\overline{u'v'}$ around 0, with, again, the "e^{iyt}" oscillation superimposed on it. Since at that time the wave source is still on, this implies a complete reflection of the wave energy at the critical level; thus the nonlinear integration gives a result which is completely different from the linear integration, i.e., the steady-state (away from the critical layer) being characterized by a wave reflection instead of a wave absorption. This result is completely in accord with Benney and Bergeron's (1969) analysis, who first proved the existence of suchasolution by showing that their steady-state had a zero jump in the Reynolds stress across the C.L.; since it had to vanish at $y \to -\infty$, it had to be zero everywhere. On the same figure, we have plotted the evolution for a quasilinear integration (curve 3). It is obviously quite different. GD (1974) however showed that eventually the same steady-state is reached, after a number of successive decaying oscillations around zero. It was not possible (due to computer time and storage limitations), to integrate long enough to check that this was indeed the case. Nevertheless, the behaviour seems to be qualitatively similar to the results they obtained i.e., a rapid decrease of $\overline{u'v'}$ to

a negative value followed by a rise. We should point out here that our model is quite different from theirs in many aspects. One of these differences and not the least, is that in their model, the $\frac{\partial \bar{u}}{\partial t}$ term is multiplied by a function $f(y) = \frac{1}{2}[1 + \tanh(-ay + y_0)]$ where a and y_0 are chosen such that $f(y) \simeq 0$ near the forcing level, and $f(y) \simeq 1$ near the critical level. (This fact, we should also point out, is not mentioned in their paper, although it was mentioned by Ward (1975)). It is not obvious to us what the effects of such a procedure are in a long term integration; it seems conceivable that it could affect the steady-state results.

Fig. 6.2 is a plot of $\overline{u'v'}$ at a point situated midway between the C.L. and the southern boundary, i.e. at $y = -0.625$. As expected, after an initial rise, during the period where the critical layer is just starting to build up, the evolution in time is characterized by an oscillation around a value of zero. Two stages can be observed; the first one is a linear stage, in which the evolution is given by a slowly decaying oscillation, as in the linear integration, and the second one during which there is a sudden increase in the amplitude of the oscillations, although the mean is still roughly zero. Note that the beginning of the second stage coincides with that of Fig. 6.1. Moreover, no significant differences were observed between the quasilinear and nonlinear integrations. Thus, whether the model is linear, quasilinear or nonlinear, there is no significant transfer of energy through the C.L., $\overline{u'v'}$ being $O(10^{-2})$ smaller at all times.

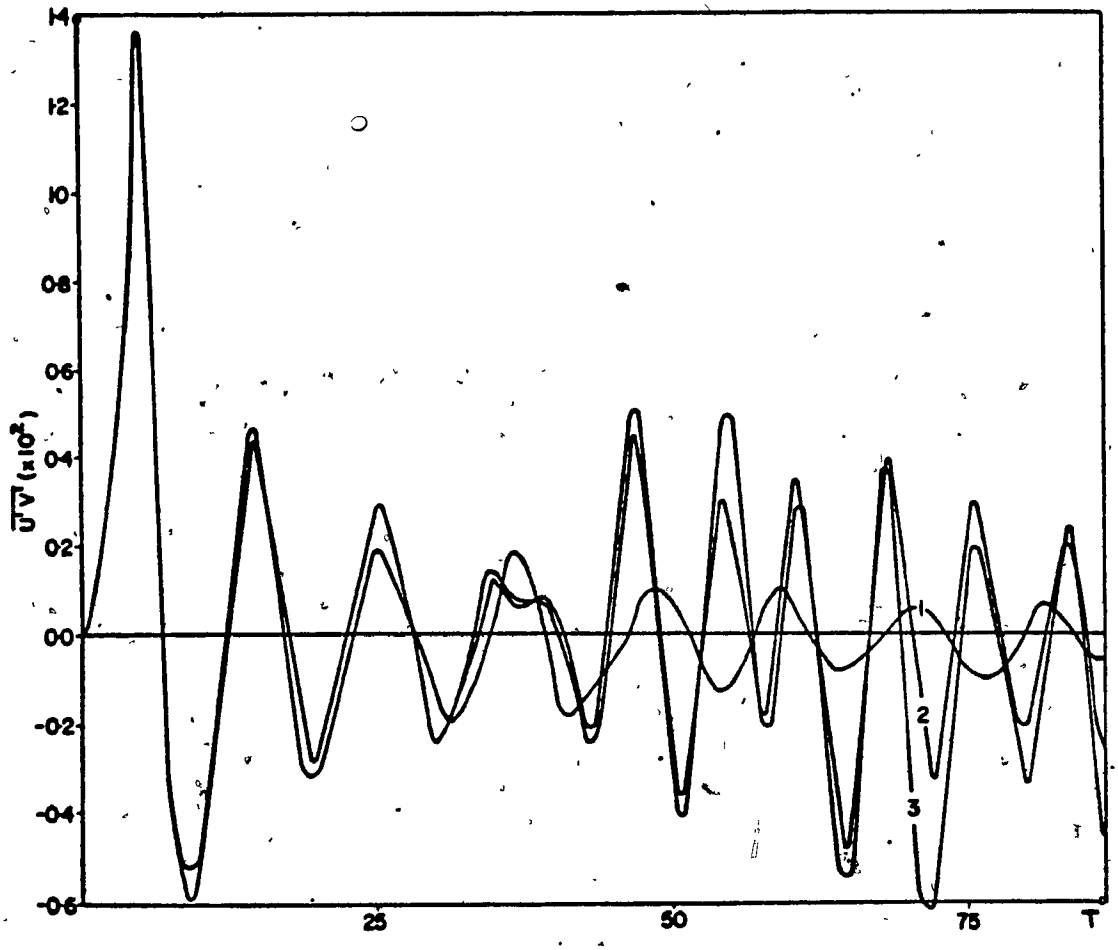

Fig. 6.2 - Same as fig. 6.1, except at y=-0.625.

Let us look now at $\overline{u'v'}$ as a function of y at a given time. Fig. 6.3.a gives the wave momentum flux of each component just at the beginning of stage 2. The usual linear quasi steady-state configuration is realized for the forced wave, including the small e^{iyt} oscillations. At that time, the other harmonics have non-zero $\overline{u'v'}$ only in the critical layer region. Fig. 6.3.b is a similar graph, for stage 3. The wave momentum flux has dropped to a value near zero for the forced wave, except in the critical layer itself. All the other harmonics have zero or near-zero momentum flux outside the critical layer region, while in the critical layer itself, each harmonic has a non-zero momentum flux. It is clear then that in the critical layer itself, no steady-state is reached. In fact, it might eventually become unstable due to the large shear developing in this region. It is obvious that the numerical model is incapable of resolving the finer and finer scales that are appearing, and hence, we had to stop the integrations before any kind of "steady situation" had developed in the critical layer itself. However, outside the critical layer region, the model can be considered to show the steady solution.

Summing up the above considerations, we can say the following: above the critical layer, the nonlinear integrations yield a quasi steady-state characterized by a zero wave momentum flux, indicating the presence of a reflected wave at the C.L.; this result is altogether different from the linear or quasilinear integrations, although in the last case, it is possible that an identical steady-state is reached, although later in time. In the critical layer itself, finer and finer scales of motion are developing, and no steady-state is reached: however, instability

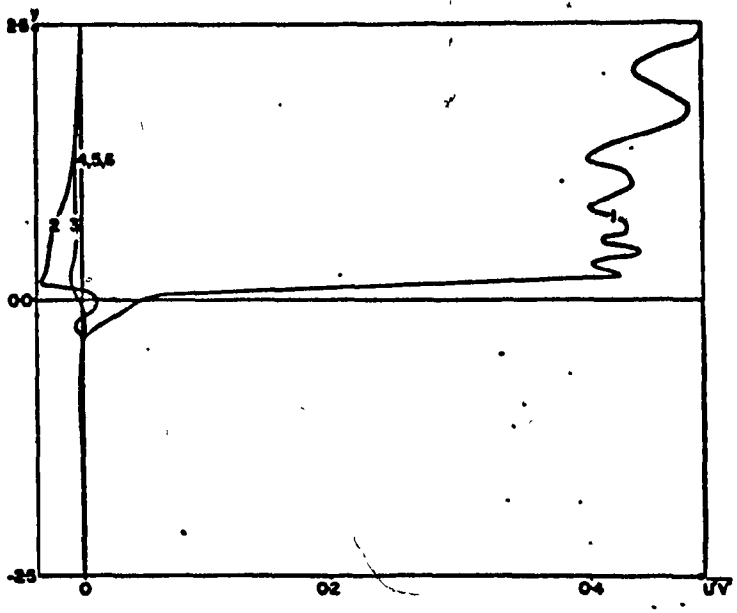

Fig. 6.3.a - $\overline{u'v'}$ as a function of y for nonlinear integration, at t=43; β=1.6, δ=0.16, ε=0.018, N=6.

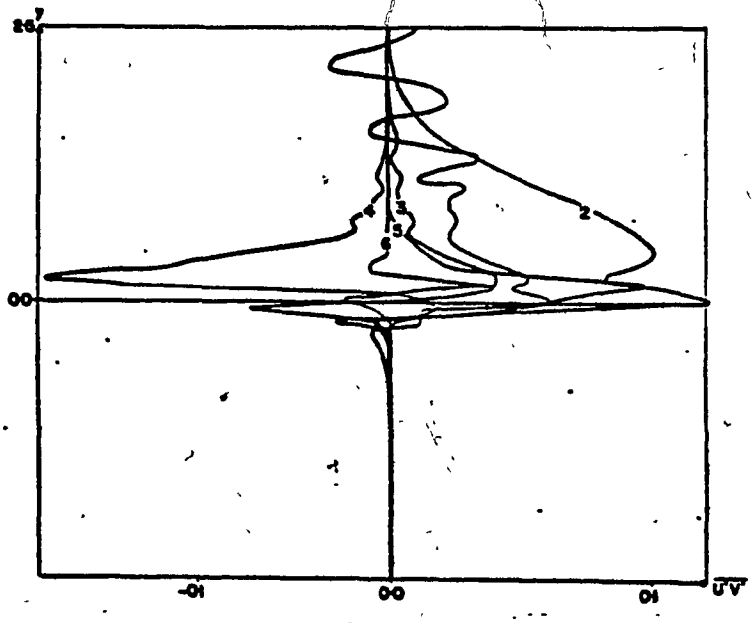

Fig. 6.3.b - Same as fig. 6.3.a, except at t=69.

could be a possible outcome, leading to a fully turbulent critical layer. Below the critical layer, their isno time-averaged energy flux, so that the C.L. can be thought of as a barrier to wave energy propagation, ultimately reflecting back all incoming energy flux towards the source.

6.1.2 $\beta - \bar{u}_{yy}$ TERM

GD pointed out the importance of $\beta - \bar{u}_{yy}$ (called β_{eff}) in their model (see chapter 3). Fig. 6.4 and Fig. 6.5 show β_{eff} as a function of y at T=43 and 86, for the nonlinear and quasilinear integrations respectively. T = 43 corresponds roughly to the beginning of stage 2 in the nonlinear integration. In the nonlinear case, β_{eff} has gone negative at two places, north of the instantaneous C.L. We should mention here that in the nonlinear integration, as in the quasilinear integration, the C.L. never moves more than a distance of $O(\varepsilon)$ (roughly 5 or 6 gridpoints) towards the source. We notice also the appearance in the profile of many wavelike oscillations in y, which are absent in the quasilinear integration (see Fig. 6.5). As time increases, the nonlinear β_{eff} develops finer and finer scales of oscillations, and it eventually becomes negative quite far north of the instantaneous C.L., whereas the quasilinear β_{eff} remains roughly steady throughout the rest of the integration period, always being negative at or very near the C.L.. This last remark agrees with the fact that $\overline{u'v'}$ near the forcing became negative after β_{eff} went negative and remained negative for the rest of the integration period. However, in the nonlinear case, as we have seen, the evolution of $\overline{u'v'}$ was quite different. And it is hard to find any

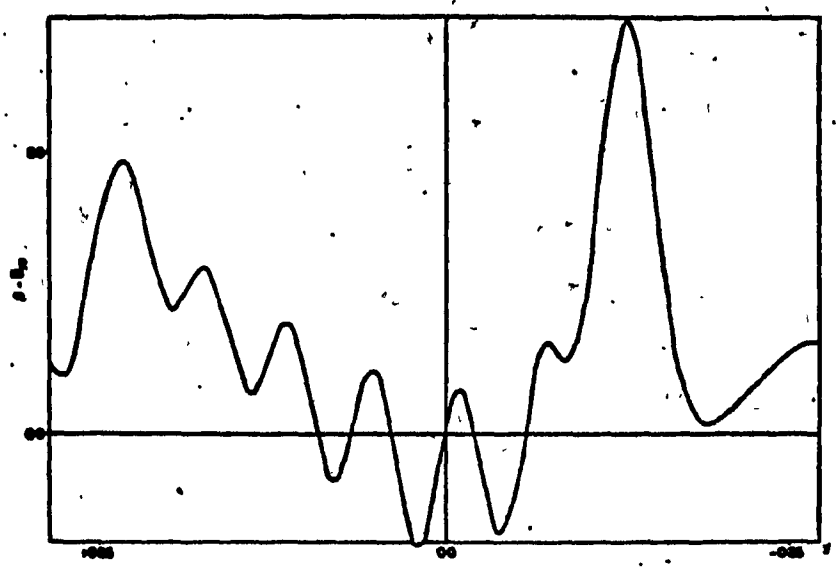

Fig. 6.4.a - $\beta - \bar{u}_{yy}$ as a function of y in nonlinear integration at t=43; β=1.6, δ=0.16, ε=0.018, N=6.

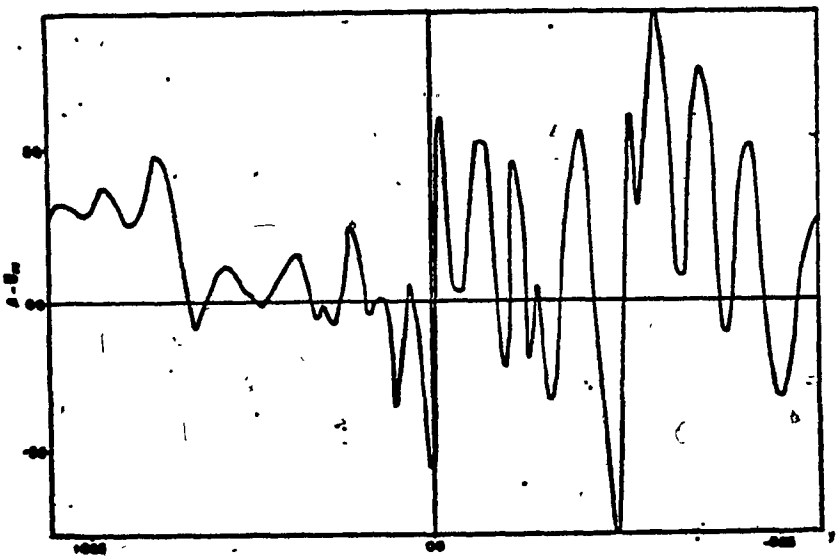

Fig. 6.4.b - Same as fig. 6.4.a, except at t=86.4.

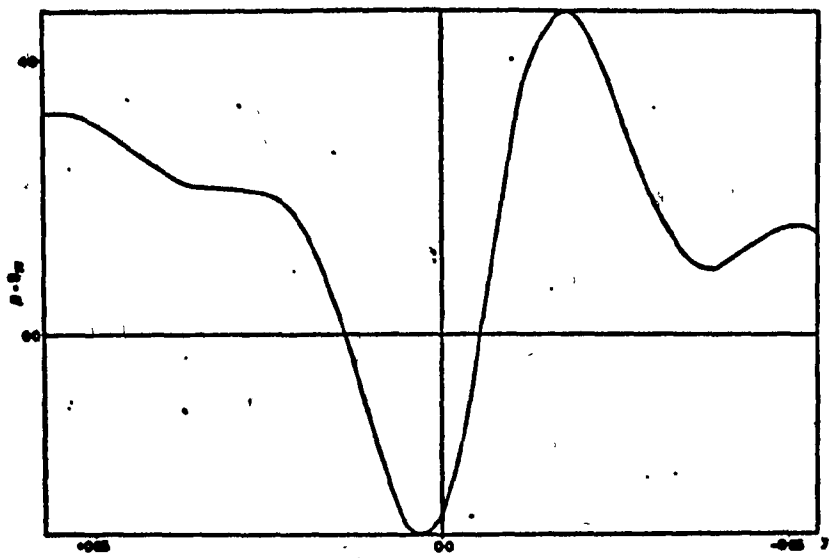

Fig. 6.5.a - Same as fig. 6.4.a, except for quasilinear integration.

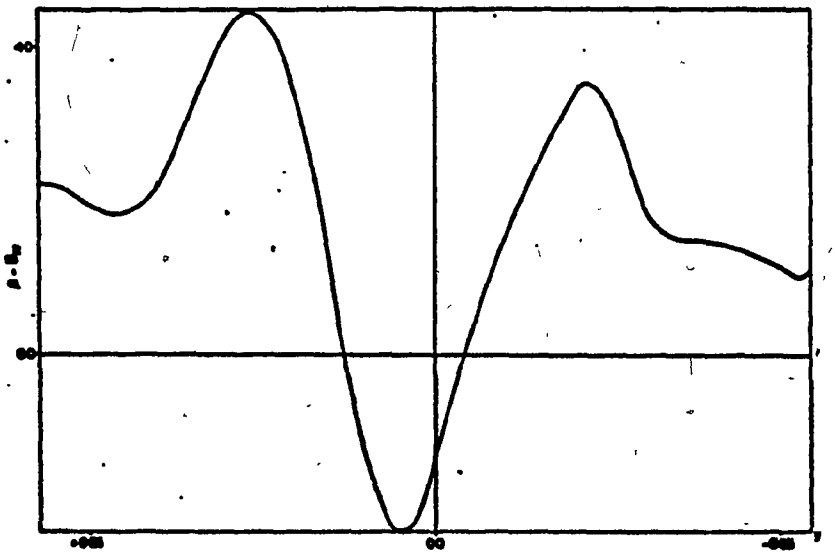

Fig. 6.5.b - Same as fig. 6.4.b, except for quasilinear integration.

clear-cut relation between β_{eff} and $\overline{u'v'}$. It might still be possible that β_{eff} triggers the drop in $\overline{u'v'}$ in the nonlinear integration, since at that time the harmonics are still small, and their effect on the mean flow, for example, through the $\overline{u'v'}$ term is also small compared to that of the forced wave. However, as time increases, their importance increases and eventually becomes comparable to that of the forced wave, in the critical layer. In fact, Warn and Warn (1976) showed that on a time scale of $O(\varepsilon^{-\frac{1}{3}})$, the vorticity of all the harmonics becomes of the same order as that of the primary wave. And in the present case, for $\varepsilon = 0.018$, this is $T \sim O(7)$. However, as can be seen from Fig. 6.1, the drop in $\overline{u'v'}$ occurs at $T \simeq 40$, although the nonlinear integration (and the quasilinear) start departing from the linear at $T \simeq 20$. To check out whether the evolution of $\overline{u'v'}$ had any relation with the nonlinear time scale $\varepsilon^{-\frac{1}{3}}$, we did a series of integrations with $\varepsilon = 0.006$, 0.012, 0.018 and 0.024, all other parameters being identical. Using the $\varepsilon = 0.024$ integration to scale the results, we have plotted the time required for $\overline{u'v'}$ at $y = 2.4$ to decrease to zero as a function of ε. The result is shown in Fig. 6.6. The full curve being the curve obtained by assuming an $\varepsilon^{-\frac{1}{3}}$ time scale. As can be seen, there is a surprisingly good agreement with the observed values. This would seem to indicate that in the nonlinear integration, it is the "ε" parameter which governs the evolution of $\overline{u'v'}$, and since ε multiplies the nonlinear Jacobian, this term must certainly be as important as the $\beta - \bar{U}_{yy}$ term in reaching a steady state of zero momentum flux. In other words,

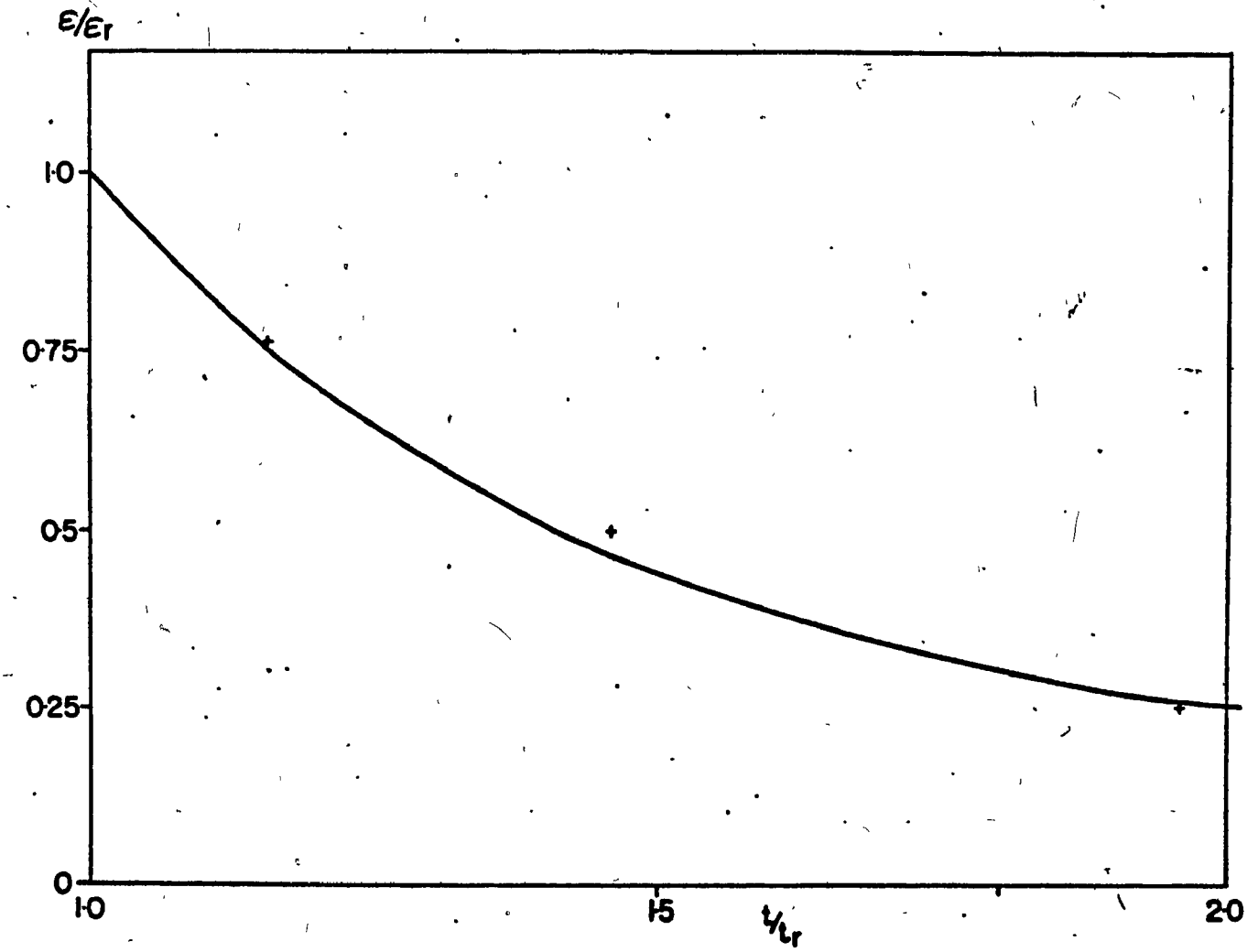

Fig. 6.6 - Time required for $\overline{u'v'}$ to decrease by two orders of magnitude at y=2.4, as a function of ε; all values scaled by those of the ε_r=0.024 integration. Full line is proposed theoretical curve.

even though GD's explanation is probably correct for the quasilinear case, it does not hold in the fully nonlinear equation, where one must take into account the nonlinear Jacobian. Moreover, Fig. 6.6 seems to indicate a strong relationship between the value of the nonlinear Jacobian and the drop in $\overline{u'v'}$.

One thing we could say also about Fig. 6.4 is that the finer and finer scales of β_{eff} could very possibly lead to instability (we shall come back to this later). In any event, they also show the need for a very fine resolution in dealing with the nonlinear problem. It is the appearance of these finer and finer scales which forced us to stop the integration at T=86.

6.1.3 MEAN FLOW DEFORMATION

By mean flow deformation, we mean the difference between $\bar{u}(y,t)$ and $\bar{u}(y,0)$, where $\bar{u}(y,0)$ is the hyperbolic tangent shear flow profile. According to Benney and Bergeron's (1969) analysis, this deformation is of $0(\varepsilon)$ in the critical layer. In other words, for example, the critical level never moves more than a distance of $0(\varepsilon)$. We have plotted in Fig. 6.7 a profile of the deformation as a function of y. The values seem to be in accord with Benney and Bergeron's results.One can also notice that away from the C.L., the deformation becomes quite small: this is to be expected since in the outer region, the flow can be assumed to be linear. Also, the deformation is negative everywhere, indicating the wave and the harmonics are actually decelerating the mean zonal flow; that is, $\frac{\partial \bar{u}}{\partial t}$ is < 0 everywhere; this implies $\bar{u}$ becomes more negative for $y < 0$, and less positive for $y > 0$.

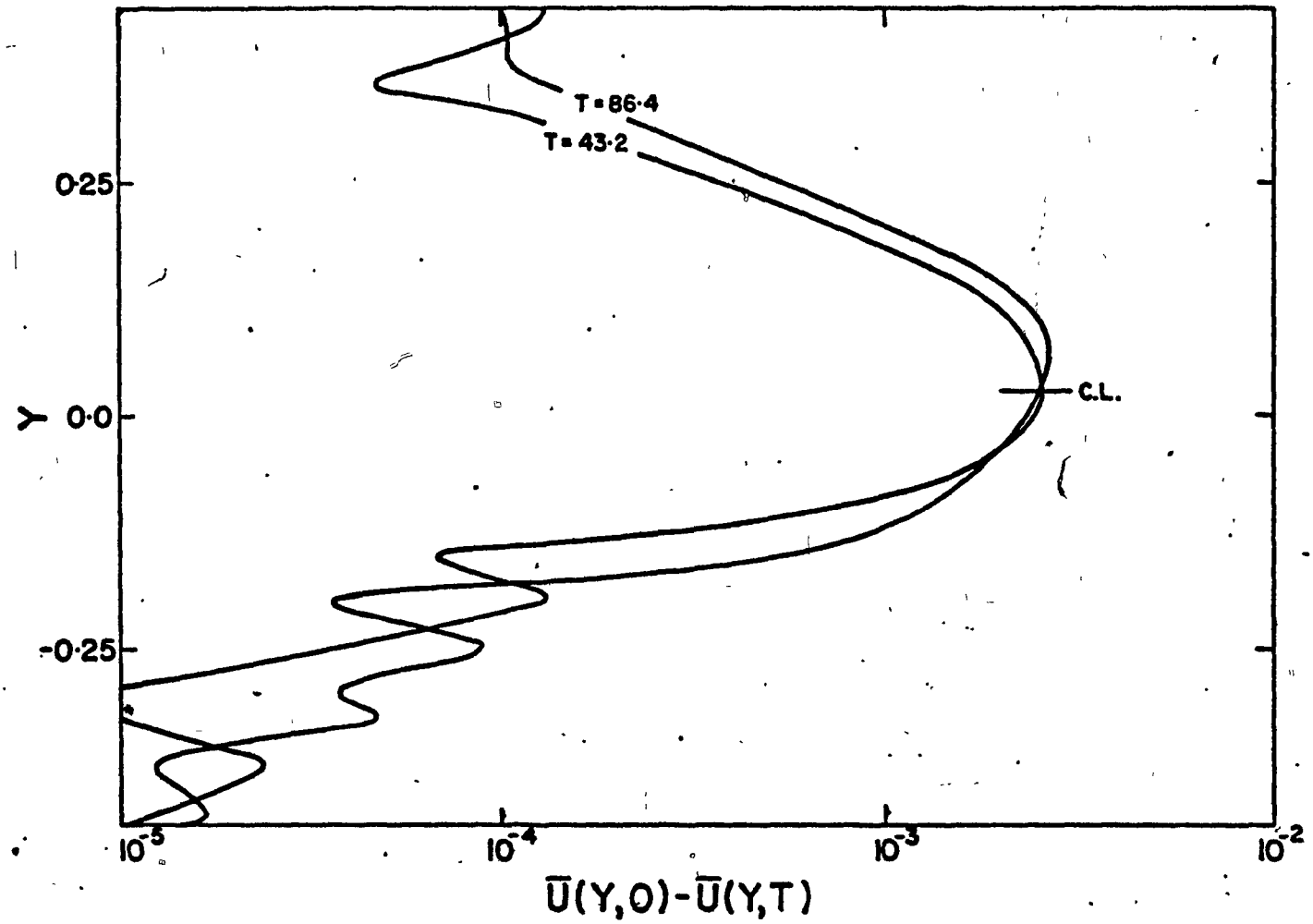

Fig. 6.7 - Mean flow deformation in nonlinear integration at two different times; $\beta = 1.6$, $\delta = 0.16$, $\epsilon = 0.018$, N=6.

6.1.4 WAVE AMPLITUDE AND PHASE

Fig. 6.8 and Fig. 6.9 are plots of the amplitude and phase at two different times, namely T=43 and T=69. As can be seen, south of the C.L., we have an exponential decay of wave amplitude, corresponding to the evanescent regime, while north of the C.L., the waves show an oscillating behaviour. According to T. Warn (private communication), the amplitude of the harmonics for $0(\varepsilon^{-1/4}) < t < 0(\varepsilon^{-1})$ should be $0(\varepsilon^{1/2})$ smaller than that of the forced wave in the critical layer, and $0(\varepsilon)$ smaller away from the critical layer. As can be seen in Figs. 6.8 and 6.9, this is roughly the case in the critical layer ($\varepsilon^{1/2} \simeq .15$). However, outside, the amplitudes are larger than $0(\varepsilon)$. We note however that T=43 or T=69 is also roughly $0(\varepsilon^{-1})$, so that we are nearing the time limit valid for the scaling to hold. For a linear zonal wind profile, this time limit can be obtained in the following way, using Warn and Warn's (1976) solution for $yt \gg 1$, with $y \sim 0(1)$ (that is, away from the critical layer). We have

$$\phi(y,t) = \phi(y,\infty) - \frac{a e^{-iyt}}{2yt^2} + \cdots \qquad (6.1)$$

Now, in the nonlinear Jacobian, the lowest order term is given by the ϕ_{yyy} term. (this can be seen by inspection of (6.1)); using (6.1), we can write that

$$\varepsilon J(\psi', \nabla^2\psi') \sim \varepsilon O(\phi\phi_{yyy}) \sim O(\varepsilon t)$$

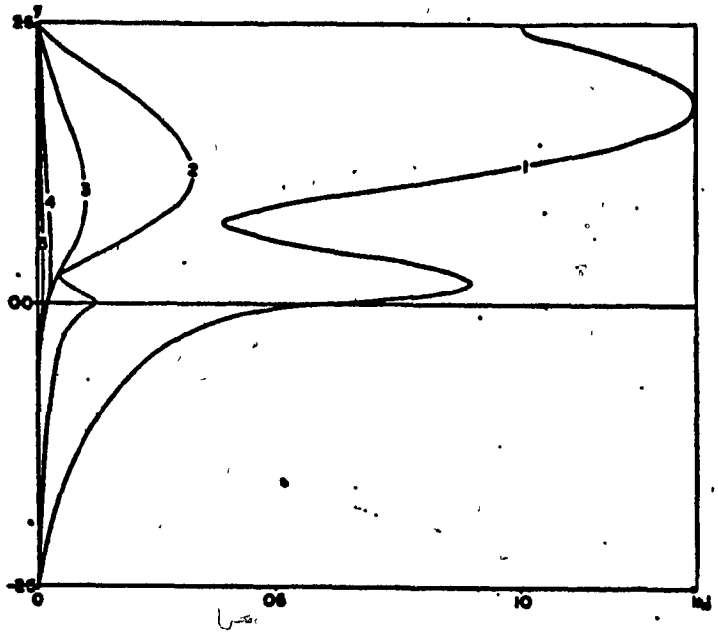

Fig. 6.8.a - Wave amplitudes as a function of y at t=43; β=1.6, δ=0.16, ε=0.018, N=6.

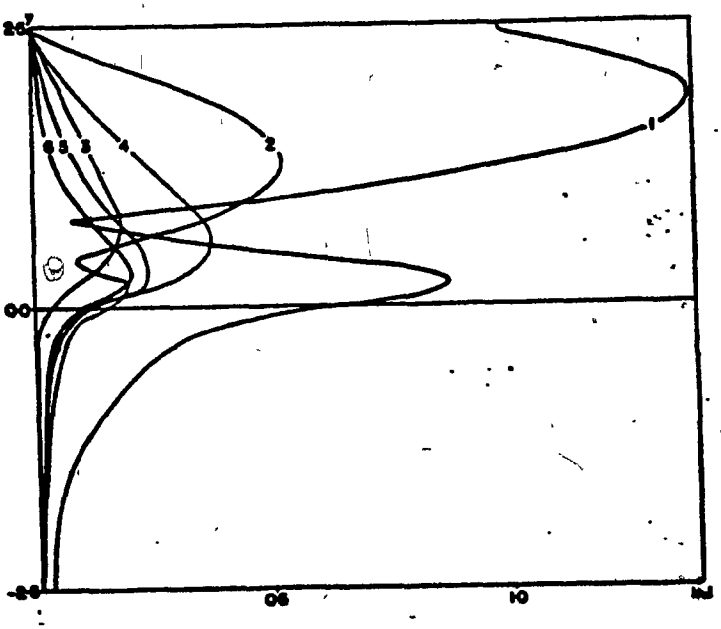

Fig. 6.8.b - Same as fig. 6.8.a, except at t=69.

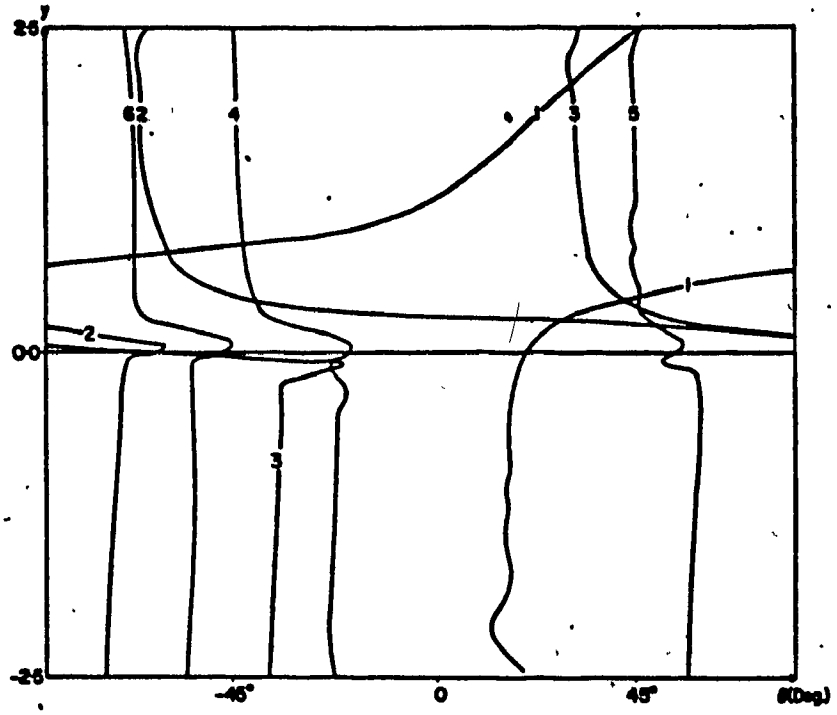

Fig. 6.9.a - Phases of the waves as a function of y at t=43; β=1.6, δ=0.16, ε=0.018, N=6.

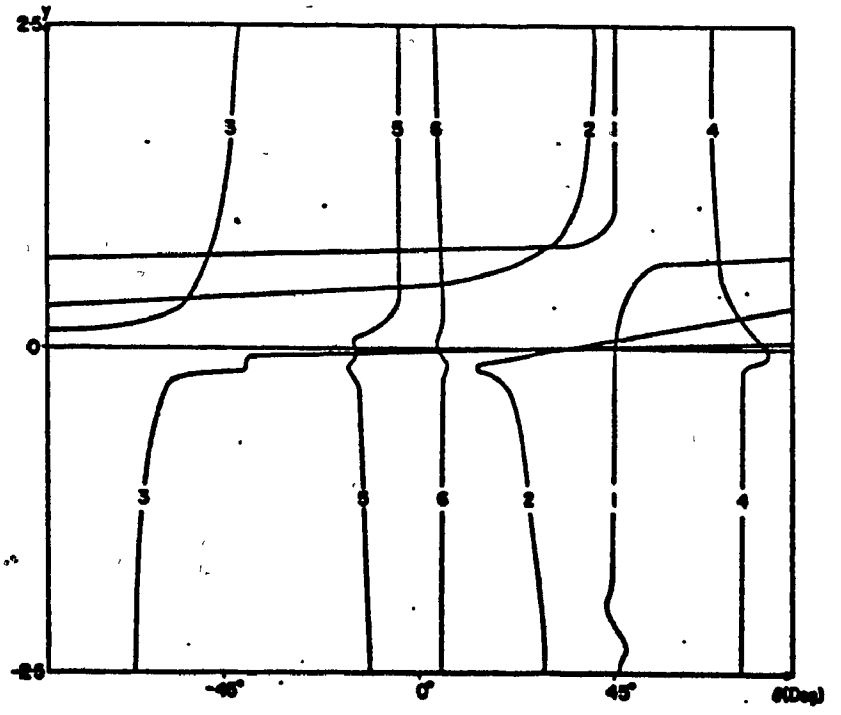

fig. 6.9.b - Same as fig. 6.9.a, except at t=69.

Similarly, the vorticity tendency term can be approximated by

$$\frac{\partial}{\partial t}\nabla^2\psi' \sim O(\phi_{yyt}) \sim O(1)$$

where again (6.1) was used. It is now easy to see that these two terms balance each other when $\epsilon t = 1$, or, in other words, when $t = 0(\epsilon^{-1})$. Since so far there does not seem to be any important differences between our linear results and Dickinson's, we think that this scaling is probably correct also for our problem. Again according to Warn, for $t > O(\epsilon^{-1})$, it is not clear what an expansion in powers of ϵ for the nonlinear solution should look like. However, we checked that for $t = 0(\epsilon^{-1/2})$, the amplitudes of the harmonics outside the critical layer are indeed $0(\epsilon)$ smaller than that of the forced wave. For $t > 0(\epsilon^{-1})$, it is possible that instability might set in, caused for example by the large shears that appear in the critical layer. However, in this case, no sustained growth was noted, and the picture at T=86 shows a similar amplitude pattern.

Looking at the phase diagram, we notice that south of the C.L., the phase lines are essentially vertical, pointing out the fact that the Reynolds stress is zero in that region. North of the C.L., at T = 43, the forced wave displays a N-E - S-W tilt, indicating a northward wave momentum flux and southward wave energy flux. The phase is fixed at 45^0 at the northern boundary. The discontinuity in phase north of the C.L. is associated with a nodal point in the amplitude. At T = 69, we notice the phase of the forced wave is vertical both above and below the

the C.L., indicating that the wave momentum flux has dropped to zero and thus the presence of a reflected wave at the C.L.. The harmonics also display vertical phase lines, except in the critical layer where a distortion is apparent; this distortion, and non-zero amplitudes in the critical layer, in turn generate momentum fluxes, indicating that no steady-state has yet been reached in the critical layer itself. We should also notice that the phase of the harmonics is not fixed at the forcing boundary, the amplitudes being set to zero at this point.

Finally, we have plotted in Fig. 6.10 the total stream function field at five different time intervals for the linear, quasilinear and non-linear integrations. Looking at the nonlinear case, we notice an eastward movement of the cat's eye, corresponding to the phase change of the forced wave. In the third picture, the phase is essentially vertical, and we have attained the "quasi" steady-state configuration. As time goes on, we see finer scales appearing in the cat's eye and above; it is not clear whether these are due to some instability slowly setting in, or if they are part of a final steady-state configuration in the critical layer itself. The phase is however still vertical throughout the channel width. The quasilinear field is decidedly different as to the shape of the cat's eyes themselves, and also as far as the movement of the cat's eye is concerned. We notice that there is a steady eastward drift of the cat's eye throughout all the integration period, due to the fact that the phase of the forced wave never stabilizes to a constant value in the y direction. The linear field is essentially steady after the first picture; the cat's eyes are

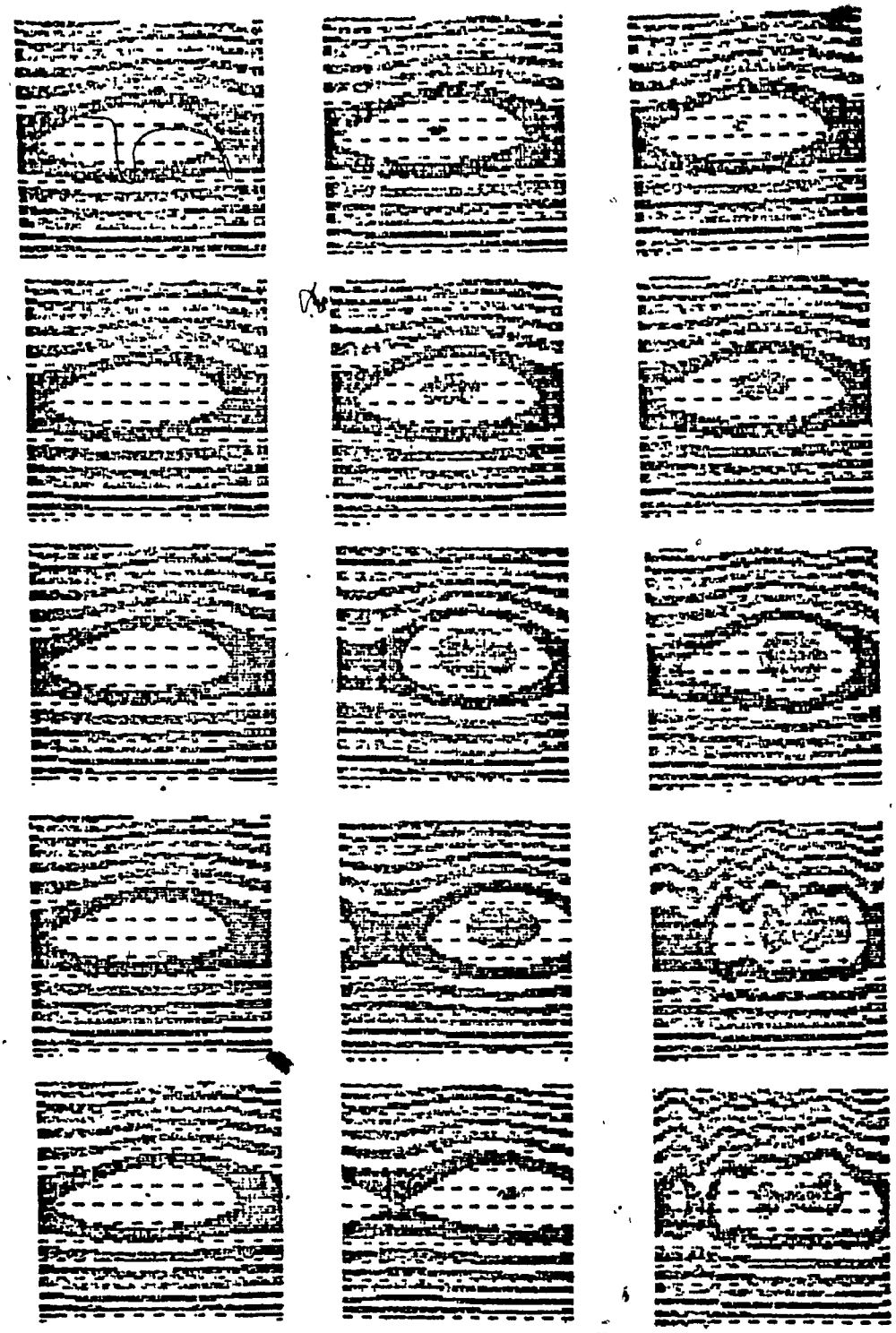

Fig. 6.10 - Total stream function field at five different times: t=17, 34, 51, 69 and 86; (a) linear, (b) quasilinear, (c) nonlinear (N=6).

"skewed" towards the N-E, and remain so, because of the steady state jump in the Reynolds stress, associated with the jump in the slope of the phase of the forcing wave.

6.1.5 LOGARITHMIC PHASE CHANGE

We have already pointed out, in discussing the linear results that the time dependent linear inviscid problem yields a logarithmic phase shift which is the same as that obtained from the steady-state linear viscous problem; that is, as one goes from $y>0$ to $y<0$, the "ln y" term in the Tollmien-Kuo solution can be written as

1) $\ln y$ for $y>0$

2) $\ln|y|-i\pi$ for $y<0$

This is equivalent to having a jump in the constant A which multiplies the ϕ_a solution, when we simply let $\ln y=\ln|y|$ for $y<0$ and $y>0$. Now if one deals with the nonlinear problem, it would prove interesting to check if the same analogy exists between the steady state nonlinear-viscous problem and the time dependent nonlinear inviscid problem; from the results we have already described, it is obvious that this is probably the case, since we have pointed out that a zero jump in the Reynolds stress across the C.L. is associated with a zero logarithmic phase shift. Nevertheless, it might prove interesting to proceed as we did for the linear integration, and evaluate the constants A, B and the associated logarithm phase shift directly from the numerical solution for the amplitude and phase of the wave. Thus the following approximation will be made, following the results

of Warn (private communication). Away from the nonlinear critical layer, we will assume that the solution is given by a series of the form

$$\Psi(x,y,t) = \int^{y} \bar{u}(y,t)\,dy + \varepsilon\left[(A(t)\phi_a + B(t)\phi_b)e^{ikx} + c.c.\right] + O(\varepsilon^{3/2})$$

where the first term is the zonal mean flow, the second, the Frobenius solution with time dependent coefficients and the third contains part of the nonlinear corrections. In order to use the scheme derived in Chapter 5, we will truncate the series before the $O(\varepsilon^{3/2})$ term. Thus, our results should have a relative error of a least $O(\varepsilon^{1/2})$; with the value of ε used, this is roughly equal to O (15%), which is quite large, since the actual value can be 4 or 5 times that order. There are also transient terms, of the form "$e^{ikt}/_{yt^2}$" which can contribute to the error. However, as time increases, their effect should become less and less important. Finally, the Frobenius series themselves we are using are given to $O(y^6)$, so that we cannot move too far away from the C.L. Taking into account these considerations, several points (in y) were chosen, and the error was found (using linear and nonlinear results) to be minimized around y=0.5. Fig. 6.11 gives a plot of $\Theta = \Theta_n + i\Theta_i$, the complex logarithmic phase shift thus obtained as a function of time. Looking at the real part, we notice a surprisingly good agreement with Benney and Bergeron's result, at t large. After an initial transient increase, Θ_n decreases to π, during the linear stage; as nonlinearities start acting, it further decreases slowly to a value very near 0, corresponding to the steady-state value of Benney and Bergeron's result. This, of course, follows

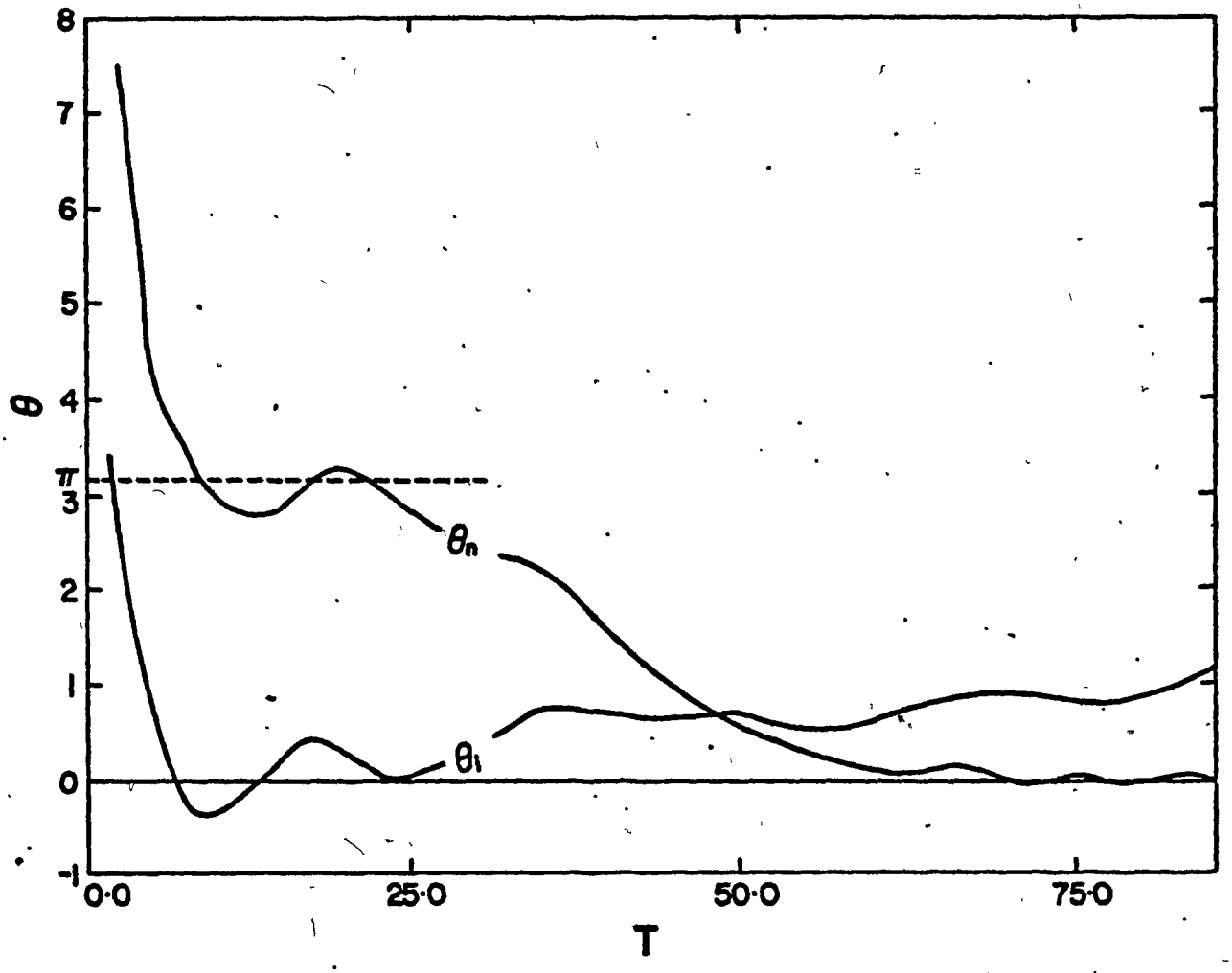

Fig. 6.11 - Complex logarithmic phase shift as a function of time in nonlinear integration; β=1.6, δ=0.16, ϵ=0.018, N=6.

closely the evolution of $\overline{u'v'}$. In fact, as we have mentioned before, a similar result can be obtained using this quantity to evaluate θ_n. Now, in both Benney and Bergeron's and Haberman's analyses, θ_i always turned out to be zero. We have plotted on the same figure θ_i as a function of time. As can be seen it is zero in the linear stage, but increases slightly as the nonlinear terms start growing, having a value of $\sim 0.5 - 0.6$ during a large part of the integration. The significance of this result is not clear. It could simply be erroneous, since it is well inside the error margin (we neglect the $t \sim 75$-80 results which are getting imprecise). However, no such error seems to be apparent in the θ_n term. We have looked at the algorithm used to evaluate θ_n and θ_i, and the error, at first glance should be equally well distributed between θ_n and θ_i. This is not the case when one evaluates A and B. It is possible to show for example that B is more precise than A. Now, since

$$\theta = \frac{i\left(A^- - A^+\right)B^*}{|B|^2 \beta}$$

and we have β, $B \neq 0$, it follows that to get $\theta_r = \theta_i = 0$, we need $A^+ = A^-$. Because of the error in A^+ and A^-, this is not the case. When the product $i(A^- - A^+)B^*$ is formed, it happens that the real part is given by the sum of two terms, approximately equal and of opposite sign. while for the imaginary part, the signs are identical. In other words, in one case, the noise (or the error) adds up, and in the other, it cancels. This is probably the reason for the non-zero θ_i. Another possibility of course, is that it might be a feature of the nonlinear time-dependent problem. This could be confirmed by an analytical solution of the problem.

Looking at B^+ and B^-, we find that they match across the C.L., the match being complete as soon as the linear stage sets in. The evolution in time of the solution can now be described as follows: in the linear stage, we have $\theta=\pi, A^+\neq A^-$, $B^+ = B^-$: The phase of the primary wave is fixed at $\pi/4$ at $y = y_0$, slopes towards the C.L., where it becomes vertical, with a constant value, dependent on β,δ and the distance between the forcing and the C.L. As the nonlinear terms start growing, B starts changing slowly; south of the C.L., the phase of the primary wave, while remaining constant in the y-direction, slowly increases to $\pi/4$; in so doing, the slope of the phase north of the C.L. diminishes, and $\overline{u'v'}$ falls to 0, when the phase is $\pi/4$ everywhere; at that point B reaches a steady value, $\Theta_r = 0$ (and $\Theta_i = .5$ or 0). Thus, even though the model is linear away from the C.L., the nonlinear interactions occurring in the critical layer force a change in A^- and B^-, which in turn modifies the solution everywhere. This shows the importance of the logarithmic phase shift: the evolution in time of this quantity is very simply related to the change in the primary wave.

6.2 VARIATION OF THE δ PARAMETER

In order to investigate further the parameter range of the problem, a series of integrations were performed with the following values of δ: 0.04, 0.16, 0.36 and 0.64. The evolution in time of the corresponding $\overline{u'v'}$ at $y \doteq 2.4$ is presented in Fig. 6.12 (south of the C.L., the wave momentum flux oscillates around zero in all cases). Looking first at the linear stage, we notice, as mentioned before, that $\overline{u'v'}_{max.}$ decreases with increasing δ .

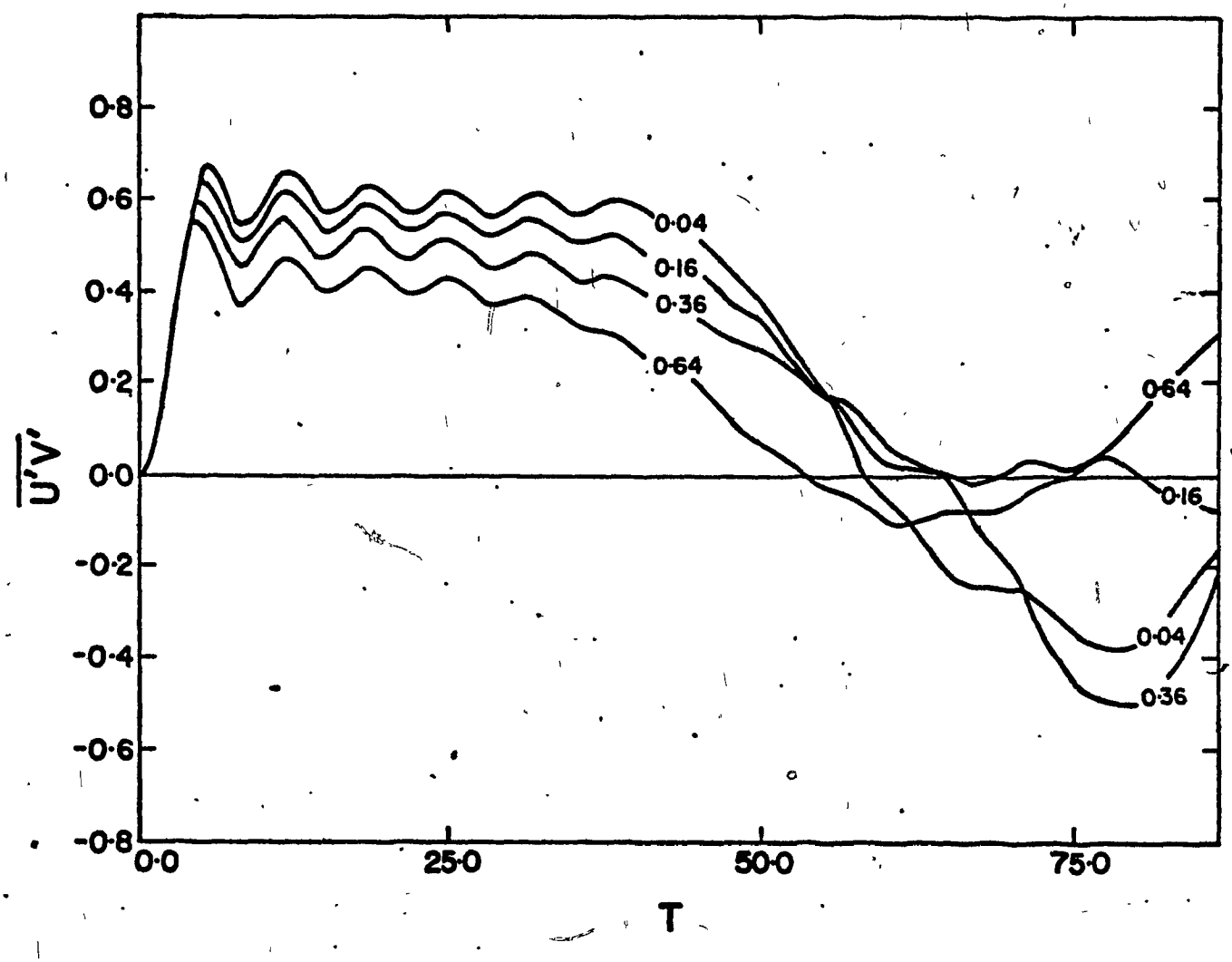

Fig. 6.12 - $\overline{u'v'}$ at y=2.4 as a function of time in nonlinear integration for different values of δ; β=1.6, ε=0.018, N=6, and δ=0.04, 0.16, 0.36, 0.64.

We also notice that for $t = 0\ (\varepsilon^{-\frac{1}{2}})$ the nonlinear $\overline{u'v'}$ starts departing from its linear value. But now, as one can see, the behaviour for $\delta = 0.04$, 0.36 and 0.64 is different from that of $\delta = 0.16$. Instead of slowly oscillating around a value of 0, $\overline{u'v'}$ becomes negative, and eventually rises back to positive values. One would be tempted to think that this behaviour is in accord with that observed by Geisler and Dickinson in their model; however, quasilinear integrations with the same values of δ, yielded quite different values of $\overline{u'v'}$. We checked that these results were not model-dependent, by modifying the forcing procedure, letting $\bar{u}$ constant in the upper grid points, checking the Poisson equation scheme, etc...

The reason behind this strange behaviour is probably the following: the two time scales $0\ (\varepsilon^{-\frac{1}{2}})$ and $0\ (\varepsilon^{-1})$ are probably not well enough separated when a value of 0.018 is used for ε. We have seen that for Benney and Bergeron's results to hold, the nonlinear interactions have to be negligible outside the critical layer. However, as shown in section 6.1.4, on a time scale of $0\ (\varepsilon^{-1})$, the model should become nonlinear everywhere. This means that the amplitudes of the harmonics should become eventually of the same order of magnitude as that of the fundamental in and out of the critical layer. In our case, $\varepsilon^{-\frac{1}{2}} = 7$, and $\varepsilon^{-1} = 54$. In other words, our period of integration clearly extends into the fully nonlinear regime. And in fact, if we look at the amplitudes of the waves, we notice that they become as big as that of the primary as t increases past $0\ (\varepsilon^{-1})$. To check that this might prove to be the correct explanation, an integration was done with $\varepsilon = 0.010$, and $\delta = 0.64$. This gives $\varepsilon^{-\frac{1}{2}} = 10$, and $\varepsilon^{-1} = 100$, so that the two time

scales are well separated. The following result was obtained : the fall of $\overline{u'v'}$ to zero was delayed due to the larger $\varepsilon^{-\frac{1}{2}}$ time scale. However, now, instead of going negative with values of $O(10^{-1})$, $\overline{u'v'}$ oscillated around zero, with an amplitude never exceeding $O(1\times10^{-2})$; in other words, the behaviour was similar to the standard $\delta = 0.16$ case. Similar results were also obtained for the $\delta = 0.04$ and $\delta = 0.36$ cases, thus adding more weight to this explanation. The fact that our standard integration did behave according to Benney and Bergeron's analysis is thus in a way fortuitous. Since our first results were obtained with $\varepsilon = 0.018$ and $\delta = 0.16$, and it is only later that we varied the parameter δ, we chose to keep it as the standard integration, as the higher value of ε used permits us to show more clearly the existence of the "quasi steady-state" characterizing the third stage.

The conclusion we draw from this experiment is that quite small values of ε are needed to separate the two time scales $\varepsilon^{-\frac{1}{2}}$ and ε^{-1} : this separation is needed if one wants to observe Benney and Bergeron's results, in the outer domain, at least. For higher values of ε (greater than say $O(10^{-2})$), the fall of $\overline{u'v'}$ to zero, even though it happens faster, might be mixed with nonlinear phenomena in the outer region.

6.3 VARIATION OF THE BETA PARAMETER

In these experiments, all parameters had their standard value, except for β which was allowed to take the following values : 1.0, 1.6, and 2.0.

The $\beta = 1.0$ integration developed instability; zonal wavenumber 2 proved to be unstable, and grew almost at the start, eventually overtaking

the primary wave. After some time, the radiation condition failed, and a blow-up was experienced. Although it is hard to pinpoint the cause of the nonlinear instability, we suspect it is the deformed basic flow; the addition of the forced wave to the hyperbolic tangent shear flow is probably unstable to wavenumber 2 for that value of β. Lorenz (1972) studied this problem, and showed that this is indeed a possible mechanism of barotropic instability. In any event, we have plotted in Fig. 6.13 the growth in time of the wave amplitude at a fixed point in y. We notice that the growth is exponential for $t < 25$, with a doubling time of 18. As the amplitude gets larger, it starts interacting nonlinearly with the other components, and departs from exponential growth. We should note here that a quasilinear integration with the same parameters remained stable, and produced an altogether different result. This is then clearly a case where a quasilinear approach would produce an erroneous result since neglect of the self-interaction of the wave changes an unstable problem into a stable one.

The $\beta = 2.0$ case yielded a truly intriguing result. Fig. 6.14 gives a plot of $\overline{u'v'}$ at $y = 2.4$ for the quasilinear and the nonlinear integration (curves 1 and 2). As can be seen, in both cases, after a certain time during which the critical layer is set up, the wave momentum flux increases relatively abruptly before eventually decreasing again. In both curves 1 and 2, $\beta_{eff.}$ has turned negative at t=30, that is, shortly before the rise. According to Geisler and Dickinson, this should be associated with a decrease in $\overline{u'v'}$; this is clearly not the case. In order to get

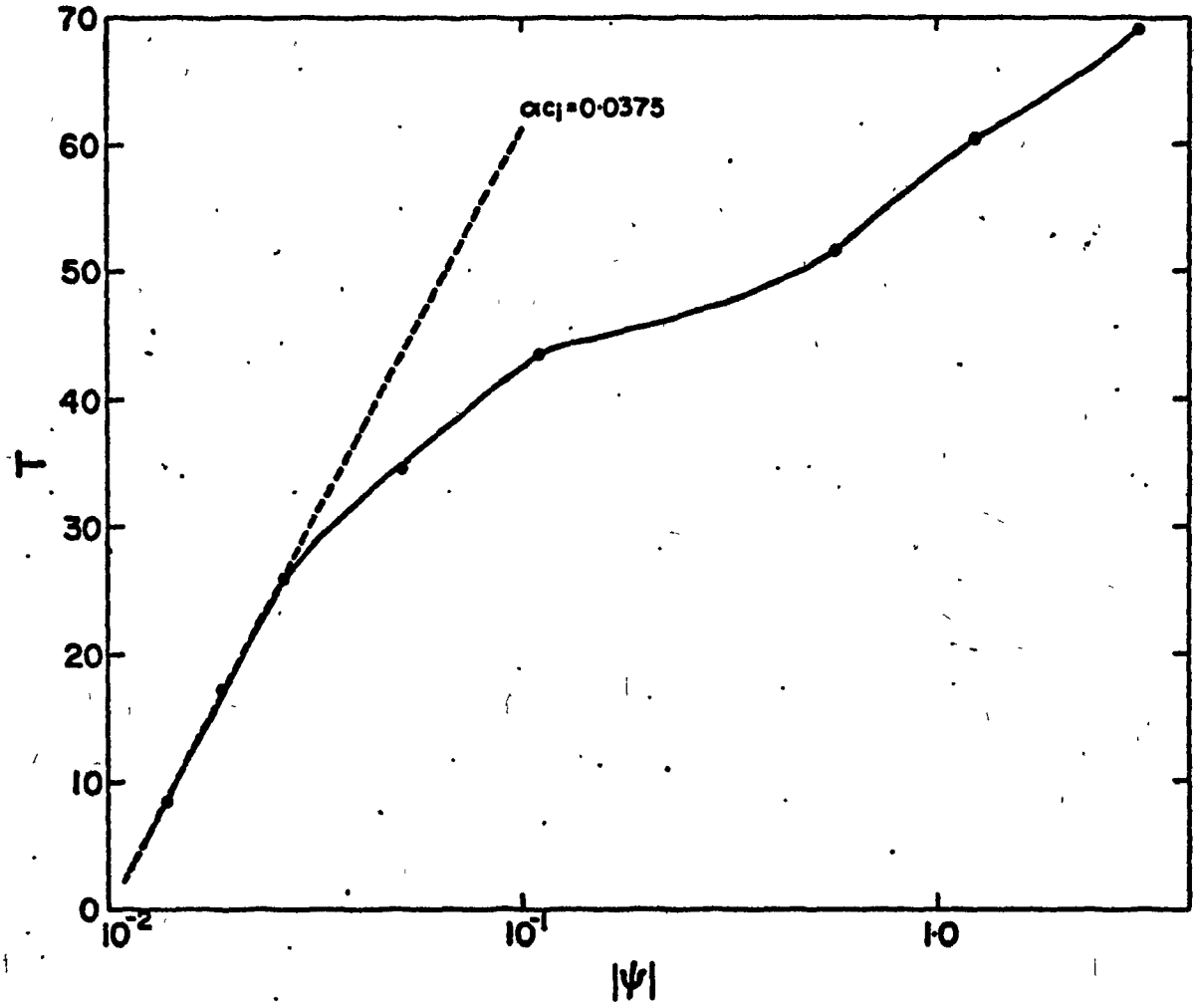

Fig. 6.13 - Growth of wavenumber 2 as a function of time in nonlinear integration; β=1.0, δ=0.16, ε=0.018, N=6.

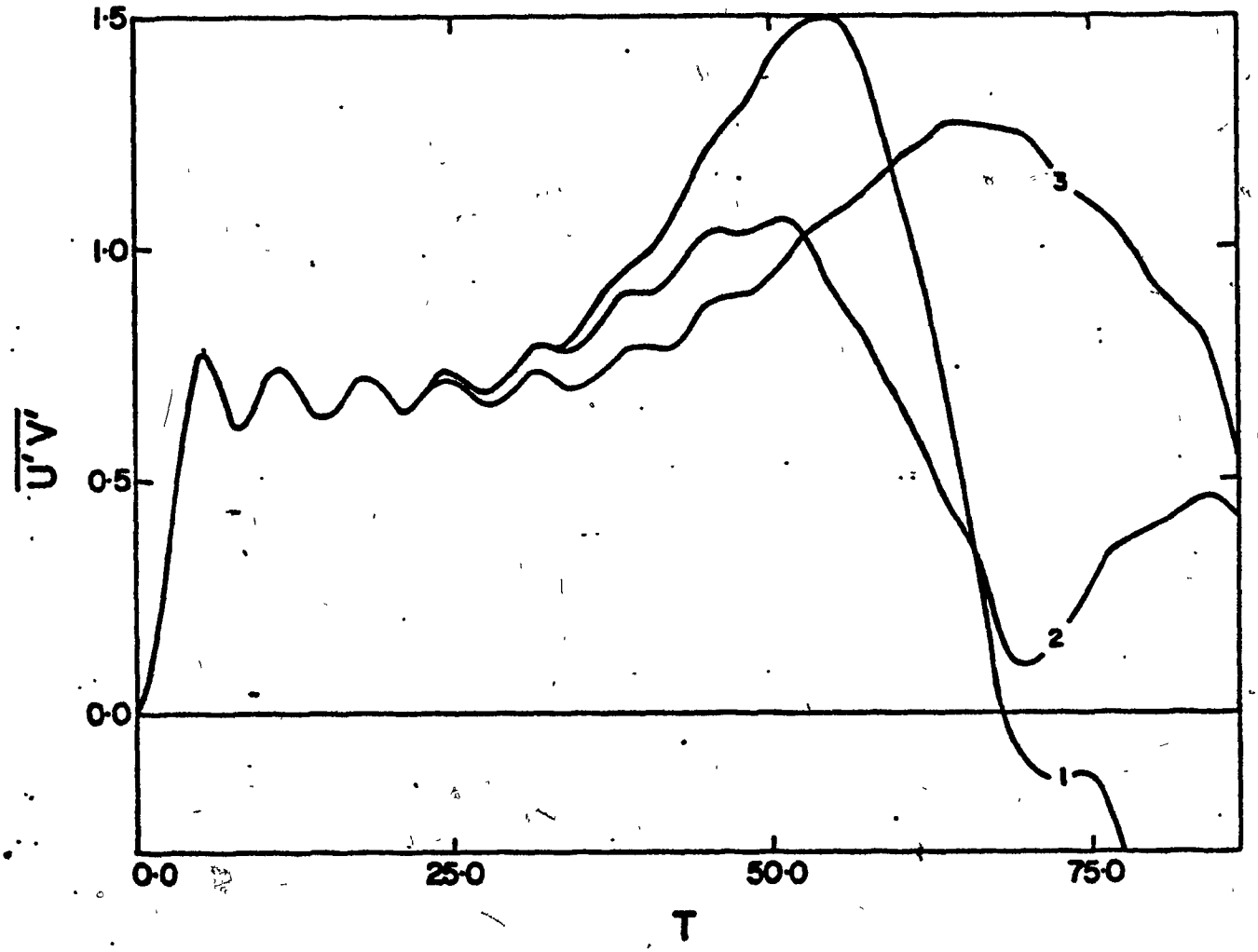

Fig. 6.14 - $\overline{u'v'}$ at y=2.4 as a function of time in nonlinear and quasilinear integrations for β=2.0; 1. quasilinear, ε=0.018, 2. nonlinear, ε=0.018, 3. nonlinear, ε=0.010.

a better separation of the time scales, another integration was done with $\varepsilon = 0.010$ (curve 3 in Fig. 6.14). Again, a similar behaviour was observed. A careful inspection of the output revealed the following: after the linear stage, the phase of the forced wave south of the C.L. has its linear value of -49 degrees; north of the C.L., $\overline{u'v'}$ is constant in y, and has its linear "steady-state" value of 0.69. It then starts growing slowly, being larger near the forcing, than near the C.L.; it can also be seen to slope from NE to SW. Simultaneously, the wave amplitude grows, until it attains a maximum amplitude of 2.5 at y = 1.75. South of the C.L., however, the phase of the wave has been steadily decreasing towards $\pi/4$. We noticed also that for the $\varepsilon = 0.010$ case, $\beta_{eff.}$ was still positive (0.85) when the increase in $\overline{u'v'}$ started. The amplitudes of the other harmonics were also very small at that time (roughly $O(\varepsilon)$ smaller than the fundamental). A short time after the maximum value of $\overline{u'v'}$ is reached at y=2.4, it becomes again constant in y north of the C.L., and then proceeds to decrease slowly, remaining constant in y.

It seems that we can attribute the increase in $\overline{u'v'}$ to the increase in the forced wave amplitude; the slope of the phase of the forced wave remains more or less constant next to the forcing wall during the increase. This growth in amplitude is clearly a nonlinear phenomenon, and since a somewhat similar behaviour is obtained in the quasilinear integration, its origin lies probably in a wave-zonal flow interaction mechanism, which for lack of analytical results is hard to pinpoint. One conclusion we draw from this experiment, and the preceding one, is that the model is quite sensitive to variations in the beta parameter. It seems that only for some limited range

of β the results of Benney and Bergeron can be reproduced with a time-dependent nonlinear model. Here again, an analytical theory would be needed to get more insight on the effect of β in the nonlinear critical layer development.

6.4 DIFFUSION

A few experiments were done with the term $\nu\nabla^4\psi$ added to the right hand side of the predictive equations. The values of ν were chosen, taking into account the value of the parameter

$$\lambda = \nu/\varepsilon^{3/2}$$

defined in Benney and Bergeron (1969) and Haberman (1972). $\lambda \ll 1$ corresponds to a very small diffusivity; this was the case treated by Benney and Bergeron. Haberman extended their analysis to the cases $\lambda = O(1)$ and $\lambda > 1$; he showed in particular that as λ is increased from values $\ll 1$ to values > 1, the logarithmic phase shift changes from 0 to $-\pi$ (see his fig. 1). This further implies that the Reynolds stress jump across the C.L. should reappear as λ is increased, or as ε is decreased, with ν finite. These results of course were derived for steady-state models, and it is not clear that they should apply to time-dependent models. However, since so far the correspondence seems to hold true in many aspects, the following experiments were done: ε was set to 0.018 as in the standard integration, and ν chosen to be equal to 2×10^{-5} and 2×10^{-4}, giving $\lambda = 0.01$ and 0.1 respectively. Fig. 6.15 is a plot of $\overline{u'v'}$ at $y = 2.4$ for the above two cases, and for the standard integration, as a function

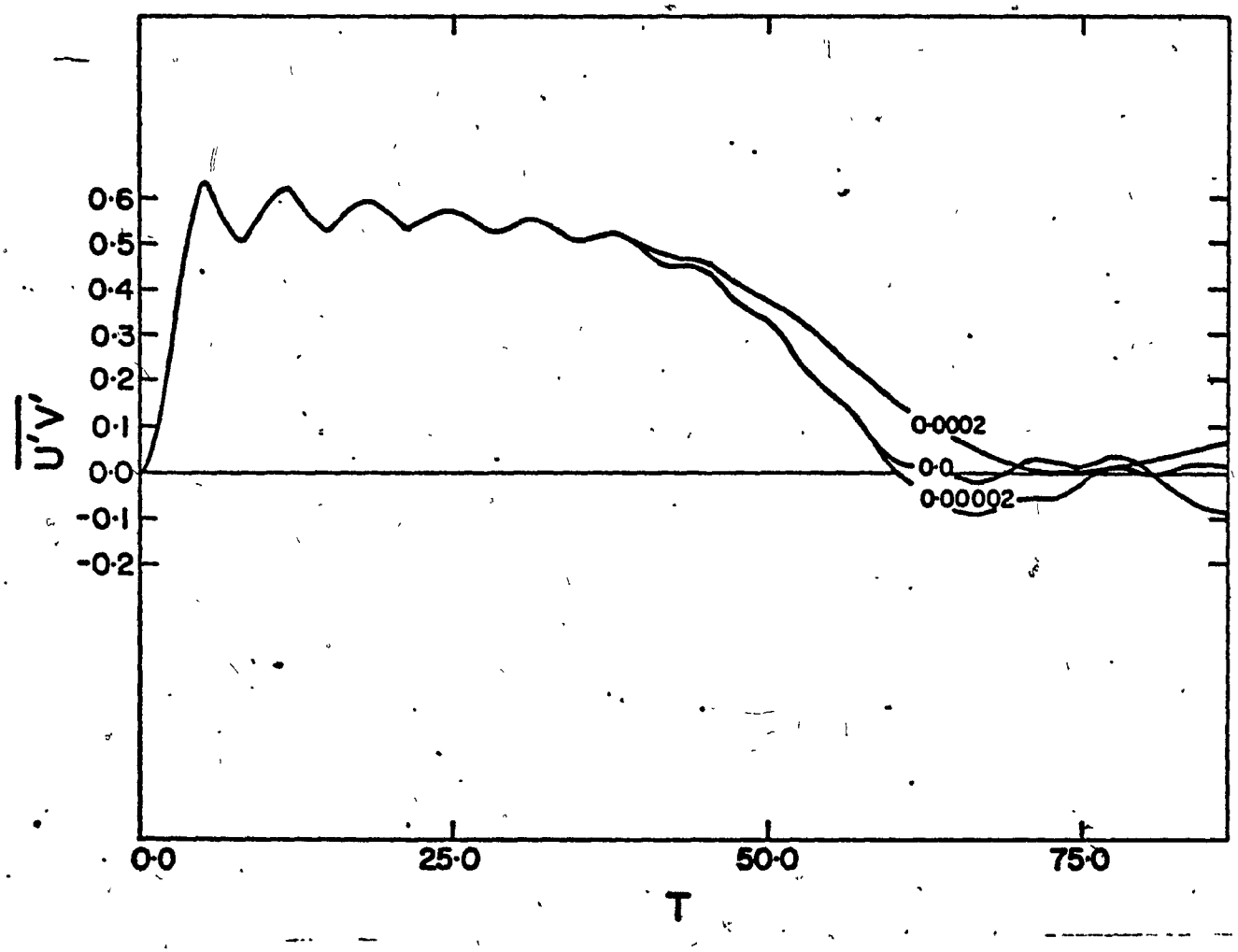

Fig. 6.15 - $\overline{u'v'}$ at y=2.4 as a function of time in nonlinear integrations with diffusion. Number on curve indicates value of ν. β=1.6, δ=0.16, ε=0.018, N=6.

of time. For $\lambda = 0.01$, the results are very close to those of the standard integration. However, for the $\lambda = 0.1$ case, some important differences arise : even at the end of the integration, a small jump in $\overline{u'v'}$ remains across the C.L. A rough evaluation of the associated phase shift gave a result which is in the range obtained by Haberman, in his Fig. 1, for that particular value of λ . The inclusion of this diffusion term also had the effect of smoothing out the wavy oscillations in y of the $\beta - \bar{u}_{yy}$ term, and also decreasing the amplitudes of the harmonics. The $\beta_{eff.}$ term, after becoming slightly negative around t=45, returned to a positive value of $0.1 \sim 0.2$ for the rest of the integration period.

We conclude from this experiment that the effect of diffusion, apart from smoothing out fine scale oscillations and decreasing slightly the amplitudes of harmonics, is to lead to a small but finite jump at the C.L. in the wave momentum flux, as suggested by Haberman.

6.5 LARGE ε CASE

So far, we have only investigated the small ε parameter range; in particular, we have shown that for values of $\varepsilon \sim O(10^{-2})$, all the results described in the standard case hold in the interval $O(\varepsilon^{-\frac{1}{2}}) < t < O(\varepsilon^{-1})$. Now, in many physical applications, ε is quite large. In order to study the development for a larger ε , an integration was performed with $\varepsilon = 0.18$, that is a value ten times larger than before. We will now describe the results.

Obviously, the two time scales are now almost identical, since $O(\varepsilon^{-\frac{1}{2}}) \cong 2$, and $O(\varepsilon^{-1}) \cong 5$. Hence, we should expect the model to become nonlinear everywhere much faster than before. This was indeed observed, since the model became unstable roughly at t = 25 (because of the failure of the radiation condition). However, quite surprisingly, in the small time span $0 < t < 20$, a development qualitatively similar to that of the $\varepsilon = 0.018$ case was observed. We have plotted in Fig. 6.16 $\overline{u'v'}$ as a function of y at t = 8.6 and t = 19.2. As can be observed, at t = 8.6, a linear "quasi-steady-state" has developed, in which the Reynolds stress is constant above the C.L., and jumps to zero across it. As t increases, $\overline{u'v'}$ decreases to zero, and the jump disappears completely; this is realized at t = 19. During this time span, the wave momentum flux of the other harmonics remains very small (of $O(10^{-2})$) at most, even though at t=19, their amplitudes are getting to be of the order of that of the primary wave. We should note that there is no increase in the amplitudes of the harmonics, or of the primary wave, south of the C.L. at that time: they all display an exponential like decay for $y < 0$. This is clearly a different result from that obtained by Ward (1974).

Another of Ward's contentions is that when nonlinear interactions are allowed, the ledge observed in Geisler and Dickinson's experiments does not form. Instead, the mean flow supposedly loses momentum uniformly, and the profile is slowly drawn upwards towards the source. We have plotted in Fig. 6.17 the mean flow configuration at t = 4.3 and t = 19.2. At t = 4.3, the critical layer has not yet developed, and the profile is almost similar

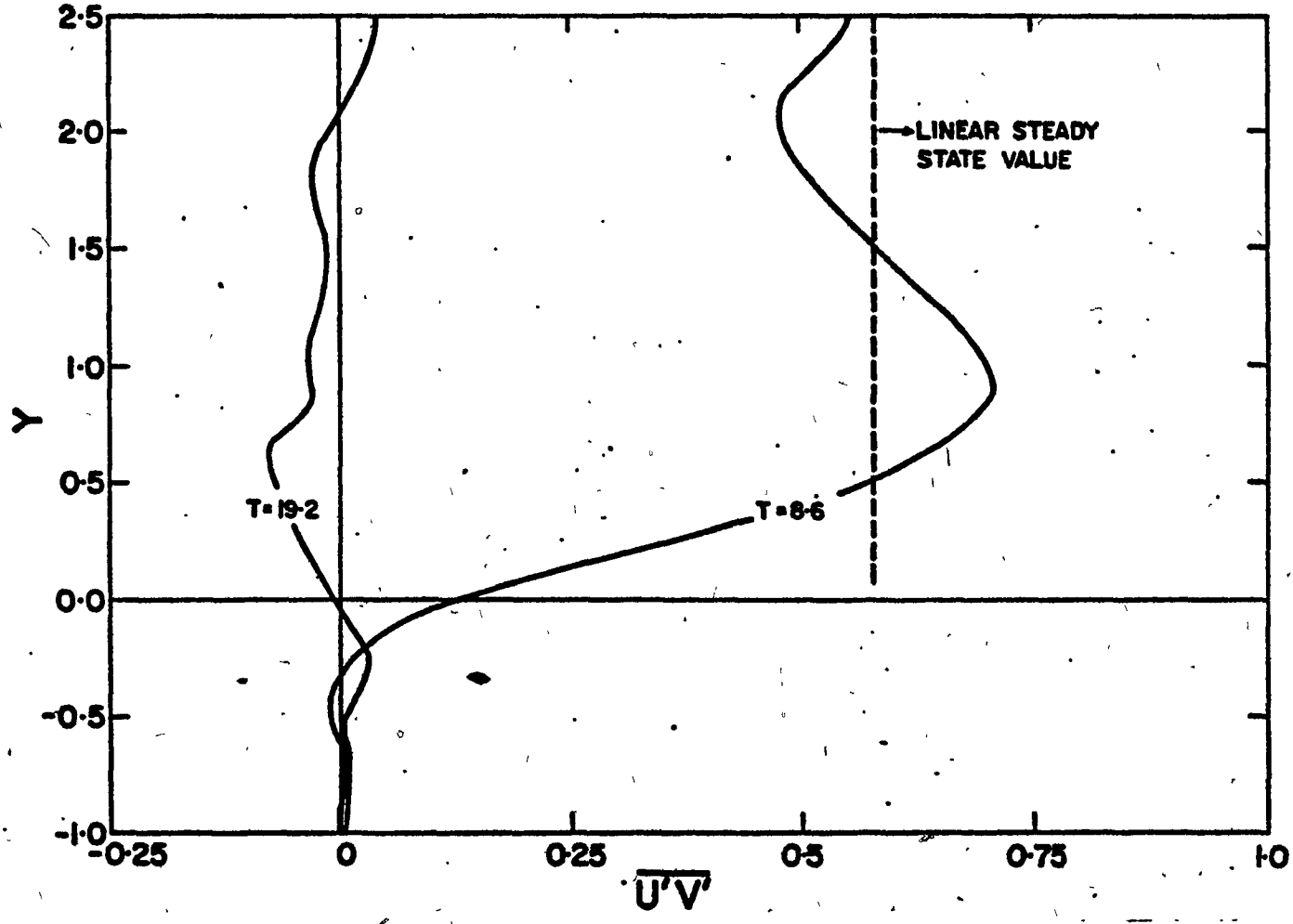

Fig. 6.16 - $\overline{u'v'}$ as a function of y in large ε experiment; number on curve indicates time. $\beta=1.6, \delta=0.16, \varepsilon=0.18, N=6$.

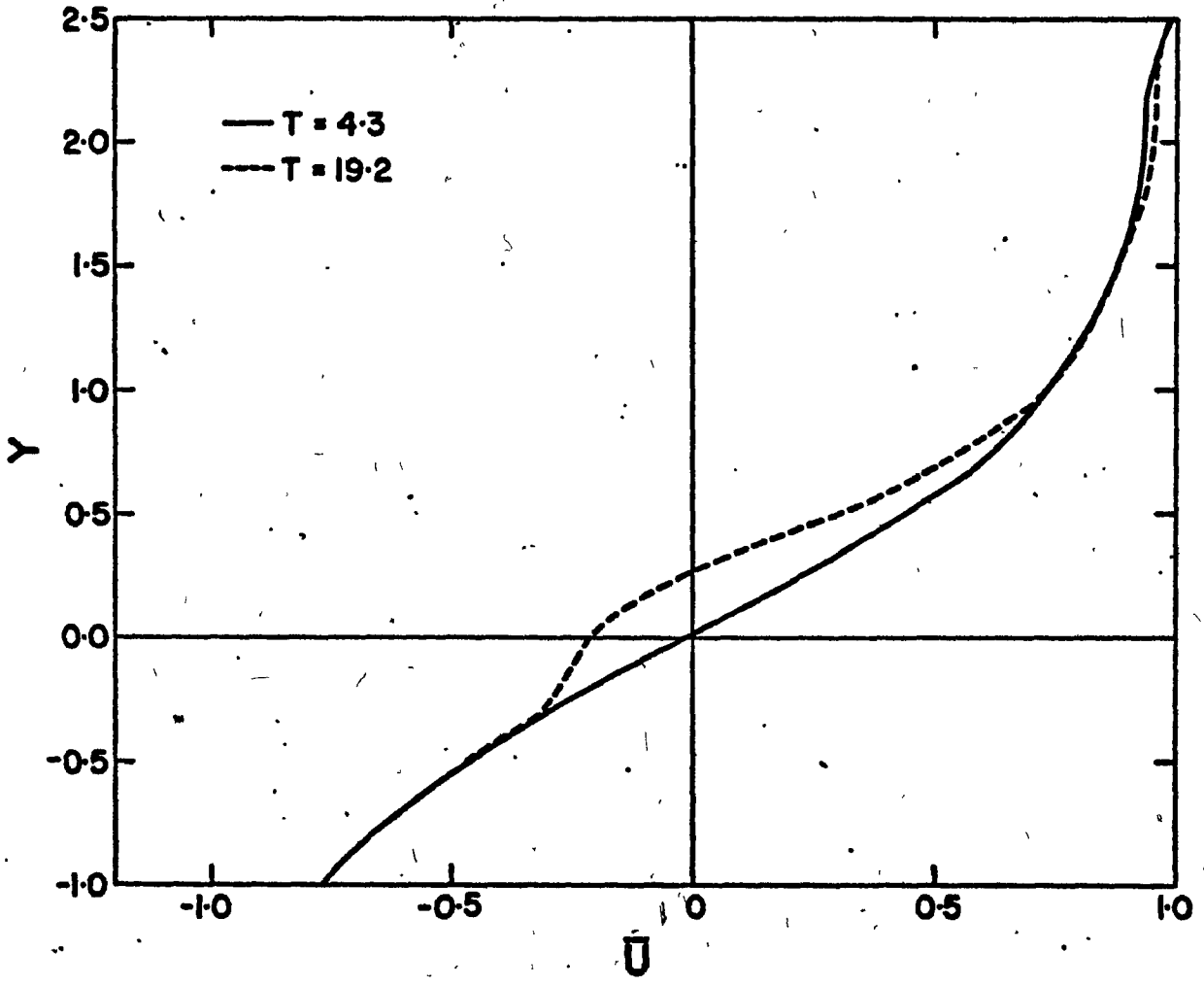

Fig. 6.17 - Mean flow profile as a function of y in large ε experiment; number on curve indicates time. β =1.6, δ =0.16, ε =0.18, N=6.

to the initial profile, except for a small deformation near the forcing boundary (which does not affect the development). However, at t = 19.2, we can observe a well-defined ledge. The C.L. has moved northward by a distance y = 0.25, that is, a distance which is in agreement with our previous experiments (i.e. $O(\varepsilon)$). Thus the result again disagrees somewhat with Ward's.

The conclusion we draw from this experiment is that even for a moderately large value of ε, the transient nonlinear critical layer development is similar in all respects to the small ε case. The important difference is now that because of the coalescence of the ε^{-1} and $\varepsilon^{-\frac{1}{2}}$ time scales, the "outer solution steady-state" does not appear, and the model becomes rapidly fully nonlinear, and eventually, in our case, unstable. The cause of this instability is hard to specify: it could be a numerical instability, for the radiation condition was derived for linear conditions at y = 1.25; the limited number of harmonics (6) could also be a possible cause.

6.6 FORCING EXPERIMENTS

Two experiments were conducted in order to check the effect of a finite time forcing, and that of a standing wave forcing; the forcing procedure used was previously described in section 5.2; in the first experiment, however, the forced wave amplitude was brought back to a value of 0.1 instead of 0 as numerical problems were encountered for the latter value.

In the first experiment (i.e. that of a finite time forcing) the following results were obtained: after an initial increase in $\overline{u'v'}$ near $y=y_0$, the wave momentum flux decreases to a smaller value corresponding to that of the linear steady-state value for that particular value of the forcing amplitude; the initial pulse eventually reaches the C.L., where it is absorbed, without producing any nonlinear critical layer development; during the course of the integration, however, $\beta_{eff.}$ does develop a number of wavy oscillations similar to the ones observed in the standard case. At the end of the integration period, some indication of numerical instability is present: the cause certainly lies in the fact that the profiles show quite large oscillations of finer and finer scales. These are produced by the e^{iyt} terms, whose "effect" is enhanced by the fact that the "steady" values are now very small. The mesh finally proves to be too coarse to resolve the oscillations.

In the second experiment, the fact that some energy is allowed to leak through the C.L., since one of the two traveling waves has no C.L., and is able to propagate freely, eventually produces an increase in the amplitudes of some of the harmonics south of the C.L. Again the radiation condition fails rapidly, and after a sudden increase in $\overline{u'v'}$ south of the C.L., a blow-up is experienced. North of the C.L., the development follows closely the pattern set by the standard integration. A jump develops, and eventually, there is a decrease in the wave momentum flux; the process is however interrupted abruptly by what is happening in the south.

The conclusion we draw from these experiments is that the model is certainly not suited to yield definitive results for this type of experiments : the boundary condition was not designed for such forcings; nevertheless, the earlier part of the development seems to agree with what was said earlier. Of particular interest is the problem of the finite time switch-on; it would be interesting to see if for some critical amplitude a nonlinear critical layer development could be triggered, even though the forcing amplitude has been brought back to zero. Some changes in the model will have to made before that problem can be tackled. As for the second problem, it is not clear yet what type of boundary condition would be best suited.

6.7 EFFECT OF INITIALLY DEFORMED MEAN FLOW OR "WAVE-WAVE ONLY" INTERACTIONS

Under this heading, we shall describe two experiments; the first one was designed to check the importance of the "zero" harmonic (i.e. the mean flow deformation), in the evolution of the critical layer. To achieve this, only wave-wave interactions were allowed. The parameters had their usual standard values. This means that (2.8.a) is replaced by $\frac{\partial \bar{u}}{\partial t} = 0$. The results, surprisingly enough, were almost identical to those of the linear integration. The wave momentum flux is identical, in time and in space, the forced wave amplitude and phase almost equal to their linear counterpart. The amplitude of the harmonics themselves is at least $O(\varepsilon)$ smaller than that of the fundamental throughout the integration period. Thus, even though it is quite small, the mean flow deformation is of paramount importance in the evolution towards the nonlinear steady-state.

In the second experiment, we performed a linear integration using the deformed mean flow of the standard nonlinear integration at t=60.48 as the initial mean wind profile. At this time, in the nonlinear integration, $\overline{u'v'}$ has fallen to zero north of the C.L., and $\beta - u_{yy}$ has gone negative at three or four places around the C.L., now at y = 0.03. The idea behind the experiment is to see if a linear steady state solution can be obtained, which would resemble the standard nonlinear solution at t = 60.48. The results confirmed only partly this hypothesis. The linear solution did possess some of the features of the nonlinear solution. For example, $\overline{u'v'}$ north of the C.L. does decay to zero; it however does not remain zero, and starts oscillating around this value: the integration did not extend long enough to see if this oscillation would eventually decay to zero. In Fig. 6.18, we have plotted the linear wave amplitude at t = 35, along with the amplitude of the corresponding forced wave in the nonlinear integration. As can be seen, they show a similar shape, even though the values are somewhat different. The phase structure is similar at that time, $\overline{u'v'}$ being zero in both cases. No instability was observed, even though the Rayleigh criterion was violated (it is however only a necessary condition).

We draw the following two conclusions from these experiments: 1) Neglect of the mean flow interaction term in the nonlinear problem leads to a completely erroneous result, at least for the case where a C.L. is present; 2) use of an observed "deformed" profile to construct a linear steady-state solution will probably give a reasonable result, at least for the case of weak nonlinearities.

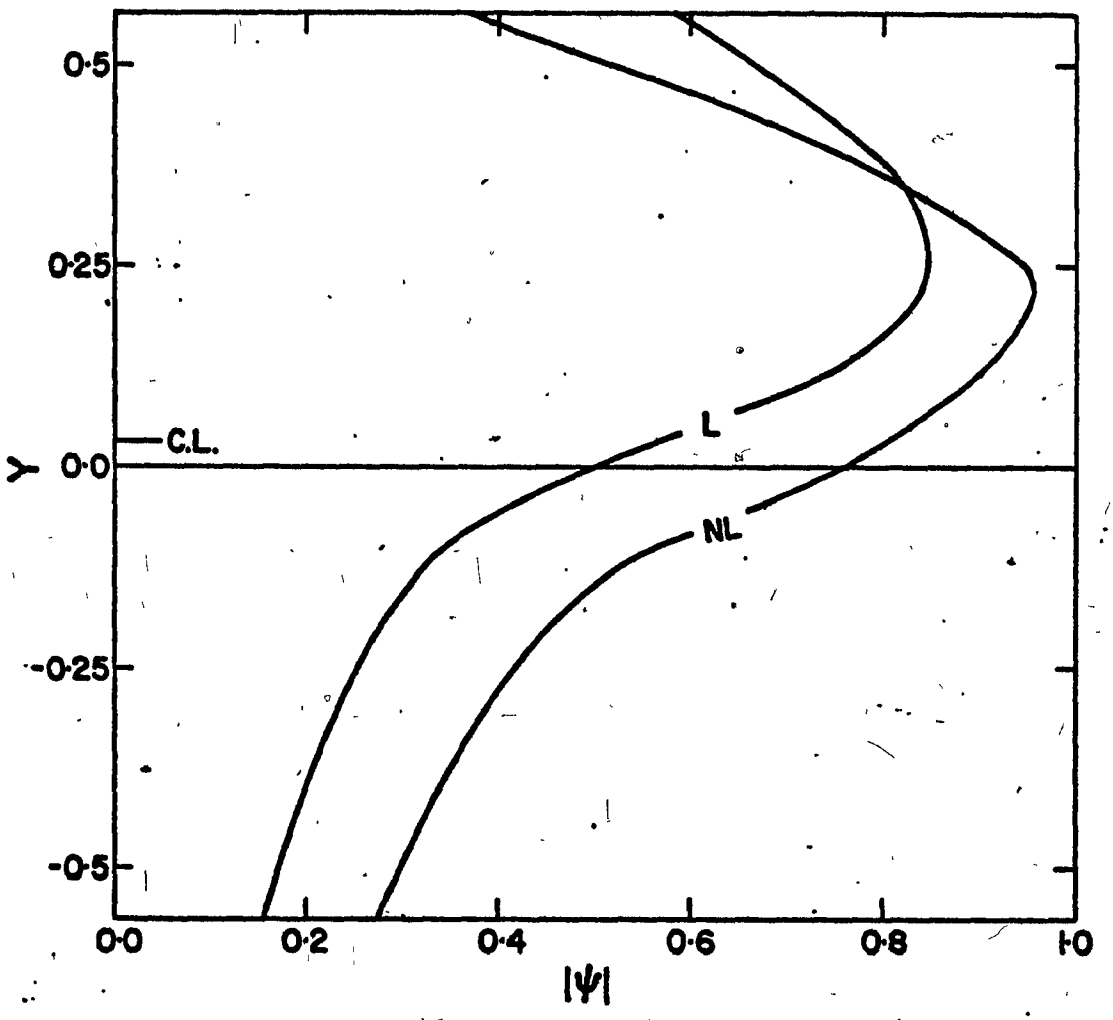

Fig. 6.18 - Primary wave amplitude in deformed mean flow integration. Curve labeled "L" is for linear integration, and "NL" for nonlinear integration.

CHAPTER 7. CONCLUSION

At the beginning of this work, we have put forth a number of questions. We feel we are now in a position to answer these questions, and perhaps add a few additional comments to what has already been said.

The main result of the thesis is to have shown that it is indeed possible to reach a steady-state for the nonlinear Rossby wave critical level problem, at least in the outer layer, which is similar to the one obtained by Benney and Bergeron, and Davis. This steady-state, as we have seen, is quite different from the linear steady-state, in that it is characterized by a total reflection of the wave at the C.L., in contrast to the absorption which characterizes the linear problem. This steady-state differs also from that of a quasilinear integration in many respects: even though they both predict a zero jump in $\overline{u'v'}$, the structure of the critical layer is markedly different, due to the presence of higher harmonics. It was also shown that the approach to that steady-state is completely different, in that the cycling of wave momentum flux in and out of the critical layer region is totally absent, and that no definite correlation between the oscillations of $\beta - u_{yy}$ and the evolution of $\overline{u'v'}$ was found. In all of the integrations for which a critical level concept holds, no significant propagation of wave energy south of the C.L. was observed. A final remark that should also be made about the main result is the following: the steady-state that we reach in the outer layer should really be called a "quasi" steady-state, for the transients excited by the switch-on procedure eventually grow in time, such that for $t \sim O(\varepsilon^{-1})$, the model becomes nonlinear everywhere, in which case the critical level concept fails to apply. Due to resolution problems, it was not possible for us to

integrate long enough to obtain useful information about what happens after that.

Interesting results were also obtained from a number of different experiments, two of which we shall discuss here. In one of these, we added an eddy diffusion term to the vorticity equation. The results tended to support Haberman's conclusion that as viscosity is increased, a jump in $\overline{u'v'}$ reappears. In other words, the ratio of nonlinearity to viscosity is also of importance in the time-dependent problem, as quite different results are obtained depending on the value of the "λ" parameter. In the second experiment, the value of ε was increased to 0.18, that is a value ten times larger than that of the standard experiment. Now for such a large value, the concept of a critical level singularity barely applies, since presumably the nonlinear terms should be retained in the equation for the whole domain. Nevertheless, a development quite similar qualitatively, and for some time, quantitatively, to that of the small ε case was observed. In particular, the migration of the C.L. was again of $O(\varepsilon)$, and a total reflection of the wave was observed, with the corresponding disappearance of the jump in $\overline{u'v'}$. The interest in this case lies in the fact that in the atmosphere, values of ε of $O(10^{-1})$ are more often encountered than those of $O(10^{-2})$.

Before going on to talk of the relevance of these results to the "real" atmosphere, we would like to make three remarks. The first is about the migration of the C.L. In all of our experiments, this migration is at most of $O(\varepsilon)$; and once the C.L. has migrated this distance, it stops. Thus, it does not make much sense to try to explain the displacement of a zero wind line

over many hundreds or thousands of kilometers by a critical layer interaction (in our $\varepsilon = 0.18$ integration for example, the migration was less than 6° lat.). This is not to say that a zero wind line cannot move for such a large distance: but the mechanism by which the migration is effected is certainly not a critical layer interaction. The second is about the argument that adding nonlinearities in a critical layer problem could permit energy transfer through the C.L. For any problem for which a critical level singularity can be defined (and that implies a small ε), this is not the case (we assume here that the $\bar{u}$ profile is such that the waves are evanescent south of the C.L.; obviously, if one forces from the evanescent side of the C.L., then wave energy propagation across the critical line is possible). The third and final remark is about using critical layer concepts for cases where ε is large. This is incorrect. This remark is related to the previous one in that it is quite possible that for a large ε , some energy transfer might be observed. For example, waves could be excited south of an ill-defined C.L. This is however a completely nonlinear phenomenon, and none of the conclusions obtained using critical layer theory remain valid anymore.

We now arrive at the final and perhaps most important question: is the Rossby wave nonlinear critical level an important phenomenon in the atmosphere? We should stress here that the barotropic vorticity equation is obviously a very crude approximation to the atmosphere, and as such, all our conclusions should be viewed in light of this limitation. That being understood, we can say the following. For small values of ε , that is of $O(10^{-2})$, the time scales involved are so large that it is quite improbable that a

nonlinear steady state may ever be reached, due to the natural variability of the atmosphere. For the standard integration, assuming the values given in section 2.3.5 for the dimensional parameters, it would take 175 days to reach the steady state. For wavenumber 10, and a maximum wind speed of 20 $m\text{-}s^{-1}$, this drops to 17.5 days, still a quite large delay, although it is more reasonable. For values of ε of $O(10^{-1})$, the critical layer development is much faster. As an example, our large ε experiment, for the values quoted above, gave times of 60 days and 6 days respectively. The last value is clearly small enough for the phenomenon to happen. Still smaller values would be obtained for a higher wind speed. However, for such values of ε , the concept of a critical level becomes questionable, although the development (at least for $\varepsilon=0.18$) seems to be qualitatively similar to the standard small ε case. Another aspect that should be taken into account is the time scale of the natural variability of the atmosphere. If this time scale is long enough, then obviously it could be possible to get a nonlinear critical layer development. On the other hand, if it is too short even for a linear critical layer development, nothing much can be said. In fact, we could summarize the above considerations in the following way.

Let us define some climatological mean state of the atmosphere, characterized by a mean wind profile $\bar{U}$, and some forcing acting on a very large time scale (in fact $t\to\infty$). Then, if we let t_U stand for the time scale of the natural variability of the atmosphere (this would imply for example that the C.L. would move in time due to some external cause), t_L for the time scale of the linear critical layer, and t_{NL} for the time scale of the nonlinear critical layer, the following four cases could possibly describe what happens in the atmosphere:

time scale interval	steady state phase shift
$t_U > t_{NL}$	$\theta = 0°$
$t_U \sim t_{NL}$	?
$t_L < t_U < t_{NL}$	$(\theta = -\pi)$?
$t_U < t_L$	?

In other words, if t_U is larger than t_{NL}, the steady state configuration would be characterized by a zero logarithmic phase shift, and no jump in $\overline{u'v'}$ across the C.L. Then, one could say : yes, the nonlinear Rossby wave critical level is an important phenomenon in the atmosphere. If on the other hand $t_U \sim t_{NL}$, then our study cannot be used to reach a conclusion. This would be an interesting problem to study. If $t_L < t_U < t_{NL}$, then it is only possible that a $-\pi$ phase shift, and hence a linear critical layer phenomenon, might be a correct representation of the situation. This problem could also be tackled using a model quite similar to ours. Finally, for $t_U < t_L$, no conclusion can as yet be reached. Thus we see that it is possible to answer that question only if t_U is known, and $> t_{NL}$. For all the other cases, we can only speculate.

In any case, we feel that one of the most important results of this study is with respect to other types of atmospheric waves. The reason is that the results obtained for the Rossby wave, although they cannot be extended to gravity waves, for example, clearly show that a totally different result is obtained from a nonlinear critical level than from a linear critical level. We feel it would thus prove worthwhile to study the case of other atmospheric waves (gravity waves, for example) since the time scales involved might be more relevant to the atmosphere. Such studies might show that a linear

treatment of the C.L. is wrong, and lead to new results. Another field worth looking into is that of the vertical propagation of Rossby waves, in the presence of a C.L. So far, only linear or quasilinear studies have been made. The results obtained using a nonlinear model could prove to be very interesting, particularly with respect to the sudden stratospheric warming phenomenon. We finally conclude by noting that this study has raised a lot of questions, some of which we intend to pursue further in the near future.

APPENDIX A: THE MODEL EQUATIONS

Equation (2.4) can be written as

$$\frac{\partial \zeta}{\partial t} + J(\psi, \zeta) + \beta \frac{\partial \psi}{\partial x} = 0 \qquad \text{(A-1)}$$

where :

$$\psi(x,y,t) = \sum_{m=0}^{N} \left\{ A^m(y,t) \cos mx + B^m(y,t) \sin mx \right\} \qquad \text{(A-2)}$$

$$\zeta = \nabla^2 \psi = \sum_{m=0}^{N} \left\{ \zeta^{A^m} \cos mx + \zeta^{B^m} \sin mx \right\} \qquad \text{(A-3)}$$

and

$$\zeta^{A^m} = A^m_{yy} - m^2 \delta A^m \quad ; \quad \zeta^{B^m} = B^m_{yy} - m^2 \delta B^m \qquad \text{(A-4)}$$

The n=0 harmonic corresponds to the mean flow; the harmonics are truncated at n=N (usually 6 in the model), and no negative wavenumbers are allowed. We are using the energy-preserving Jacobian, that is we write

$$J(\psi, \zeta) = \frac{\partial}{\partial y}\left(\zeta \frac{\partial \psi}{\partial x}\right) - \frac{\partial}{\partial x}\left(\zeta \frac{\partial \psi}{\partial y}\right) \qquad \text{(A-5)}$$

Substitution of (A-2) and (A-3) in (A-5) yields:

$$\frac{\partial}{\partial y}\left(S\frac{\partial \psi}{\partial x}\right) = \sum_{m=0}^{N}\sum_{l=0}^{L} l\left(C_1^{m,l}\sin mx\cos lx - C_2^{m,l}\sin mx\sin lx + C_3^{m,l}\cos mx\cos lx - C_4^{m,l}\cos mx\sin lx\right) \qquad (A\text{-}6)$$

$$\frac{\partial}{\partial x}\left(S\frac{\partial \psi}{\partial y}\right) = \frac{\partial}{\partial x}\left\{\sum_{m=0}^{N}\sum_{l=0}^{L}\left(D_1^{m,l}\sin mx\sin lx + D_2^{m,l}\sin mx\cos lx + D_3^{m,l}\cos mx\sin lx + D_4^{m,l}\cos mx\cos lx\right)\right. \qquad (A\text{-}7)$$

where:

$$C_1^{m,l} = \frac{\partial}{\partial y}\left(S^{A^m}A^l\right) \qquad D_1^{m,l} = S^{A^m}A_y^l$$

$$C_2^{m,l} = \frac{\partial}{\partial y}\left(S^{A^m}B^l\right) \qquad D_2^{m,l} = S^{A^m}B_y^l$$

$$C_3^{m,l} = \frac{\partial}{\partial y}\left(S^{B^m}A^l\right) \qquad D_3^{m,l} = S^{B^m}A_y^l$$

$$C_4^{m,l} = \frac{\partial}{\partial y}\left(S^{B^m}B^l\right) \qquad D_4^{m,l} = S^{B^m}B_y^l$$

We will be using the following identities:

$$\begin{aligned}
\sin nx\sin lx &= \tfrac{1}{2}(\cos(n-l)x - \cos(n+l)x)\\
\sin nx\cos lx &= \tfrac{1}{2}(\sin(n-l)x + \sin(n+l)x)\\
\sin lx\cos nx &= \tfrac{1}{2}(\sin(l-n)x + \sin(n+l)x)\\
\cos nx\cos lx &= \tfrac{1}{2}(\cos(n-l)x + \cos(n+l)x)
\end{aligned} \qquad (A\text{-}8)$$

The zonal flow equation (2.13) is obtained by integrating (A-1) from 0 to 2π, using the following identities:

$$\begin{aligned}
&\frac{1}{2\pi}\int_0^{2\pi} \sin nx \cos \ell x \, dx = 0 \\
&\frac{1}{2\pi}\int_0^{2\pi} \sin nx \sin \ell x \, dx = \begin{cases} \frac{1}{2} & n = \ell \\ 0 & n \neq \ell \end{cases} \\
&\frac{1}{2\pi}\int_0^{2\pi} \cos nx \cos \ell x \, dx = \begin{cases} \frac{1}{2} & n = \ell \\ 0 & n \neq \ell \end{cases} \\
&\frac{1}{2\pi}\int_0^{2\pi} \sin nx \, dx = \frac{1}{2\pi}\int_0^{2\pi} \cos nx \, dx = 0
\end{aligned} \tag{A-9}$$

We get

$$\frac{\partial}{\partial t} B^0_{yy} = -\sum_{m=0}^{N} \frac{m}{2}\left(C_3^{m,m} - C_2^{m,m}\right)$$

since $B^0 = \overline{\Psi}(y,t)$, and substituting for $C_3^{n,n}$ and $C_2^{n,n}$, we get

$$\frac{\partial \overline{\zeta}}{\partial t} = -\sum_{m=0}^{N} \frac{m}{2}\left\{\frac{\partial}{\partial y}\left(A^m \zeta^{B^m}\right) - \frac{\partial}{\partial y}\left(B^m \zeta^{A^m}\right)\right\}$$

Again, we have $\overline{\zeta} = -\frac{\partial \overline{u}}{\partial y}$, so that we can integrate once with respect to y, to finally obtain (2.13):

$$\frac{\partial \overline{u}}{\partial t} = \sum_{m=0}^{N} \frac{m}{2}\left(A^m \zeta^{B^m} - B^m \zeta^{A^m}\right) \tag{A-10}$$

The A^p equation is obtained by multiplying (A-1) by sin px, and taking $\frac{1}{2\pi}\int_0^{2\pi}(\,)\,dx$ of the resulting equation. In the "$\frac{\partial}{\partial y}$" part of the Jacobian, only the $C_1^{n,\ell}$ and $C_4^{n,\ell}$ terms contribute; we have:

$$\frac{1}{2}\sum_{m=0}^{N}\sum_{\ell=0}^{L}\left\{\ell C_1^{m,\ell}\frac{1}{2\pi}\int_0^{2\pi}\left(\sin(m-\ell)\alpha\sin p\alpha+\sin(m+\ell)\sin p\alpha\right)d\alpha\right\}$$

$$-\frac{1}{2}\sum_{m=0}^{N}\sum_{\ell=0}^{L}\left\{\ell C_4^{m,\ell}\frac{1}{2\pi}\int_0^{2\pi}\left(\sin(\ell-m)\alpha\sin p\alpha+\sin(m+\ell)\alpha\sin p\alpha\right)d\alpha\right\}$$

Using formulas (A-8), the integrals can be rewritten as follows :

$$\frac{1}{2}\sum_{m=0}^{N}\sum_{\ell=0}^{L}\left\{\ell C_1^{m,\ell}\frac{1}{4\pi}\int_0^{2\pi}\left[\underset{(1)}{\cos(m-\ell-p)\alpha}-\underset{(2)}{\cos(m-\ell+p)\alpha}+\underset{(3)}{\cos(m+\ell-p)\alpha}-\underset{(4)}{\cos(m+\ell+p)\alpha}\right]d\alpha\right\}$$

$$-\frac{1}{2}\sum_{m=0}^{N}\sum_{\ell=0}^{L}\left\{\ell C_4^{m,\ell}\frac{1}{4\pi}\int_0^{2\pi}\left[\underset{(5)}{\cos(\ell-m-p)\alpha}-\underset{(6)}{\cos(\ell-m+p)\alpha}+\underset{(7)}{\cos(m+\ell-p)\alpha}-\underset{(8)}{\cos(m+\ell+p)\alpha}\right]d\alpha\right\}$$

Using (A-9), we get the following results for the above eight integrals (e.g. $\frac{1}{4\pi}\int_0^{2\pi}(\quad)d\alpha$)

(1) = $\frac{1}{2}$ for $n = p+\ell$

(2) = $-\frac{1}{2}$ for $n = \ell - p$

(3) = $\frac{1}{2}$ for $n = p - \ell$

(4) = $-\frac{1}{2}$ for $n = -p-\ell$

(5) = $-\frac{1}{2}$ for $n = \ell - p$

(6) = $\frac{1}{2}$ for $n = \ell + p$

(7) = $-\frac{1}{2}$ for $n = p - \ell$

(8) = $\frac{1}{2}$ for $n = -p - \ell$

Since we require $n \geq 0$, (4) and (8) must be discarded; the final result is then:

$$\frac{1}{4}\sum_{\ell=0}^{L}\ell\left\{C_1^{p+\ell,\ell}+C_1^{p-\ell,\ell}-C_1^{\ell-p,\ell}-C_4^{\ell-p,\ell}-C_4^{p-\ell,\ell}+C_4^{p+\ell,\ell}\right\} \qquad \text{A-11}$$

where it is understood that only terms with positive indices are retained, and $p + \ell \leq L$. The "$\frac{\partial}{\partial \pi}$" part of the Jacobian is integrated by parts to yield terms of the form

$$\Big[\quad\Big]_0^{2\pi} - p\int_0^{2\pi}\Big[\quad\Big]\,d\pi$$

where the parenthesis encloses a product of 3 trigonometric functions. The first parenthesis is obviously 0, and we are left with

$$-\tfrac{1}{2}\sum_{n=0}^{N}\sum_{\ell=0}^{L}\Big\{p D_1^{n,\ell}\,\frac{1}{2\pi}\int_0^{2\pi}\big[\cos(m-\ell)\pi\cos p\pi - \cos(m+\ell)\pi\cos p\pi\big]\,d\pi$$

$$-\tfrac{1}{2}\sum_{n=0}^{N}\sum_{\ell=0}^{L}\Big\{p D_4^{n,\ell}\,\frac{1}{2\pi}\int_0^{2\pi}\big[\cos(m-\ell)\pi\cos p\pi + \cos(m+\ell)\pi\cos p\pi\big]\,d\pi$$

Again, using (A-8), the integrals can be simplified as follows:

$$-\tfrac{1}{2}\sum_{n=0}^{N}\sum_{\ell=0}^{L} p D_1^{n,\ell}\,\frac{1}{4\pi}\int_0^{2\pi}\big[\underbrace{\cos(m-\ell-p)\pi}_{(1)} + \underbrace{\cos(m-\ell+p)\pi}_{(2)} - \underbrace{\cos(m+\ell-p)\pi}_{(3)} - \underbrace{\cos(m+\ell+p)\pi}_{(4)}\big]\,d\pi$$

$$-\tfrac{1}{2}\sum_{n=0}^{N}\sum_{\ell=0}^{L} p D_4^{n,\ell}\,\frac{1}{4\pi}\int_0^{2\pi}\big[\underbrace{\cos(m-\ell-p)\pi}_{(5)} + \underbrace{\cos(m-\ell+p)\pi}_{(6)} + \underbrace{\cos(m+\ell-p)\pi}_{(7)} + \underbrace{\cos(m+\ell+p)\pi}_{(8)}\big]\,d\pi$$

Using (A-9), we then get the following results for the above integrals:

(1) = $-\frac{1}{2}$ for $n = \ell + p$

(2) = $-\frac{1}{2}$ for $n = \ell - p$

(3) = $\frac{1}{2}$ for $n = p - \ell$

(4) = $\frac{1}{2}$ for $n = -p - \ell$

(5) = $-\frac{1}{2}$ for $n = \ell + p$

(6) = $-\frac{1}{2}$ for $n = \ell - p$

(7) = $-\frac{1}{2}$ for $n = p - \ell$

(8) = $-\frac{1}{2}$ for $n = -p - \ell$

Again, we discard (4) and (8) since $n \gg 0$; the result is finally

$$\frac{1}{4}\sum_{\ell=0} p\left\{ D_1^{p-\ell,\ell} - D_1^{\ell+p,\ell} - D_1^{\ell-p,\ell} - D_4^{\ell+p,\ell} - D_4^{\ell-p,\ell} - D_4^{p-\ell,\ell} \right\} \qquad \text{(A-12)}$$

The complete Jacobian can now be written as (A-11) - (A-12). The beta term gives:

$$\beta p \sum_{n=0}^{N} \left\{ \frac{1}{2\pi} A^n \int_0^{2\pi} \cos nx \sin px \, dx - \frac{1}{2\pi} B^n \int_0^{2\pi} \sin nx \sin px \, dx \right\} = -\tfrac{1}{4}\beta p B^p \qquad \text{(A-13)}$$

The vorticity tendency term gives:

$$\frac{\partial}{\partial t}\left\{ \sum_{n=0}^{N} \left[\frac{1}{2\pi} S^{A^n} \int_0^{2\pi} \sin nx \sin px \, dx + \frac{1}{2\pi} S^{B^n} \int_0^{2\pi} \cos nx \sin px \, dx \right] \right\} = \frac{1}{2}\frac{\partial}{\partial t} S^{A^p} \qquad \text{(A-14)}$$

We can further isolate the wave-zonal flow interaction terms in the following way. First notice that these terms are characterized by the appearance of a zero value in one of the two indices n, ℓ in the interaction terms "$C^{n,\ell}$" and "$D^{n,\ell}$". This is because, as noted earlier, harmonic number zero corresponds to the zonal flow. Looking at (A-11) and (A-12), we note that a zero index can appear when either $\ell = 0$, or $|p - \ell| = 0$. For $\ell = 0$, (A-11) is identically zero, while (A-12) yields

$$p/4\left\{ D_1^{p,0} - D_1^{p,0} - D_1^{-p,0} - D_4^{p,0} - D_4^{-p,0} - D_4^{p,0} \right\}$$

Now, as mentioned before, we retain only interaction terms with positive indices; since $D_4^{p,0} = S^{B^p} B_y^0$, we end up with

$$-\tfrac{p}{2} S^{B^p} B_y^0$$

Extracting now the terms with $|p-\ell| = 0$ in (A-11) and (A-12), and noting that $C_1^{0,p}$ is zero, we get

$$\frac{\rho}{2}\left\{-C_4^{0,p} + D_4^{0,p}\right\}$$

which can be written as

$$-\frac{\rho}{2}\left\{\frac{\partial}{\partial y}\left(\zeta^{B^0}B^p\right) - \zeta^{B^0}B_y^p\right\}$$

Using the fact that $B^0 = \bar{\psi}$, $B_y^0 = -\bar{u}$ and $\zeta^{B^0} = B_{yy}^0 = -\bar{u}_y$, the wave-zonalflow interaction terms can be written as

$$\frac{\rho}{2}\left\{-\bar{v}\zeta^{B^p} + \frac{\partial}{\partial y}\left(\bar{u}_y B^p\right) - \bar{u}_y B_y^p\right\}$$

This is the energy-preserving form for the linear Jacobian. Now in our model, we found that because of the error introduced by evaluating the $\frac{\partial}{\partial y}(\bar{u}_y B^p)$ derivative at the first interior grid point (notice that $\bar{u}_y$ is not given on the boundary and has to be computed by an off-centered difference scheme), it did not matter whether the energy-conserving form was used or the simpler form

$$\frac{\rho}{2}\left\{-\bar{v}\zeta^{B^p} + B^p\bar{u}_{yy}\right\}$$

which has the advantage of avoiding the computation of $\bar{u}_y$ at the boundary. Since integrations with both forms yielded similar results, we chose to use the latter form as it was simpler to implement. The nonlinear part of the Jacobian does however remain energy-conserving. We can now write down the complete predictive equation for the A^p component, with

the linear wave-zonal flow interaction terms isolated, by starting the summation in (A-11) and (A-12) at $\ell = 1$, and requiring $|\ell - p| \neq 0$, since these terms are now written separately. This yields:

$$\frac{\partial}{\partial t} S^{Ap} = p\left[\bar{u} S^{Bp} + B^p(\beta - \bar{u}_{yy})\right] - \frac{1}{2}\sum_{\ell=1}^{L} \ell\left[C_1^{p+\ell,\ell} + C_1^{p-\ell,\ell} - C_1^{\ell-p,\ell}\right.$$

$$\left. + C_4^{p+\ell,\ell} - C_4^{|\ell-p|,\ell}\right] + p\left[D_1^{p+\ell,\ell} + D_1^{\ell-p,\ell} - D_1^{p-\ell,\ell} + D_4^{p+\ell,\ell} + D_4^{|\ell-p|,\ell}\right] \qquad \text{(A-15)}$$

where we require $|\ell - p| \neq 0$, $p+\ell \leq L$, and again retain only the interaction terms which have positive indices.

Equation (2.12) can be derived in a similar fashion. We multiply (A-1) by cos px, and integrate from 0 to 2π. In the "$\frac{\partial}{\partial y}$" part of the Jacobian, only the $C_2^{n,\ell}$ and $C_3^{n,\ell}$ terms contribute, and we get:

$$-\frac{1}{2}\sum_{m=0}^{N}\sum_{\ell=0}^{L} \ell C_2^{m,\ell} \frac{1}{2\pi}\int_0^{2\pi}\left[\cos(n-\ell)x \cos px - \cos(n+\ell)x \cos px\right] dx$$

$$+\frac{1}{2}\sum_{m=0}^{N}\sum_{\ell=0}^{L} \ell C_3^{m,\ell} \frac{1}{2\pi}\int_0^{2\pi}\left[\cos(n-\ell)x \cos px + \cos(n+\ell)x \cos px\right] dx$$

Again, using (A-8) and (A-9), we obtain:

$$-\frac{1}{2}\sum_{m=0}^{N}\sum_{\ell=0}^{L} \ell C_2^{m,\ell} \frac{1}{4\pi}\int_0^{2\pi}\Big[\underbrace{\cos(n-\ell-p)x}_{(1)} + \underbrace{\cos(n-\ell+p)x}_{(2)} - \underbrace{\cos(n+\ell-p)x}_{(3)} - \underbrace{\cos(n+\ell+p)x}_{(4)}\Big] dx$$

$$+\frac{1}{2}\sum_{m=0}^{N}\sum_{\ell=0}^{L} \ell C_3^{m,\ell} \frac{1}{4\pi}\int_0^{2\pi}\Big[\underbrace{\cos(n-\ell-p)x}_{(5)} + \underbrace{\cos(n-\ell+p)x}_{(6)} + \underbrace{\cos(n+\ell-p)x}_{(7)} + \underbrace{\cos(n+\ell+p)x}_{(8)}\Big] dx$$

with the following values for the integrals (of the form $\frac{1}{4\pi}\int_0^{2\pi}(\ )dx$) :

(1) $= -\frac{1}{2}$ for $n = p + \ell$

(2) $= -\frac{1}{2}$ for $n = \ell - p$

(3) $= \frac{1}{2}$ for $n = p - \ell$

(4) $= \frac{1}{2}$ for $n = -\ell - p$

(5) $= \frac{1}{2}$ for $n = \ell + p$

(6) $= \frac{1}{2}$ for $n = \ell - p$

(7) $= \frac{1}{2}$ for $n = p - \ell$

(8) $= \frac{1}{2}$ for $n = -p - \ell$

Again, (4) and (8) are discarded, and we get:

$$\frac{1}{4}\sum_{\ell=0}^{L}\ell\left(C_2^{p-\ell,\ell} - C_2^{\ell-p,\ell} - C_2^{p+\ell,\ell} + C_3^{p+\ell,\ell} + C_3^{\ell-p,\ell} + C_3^{p-\ell,\ell}\right) \qquad \text{(A-17)}$$

In the "$\frac{\partial}{\partial A^p}$" part of the Jacobian, only the $D_2^{m,\ell}$ and $D_3^{m,\ell}$ terms contribute, and integrating by parts as for the A^p component, we end up with the following:

$$\frac{1}{2}\sum_{m=0}^{N}\sum_{\ell=0}^{L} p D_2^{m,\ell}\frac{1}{2\pi}\int_0^{2\pi}\left[\sin(m-\ell)x\sin px + \sin(m+\ell)x\sin px\right]dx$$

$$+\frac{1}{2}\sum_{m=0}^{N}\sum_{\ell=0}^{L} p D_3^{m,\ell}\frac{1}{2\pi}\int_0^{2\pi}\left[\sin(\ell-m)x\sin px + \sin(m+\ell)x\sin px\right]dx$$

Using (A-8) and (A-9), we get

$$\frac{1}{2}\sum_{m=0}^{N}\sum_{\ell=0}^{L} p D_2^{m,\ell}\frac{1}{4\pi}\int_0^{2\pi}\underbrace{\cos(n-\ell-p)x}_{(1)} - \underbrace{\cos(n-\ell+p)x}_{(2)} + \underbrace{\cos(n+\ell-p)x}_{(3)} - \underbrace{\cos(n+\ell+p)x}_{(4)}\Big]dx$$

$$+\frac{1}{2}\sum_{m=0}^{N}\sum_{\ell=0}^{L} p D_3^{m,\ell}\frac{1}{4\pi}\int_0^{2\pi}\underbrace{\cos(\ell-n-p)x}_{(5)} - \underbrace{\cos(\ell-n+p)x}_{(6)} + \underbrace{\cos(n+\ell-p)x}_{(7)} - \underbrace{\cos(n+\ell+p)x}_{(8)}\Big]dx$$

with:

(1) = ½ for n=p+ℓ

(2) = -½ for n = ℓ - p

(3) = ½ for n = p - ℓ

(4) = - ½ for n = -p -ℓ

(5) = ½ for n = ℓ - p

(6) = -½ for n = ℓ + p

(7) = ½ for n = p -ℓ

(8) = -½ for n = -p - ℓ

Discarding (4) and (8), we get :

$$\frac{1}{4}\sum_{\ell=0}^{L} p\left[D_2^{p+\ell,\ell} - D_2^{\ell-p,\ell} + D_2^{p-\ell,\ell} + D_3^{\ell-p,\ell} - D_3^{p+\ell,\ell} + D_3^{p-\ell,\ell}\right] \qquad \text{(A-18)}$$

Again, we can write the linear interaction terms separately by extracting the $\ell = 0$, $p - \ell = 0$ and $\ell - p = 0$ terms from (A-17) and (A-18); their sum is

$$-\tfrac{1}{2}(D_2^{p,0} + D_3^{0,p}) + \tfrac{1}{2}pC_3^{0,p}$$

or, in terms of A_p and B_p:

$$\frac{p}{2}\left[S_y^{B^0} A^p - S^{A^p} B_y^0\right]$$

Since $B_y^0 = -\bar{u}$, and $S_y^{B^0} = -\bar{u}_{yy}$, we can rewrite as :

$$\tfrac{1}{2}p\left(\bar{v}\, S^{A^p} - A^p \bar{v}_{yy}\right)$$

The beta term integrates to :

$$\beta \sum_{m=0}^{N} m\left[A^m \frac{1}{2\pi}\int_0^{2\pi} \cos mx \cos px\, dx - B^m \frac{1}{2\pi}\int_0^{2\pi} \sin mx \cos px\, dx\right] = \tfrac{1}{2}p\beta A^p$$

and the vorticity tendency term to:

$$\frac{\partial}{\partial t}\left[\sum_{n=0}^{N}\left\{\zeta^{A^n}\frac{1}{2\pi}\int_0^{2\pi}\sin nx\cos px\,dx+\zeta^{B^n}\frac{1}{2\pi}\int_0^{2\pi}\cos nx\cos px\,dx\right\}\right]=\frac{1}{2}\frac{\partial}{\partial t}\zeta^{B^p}$$

The complete equation can now be written:

$$\frac{\partial}{\partial t}\zeta^{B^p}=p\left(A^p\bar{v}_{yy}-\bar{v}\zeta^{A^p}-\beta A^p\right)-\frac{1}{2}\sum_{l=0}^{L}\left\{l\left(C_2^{p-l,l}-C_2^{l-p,l}-C_2^{p+l,l}+C_3^{p+l,l}+C_3^{|p-l|,l}\right)\right.$$

$$\left.-p\left(D_2^{p+l,l}-D_2^{l-p,l}+D_2^{p-l,l}+D_3^{|l-p|,l}-D_3^{p+l,l}\right)\right\}$$

(A-19)

where we require $|p-l|\neq 0$, $p+l\leq L$, and we retain only interaction terms with positive indices. Equations (A-10), (A-16) and (A-19) are the three predictive equations used in the numerical model.

APPENDIX B : TOLLMIEN-KUO SOLUTIONS

The equation to be solved is

$$\phi'' - \left(\frac{\bar{u}'' - \beta}{\bar{u} - c} + \alpha^2 \right) \phi = 0 \qquad \text{(B-1)}$$

At $y = 0$, $\bar{u} = c$, so that there is a regular singular point at $y = 0$.

Let :

$$f(y) = \left(\frac{\bar{u}'' - \beta}{\bar{u} - c} + \alpha^2 \right)$$

Then :

$$\phi'' - f(y)\,\phi = 0 \qquad \text{(B-2)}$$

Let :

$$f(y) = \sum_{m=-1}^{\infty} a_m y^m \qquad \text{(B-3)}$$

$$\phi_a(y) = y^n \sum_{m=0}^{\infty} b_m y^m \qquad \text{(B-4)}$$

Let $y - y_c = Y$, y_c being the point where $\bar{u} = c$; we expand around this point $\bar{u}$ and $\bar{u}''$ in Taylor series:

$$\bar{u} - c = Y\bar{u}'_c + \frac{Y^2}{2}\bar{u}''_c + \frac{Y^3}{6}\bar{u}'''_c + \ldots$$

$$\bar{u}'' = u''_c + Y\bar{u}'''_c + \frac{Y^2}{2}\bar{u}^{IV}_c + \ldots$$

Using the fact that $(1+x)^{-1} = 1 - x + x^2 - x^3 + \ldots$, one obtains the following series for $f(y)$:

$$f(y) = a_{-1}/y + a_0 + a_1 y + a_2 y^2 + a_3 y^3 + a_4 y^4 + O(y^5) \qquad \text{(B-5)}$$

where

$$a_{-1} = \frac{\bar{v}_c'' - \beta}{\bar{v}_c'}$$

$$a_0 = \frac{\bar{v}_c'''}{\bar{v}_c'} - (\bar{v}_c'' - \beta)\frac{\bar{v}_c''}{2\bar{v}_c'^2} + \alpha^2$$

$$a_1 = (\bar{v}_c'' - \beta)\left\{\frac{\bar{v}_c''^2}{4\bar{v}_c'^3} - \frac{\bar{v}_c^{iv}}{6\bar{v}_c'^2}\right\} - \frac{\bar{v}_c'''\bar{v}_c''}{2\bar{v}_c'^2} + \frac{\bar{v}_c^{iv}}{2\bar{v}_c'}$$

$$a_2 = \frac{1}{\bar{v}_c'^4}\left\{\frac{(\beta - \bar{v}_c'')\bar{v}_c''^3}{8}\right\} + \frac{1}{\bar{v}_c'^3}\left\{\frac{5}{12}\bar{v}_c'''\bar{v}_c''^2 - \frac{\beta\bar{v}_c^{iv}\bar{v}_c''}{6}\right\} + \frac{1}{\bar{v}_c'^2}\left\{-\frac{7}{24}\bar{v}_c''\bar{v}_c^{iv} + \frac{\beta\bar{v}_c^{iv}}{24} - \frac{\bar{v}_c'''^2}{6}\right\} + \frac{\bar{v}_c^{v}}{6\bar{v}_c'}$$

$$a_3 = \frac{1}{\bar{v}_c'^5}\left\{\frac{(\bar{v}_c'' - \beta)\bar{v}_c''^4}{16}\right\} + \frac{1}{\bar{v}_c'^4}\left\{\frac{(\beta - \bar{v}_c'')\bar{v}_c'''\bar{v}_c''^2}{8} - \frac{\bar{v}_c'''\bar{v}_c''^3}{8}\right\} + \frac{1}{\bar{v}_c'^3}\left\{\frac{(\bar{v}_c'' - \beta)(6\bar{v}_c^{iv}\bar{v}_c'' + 4\bar{v}_c'''^2)}{144}\right.$$

$$\left. + \frac{\bar{v}_c'''^2\bar{v}_c''}{6} + \frac{\bar{v}_c''^2\bar{v}_c^{iv}}{8}\right\} + \frac{1}{\bar{v}_c'^2}\left\{\frac{-(\bar{v}_c'' - \beta)\bar{v}_c^{v}}{120} - \frac{\bar{v}_c^{iv}\bar{v}_c^{iv}}{24} - \frac{\bar{v}_c'''\bar{v}_c^{iv}}{12} - \frac{\bar{v}_c^{v}\bar{v}_c''}{12}\right\} + \frac{1}{\bar{v}_c'}\left\{\frac{\bar{v}_c^{vi}}{24}\right\}$$

$$a_4 = \frac{(\bar{v}_c'' - \beta)}{\bar{v}_c'}\left\{\frac{-\bar{v}_c^{vi}}{720\bar{v}_c'} + \frac{1}{\bar{v}_c'^2}\left(\frac{\bar{v}_c^{v}\bar{v}_c''}{120} + \frac{\bar{v}_c^{iv}\bar{v}_c'''}{72}\right) - \frac{1}{240\bar{v}_c'^3}\left(\frac{3\bar{v}_c^{iv}\bar{v}_c''^2}{4} + \bar{v}_c'''^2\bar{v}_c''\right) + \frac{1}{12}\frac{\bar{v}_c'''\bar{v}_c''^3}{\bar{v}_c'^4}\right.$$

$$\left. - \frac{\bar{v}_c''^5}{32\bar{v}_c'^5}\right\} + \frac{\bar{v}_c'''}{\bar{v}_c'}\left\{-\frac{\bar{v}_c^{v}}{120\bar{v}_c'} + \frac{1}{144\bar{v}_c'^2}\left(6\bar{v}_c^{iv}\bar{v}_c'' + 4\bar{v}_c'''^2\right) - \frac{1}{8}\frac{\bar{v}_c'''\bar{v}_c''^2}{\bar{v}_c'^3} + \frac{\bar{v}_c''^4}{16\bar{v}_c'^4}\right\}$$

$$+ \frac{\bar{v}_c^{iv}}{2\bar{v}_c'}\left\{\frac{-\bar{v}_c^{iv}}{240\bar{v}_c'} + \frac{\bar{v}_c'''\bar{v}_c''}{6\bar{v}_c'^2} - \frac{\bar{v}_c''^3}{8\bar{v}_c'^3}\right\} + \frac{\bar{v}_c^{v}}{6\bar{v}_c'}\left\{\frac{-\bar{v}_c'''}{6\bar{v}_c'} + \frac{\bar{v}_c''^2}{4\bar{v}_c'^2}\right\} + \frac{\bar{v}_c^{vi}}{240\bar{v}_c'}\left\{\frac{-\bar{v}_c''}{2\bar{v}_c'}\right\} + \frac{\bar{v}_c^{vii}}{120\bar{v}_c'}$$

Substituting (B-4) and (B-3) in (B-2) gives the indicial equation for r; the two roots are r = 1 and r = 0. Choosing r = 1 yields the following formulae for the "b_n" coefficients (the substitution $n \to n+1$ has been made).

$$
\begin{aligned}
b_1 &= 1 \\
b_2 &= \frac{a_{-1} b_1}{2} \\
b_3 &= \frac{a_{-1} b_2 + a_0 b_1}{6} \\
&\vdots \\
b_n &= \frac{a_{-1} b_{n-1} + a_0 b_{n-2} + \cdots + a_{n-3} b_1}{n(n-1)} \qquad , \quad n > 1
\end{aligned}
\tag{B-6}
$$

Since the two roots of the indicial equation differ by an integer, another linearly independent solution is given by:

$$\phi_b(y) = C \phi_a \ln y + \sum_{m=0}^{\infty} c_m y^m \tag{B-7}$$

Substituting (B-7) and (B-3) into (B-2) yields the following formulae for the "c_n" coefficients:

$$
\begin{aligned}
c &= a_{-1} \\
c_0 &= 1 \\
c_1 &= 0 \\
c_2 &= \frac{a_{-1} c_1 + a_0 c_0 - 3 c b_2}{2}
\end{aligned}
$$

$$c_3 = \frac{a_{-1}c_2 + a_0 c_1 + a_1 c_0 - 5cb_3}{6}$$

$$\vdots$$

$$c_n = \frac{a_{-1}c_{n-1} + a_0 c_{n-2} + \cdots + a_{n-2}c_0 - (2n-1)cb_n}{n(n-1)} \quad , n>1 \qquad \text{(B-8)}$$

(B-7) and (B-4) are the so-called "Tollmien solutions" (here, a "β" term is added in the Rayleigh equation), rewritten explicitly below as:

$$\Phi_a = \gamma + b_2\gamma^2 + b_3\gamma^3 + b_4\gamma^4 + \cdots + b_n\gamma^n$$

$$\Phi_b = 1 + c\Phi_a \ln\gamma + c_2\gamma^2 + c_3\gamma^3 + \cdots + c_n\gamma^n$$

APPENDIX C: THE RADIATION CONDITION

The integral appearing in (2.18.a) and (2.18.b) is evaluated using the trapezoidal rule; that is, we let $t = \ell\Delta t$, $\ell = 0,1,\ldots,L$, and we write:

$$\int_0^{L\Delta t} f(t)\,dt = \frac{\Delta t}{2}\left[f(0) + 2f(\Delta t) + 2f(2\Delta t) + \cdots + 2f((L-1)\Delta t) + f(L\Delta t)\right]$$

It is obvious that the values of the stream function tendencies at $t = L\Delta t$ are unknown; so we break up the right hand side of (2.18.a) and (2.18.b) into two parts: one which contains known values (that is values evaluated at $t = (L-1)\Delta t$ and less) and one containing the unknown values. The part containing values at $t = (L-1)\Delta t$ and less will be designated by w_A in (2.18.a) and w_B in (2.18.b). We further let B_m and A_m stand for $\frac{\partial B}{\partial t}\Big|_{\ell\Delta t, m\Delta y}$ and $\frac{\partial A}{\partial t}\Big|_{\ell\Delta t, m\Delta y}$ respectively, and let $h_R(\ell\Delta t)$ and $h_I(\ell\Delta t)$ stand for $\mathrm{Re}\{h(t)\}$ and $\mathrm{Im}\{h(t)\}$ in (2.17). We also let :

$$A_m = A_m^h + A_m^p = C_A I_m + D_A H_m + A_m^p$$

$$B_m = B_m^h + B_m^p = C_B I_m + D_b H_m + B_m^p$$

with

$$I_m = e^{(\lambda+\pi)(m-M)}$$

$$H_m = e^{\lambda(m-M)} \sinh \pi(m-M)$$

"h" and "p" stand for homogeneous and particular solution respectively. We recall that the unknowns are D_A and D_B, C_A and C_B having been determined by using the northern boundary condition. We also define:

$$\Delta f = -\frac{\partial f}{\partial y}\Big|_{y=0} = \frac{1}{2\Delta y}\left[3f(y) - 4f(y+\Delta y) + f(y+2\Delta y)\right]$$

In all of the above, "ℓ" designates the time step, "m" the gridpoint and "n" the wave number. Substituting in (2.18a) and (2.18b), we obtain the following

$$C_A \Delta I_1 + D_A \Delta H_1 + m\delta^{1/2} C_A I_1 + m\delta^{1/2} D_A H_1 = -\frac{\Delta t}{2} h_I(0) \left[B_1^\rho + C_B I_1 + D_B H_1 \right]$$

$$+ \frac{\Delta t}{2} h_R(0) \left[A_1^\rho + C_A I_1 + D_A H_1 \right] - w_A - \Delta A_1^\rho - m\delta^{1/2} A_1^\rho \qquad \text{(C-1)}$$

$$C_B \Delta I_1 + D_B \Delta H_1 + m\delta^{1/2} C_B I_1 + m\delta^{1/2} D_B H_1 = \frac{\Delta t}{2} h_R(0) \left[B_1^\rho + C_B I_1 + D_B H_1 \right]$$

$$+ \frac{\Delta t}{2} h_I(0) \left[A_1^\rho + C_A I_1 + D_A H_1 \right] + w_B - \Delta B_1^\rho - m\delta^{1/2} B_1^\rho \qquad \text{(C-2)}$$

Equations (C-1) and (C-2) form a set of two equations in two unknowns D_A and D_B. Noting that $h_R(0) = 0$, we get

$$D_A = \frac{D_B \left(-\frac{\Delta t}{2} h_I(0) H_1 \right) + \Theta_A}{\Delta H_1 + m\delta^{1/2} H_1} \qquad \text{(C-3)}$$

$$D_B = \frac{D_A \left(\frac{\Delta t}{2} h_I(0) H_1 \right) + \Theta_B}{\Delta H_1 + m\delta^{1/2} H_1} \qquad \text{(C-4)}$$

where

$$\Theta_A = -C_B\left[\frac{\Delta t}{2} h_I(0) I_1\right] - C_A\left[\Delta I_1 + m\delta^{1/2} I_1\right] - B_1^P\left[\frac{\Delta t}{2} h_I(0)\right] - \Delta A_1^P - m\delta^{1/2} A_1^P - W_A$$

$$\Theta_B = C_A\left[\frac{\Delta t}{2} h_I(0) I_1\right] - C_B\left[\Delta I_1 + m\delta^{1/2} I_1\right] + A_1^P\left[\frac{\Delta t}{2} h_I(0)\right] - \Delta B_1^P - m\delta^{1/2} B_1^P + W_B$$

and are known quantities. Solving for D_A and D_B in (C-3) and (C-4), we finally get

$$D_A = \frac{-\Theta_B \theta + (\Delta H_1 + m\delta^{1/2} H_1)\Theta_A}{(\Delta H_1 + m\delta^{1/2} H_1)^2 + \theta^2} \qquad \text{(C-5)}$$

$$D_B = \frac{\Theta_A \theta + (\Delta H_1 + m\delta^{1/2} H_1)\Theta_B}{(\Delta H_1 + m\delta^{1/2} H_1)^2 + \theta^2} \qquad \text{(C-6)}$$

where $\theta = \frac{\Delta t}{2} h_I(0) H_1$

We note in passing that the evaluation of D_A and D_B requires the knowledge of all the previous values of the streamfunction tendencies (in W_A and W_B) at $y = 0$, and thus a non-negligible amount of core memory has to be used to store these values at every time step. Once D_A and D_B are known, A_m and B_m, or, equivalently, $\frac{\partial A}{\partial t}$ and $\frac{\partial B}{\partial t}$ can be computed, and one can proceed with the time differencing scheme.

BIBLIOGRAPHY

Arakawa, A., 1966: Computational design for long-term numerical integration of the equations of fluid motion: Two-dimensional incompressible flow. Part 1. J. Comp. Phys., 1, 119-143.

Asselin, R., 1972: Frequency filter for time integrations. Monthly Weather Review, 100, 487-490.

Béland, M., and T. Warn, 1975: The radiation condition for transient Rossby waves. J. Atmos. Sci., 32, 1873-1880.

Bennett, J.R., and J.A. Young, 1971: The influence of latitudinal wind shear upon large-scale wave propagation in the tropics. Mon. Wea. Rev., 99, 202-214.

Benney, D.J., and R.F. Bergeron, 1969: A new class of nonlinear waves in parallel flows. Studies Appl. Math., 48, 181-204.

Booker, J.R., and F.P. Bretherton, 1967: The critical layer for gravity waves in a shear flow. J. Fuid Mech., 27, 513-539.

Burger, A.P., 1958: Scale considerations of planetary motions of the atmosphere. Tellus, 10, 195-205.

Charney, J.G., 1963: A note on large-scale motions in the tropics J. Atmos. Sci., 20, 607-609.

Davis, R.E., 1969: On the high Reynolds number flow over a wavy boundary. J. Fluid Mech., 36, 337-346.

Dickinson, R.E., 1970: Development of a Rossby wave critical level J. Atmos Sci., 27, 627-633.

Dietrich, D.E., 1973: A numerical study of rotating annulus flows using a modified Galerkin Method. Birkauser Verlag, 109, 1826-1861.

Eliassen, A., and E. Palm, 1961: On the transfer of energy in stationary mountain waves. Geofysiske Publikasjoner, 22, no. 3, 1-23.

Geisler, J.E., and R.E. Dickinson, 1974: Numerical study of an interacting Rossby wave and barotropic zonal flow near a critical level. J. Atmos. Sci., 31, 946-955.

Haberman, R., 1972: Critical layers in parallel flows. Stud. Appl. Math., 51, 139-162.

Henrici, P., 1962: Discrete variable methods in ordinary differential equations. New York: John Wiley & Sons, Inc.

_____, 1964: Elements of numerical analysis. New York: John Wiley & Sons Inc.

Kelly, R.E., and S. Maslowe, 1970: The nonlinear critical layer in a sligthly stratified shear flow. Studies Appl. Math., 69, 301-326.

Kuo, H.L., 1949: Dynamic instability of two-dimensional non-divergent flow in a barotropic atmosphere. J. Meteor., 6, 105-122.

Lilly, D.K., 1965: On the computational stability of numerical solutions of time-dependent nonlinear geophysical fluid dynamic problems. Mon. Wea. Rev., 93, 11-25.

Lin, C.C., 1944: On the stability of two-dimensional parallel flows Proc. Nat. Acad. Sci., Wash., 30, 316-23.

_____, 1945: On the stability of two-dimensional paralled flows. Parts I, II, III. Quart. Appl. Math., 3, 177-42, 218-34, 277-301.

Lin, C.C., 1955: On the Theory of hydrodynamic stability. Cambridge University Press, 155 pp.

_____, 1957: On the instability of laminar flow and its transition to turbulence. Proc. Symp. Boundary Layer Research, Freiburg/BR, H. Gortler, Ed., 144-160.

Lorenz, E.N., 1972: Barotropic instability of Rossby wave motion. J. Atmos. Sci., 29, 258-264.

Maslowe, S.A., 1972: The generation of clear air turbulence by nonlinear waves. Stud. Appl. Math., 51, 1-16.

_____, 1973: Finite-amplitude Kelvin-Helmholtz billows. Bound. - Layer Meteor., 5, 43-52.

Matsuno, T., 1966: False reflection of waves at the boundary due to the use of finite differences. J. Meteor. Soc. Japan, 44, 145-157.

_____ , 1966: Numerical integrations of the primitive equations using a simulated backward difference method. J. Meteor. Soc. Japan, 44, 76-83.

_____ , 1971: A dynamical model of the stratospheric sudden warming. J. Atmos. Sci., 28, 1479-1494.

Murakami, M., 1974: Influence of mid-latitudinal planetary waves on the tropics under the existence of a critical latitude. J. Meteor. Soc. Japan, 52, 261-271.

Pedlosky, J., 1964: The stability of currents in the atmosphere and the ocean: Part 1, J. Atmos. Sci., 21, 201-219.

Robert, A.J., 1966: The integration of a low order spectral form of the primitive meteorological equations. J. Meteor. Soc. Japan, 44, 237-245.

Ward, G.H., 1974: Aspects of the nonlinear dynamics of planetary scale barotropic waves. Ph.D. thesis, University of Texas, 169 pp.

Warn, T., and H. Warn, 1976: On the development of a Rossby wave critical level. J. Atmos. Sci., 33, 2021-2024.